FAA-RD-75-23

Project Report
ATC-47

Scale Model Pattern Measurements of Aircraft L-Band Beacon Antennas

K. J. Keeping
J. C. Sureau

4 April 1975

Lincoln Laboratory
MASSACHUSETTS INSTITUTE OF TECHNOLOGY
LEXINGTON, MASSACHUSETTS

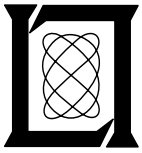

Prepared for the Federal Aviation Administration,
Washington, D.C. 20591

Technical Report Documentation Page

1. Report No.	2. Government Accession No.	3. Recipient's Catalog No.
FAA-RD-75-23		

4. Title and Subtitle	5. Report Date
Scale Model Pattern Measurements of Aircraft L-Band Beacon Antennas	4 April 1975
	6. Performing Organization Code
7. Author(s)	8. Performing Organization Report No.
K.J. Keeping and J.C. Sureau	ATC-47
9. Performing Organization Name and Address	10. Work Unit No. (TRAIS) 45364
Massachusetts Institute of Technology Lincoln Laboratory P.O. Box 73 Lexington, Massachusetts 02173	Project No. 034-241-012
	11. Contract or Grant No. DOT-FA72-WAI-261
	13. Type of Report and Period Covered
12. Sponsoring Agency Name and Address	Project Report
Department of Transportation Federal Aviation Administration Systems Research and Development Service Washington, D.C. 20591	14. Sponsoring Agency Code

15. Supplementary Notes

The work reported in this document was performed at Lincoln Laboratory, a center for research operated by Massachusetts Institute of Technology.

16. Abstract

This report describes the techniques and apparatus used to measure the directional patterns of aircraft ATC transponder antennas (L-Band) using digital techniques and magnetic tapes for data storage. Algorithms involved in data normalization, cross-polarization correction and coordinate conversions are discussed. Some typical applications of the data are illustrated with actual computer outputs obtained from the model measurements.

17. Key Words	18. Distribution Statement
Aircraft antenna patterns ATC antenna patterns Scale model measurements	Document is available to the public through the National Technical Information Service, Springfield, Virginia 22151.

19. Security Classif. (of this report)	20. Security Classif. (of this page)	21. No. of Pages	
Unclassified	Unclassified		

Form DOT F 1700.7 (8-72) Reproduction of completed page authorized

AIR FORCE (1) MAY 8, 1975--355

ACKNOWLEDGMENTS

The work reported in this paper was begun by Dr. John Ruddy who did the initial planning, set up the procedures for obtaining accurate aircraft scale models, and participated in selection of the antenna range instrumentation. Earl Hunter operated the antenna range apparatus. Ms. Kathleen Knox did the necessary computer programming which proved to be a very frustrating job due to initial equipment problems and to insidious machine-language problems that took a great deal of time and consultation to clean up. Many conversations with Dr. William Harman and Gary Schlieckert were of great use in directing the overall program. Without the assistance of all of the above and of Group 61 and Group 28 personnel, this work could not have been successfully carried out.

TABLE OF CONTENTS

LIST OF ILLUSTRATIONS

LIST OF ILLUSTRATIONS (cont.)

SCALE MODEL PATTERN MEASUREMENTS OF AIRCRAFT L-BAND BEACON ANTENNAS

I. INTRODUCTION

The Technical Development Plan for DABS discusses, under the heading of design options [Ref. 1], the possibility of aircraft antenna diversity as a means of overcoming the limitations on system performance arising from nulls in aircraft antenna patterns. Under Phase I of the DABS Development Plan it also calls for a program of aircraft antenna pattern measurements [Ref. 2] with special attention being given to general aviation aircraft for which little information is available.

Accordingly, a program was initiated at Lincoln Laboratory to obtain these pattern data in the most convenient form for use in further studies. The directional gain of aircraft antennas was to be measured over a complete spherical surface with uniform density, and the number of measurements was to be great enough so that all significant pattern data would be recorded. These data must cover a variety of typical flight conditions (such as wheels up, wheels down, and flaps up, flaps down, etc.). Various possible antenna locations on the aircraft should be used so that comparisons can be made as to the relative suitability of the position considered. Clearly, diversity schemes must be based on such comparative data.

II. DESCRIPTION OF EQUIPMENT AND MEASUREMENTS TECHNIQUES

There are many reasons, which will not be enumerated here, that it is impractical to make antenna measurements on a full scale aircraft. Considering the position apparatus, which was available to hold the model aircraft at accurately known angular coordinates while the measurements are made, it appeared that the maximum dimension of the model should not exceed about 30 inches. Consideration of actual dimensions of general aviation aircraft indicated that a scale factor of 1/20 would be suitable. Since the actual frequency of the proposed DABS system is 1060 ± 30 MHz, this means that the pattern measurements must be carried out at 20 × 1060 = 21200 MHz = 21.2 GHz (wavelength ≈ 0.56"). Although the antenna gain itself is very low, the whole aircraft (fuselage, wings, etc.) makes up a very complex antenna structure and, to assure that the measured patterns would be like those that would be seen at "infinite distance" from the model aircraft, it was decided that the distance separating the antenna, used to illuminate the model on the positioner, should be large compared to $2D^2/\lambda$ where D is the maximum dimension of the model. Since D_{max} is approximately 30 inches, the required length of the antenna range is about 270 feet. The available range length of 2000 feet is clearly more than adequate.

Through the cooperation of the manufacturers, loft line drawings were obtained for the following types of general aviation aircraft:

The Lear Jet
Piper "Cherokee" 140
Shrike "Commander"
Cessna 150
Cessna "Cardinal"
Cessna "402B"
Beech "Baron"
Beech "B-99"
Twin Otter
Helio V10D
Grumman Gulfstream II

Scale models (1/20 scale) were obtained of each type. These models have dimensional tolerance of ±0.30" with rigging tolerance no greater than ±0.060". Thus the largest dimensional errors are just over ±0.1 wavelength and as such should be of negligible importance, since the pattern of a flying aircraft is difficult, if not impossible, to define exactly due to surface flexures and vibrational modes. The actual form of the aircraft is a function of time and it may never exactly regain any form it had in the past.

The aircraft models have removable wheels (where appropriate) to simulate wheels-up conditions and removable flaps. They also have hollow fuselages with several antenna locations at or near the upper and lower center lines; these antenna locations are shown in more detail in Appendix A. In addition to this an adapter plate is fixed on the top and bottom of the fuselage to permit attaching the model to the positioner.

The site of the aircraft models during measurement was probed before making any measurements and it was found that the field intensity was constant within ±0.1 dB over the area to be occupied by the aircraft model during measurement (see Fig. 1).

A simplified block diagram of the overall data gathering facility is shown on Fig. 2. The analog-to-digital converters used for angle readout make use of synchro-to-digital conversion having a stated accuracy of 0.01 degree and a resolution of 0.01 degree. Thumbwheel offsets are provided as a convenient means of zeroing the readout to correspond to any desired reference angle.

The analog-to-digital converter used for amplitude ratio readout provides either logarithmic or linear outputs. With the logarithmic option, the selected sampling has a dynamic range of 85 dB and an accuracy and resolution of readout of 0.1 dB. The associated tape recording system is shown on Fig. 3.

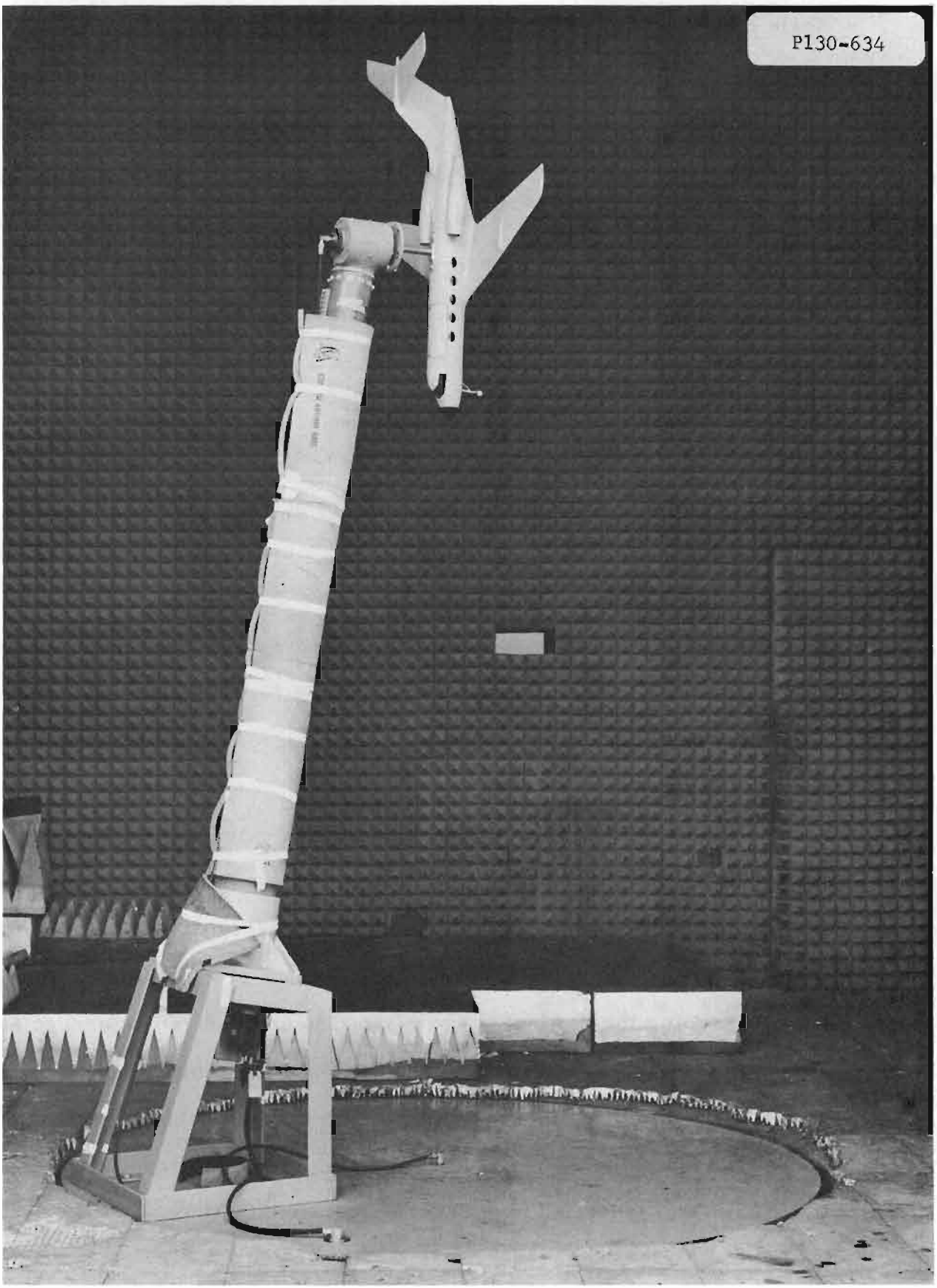

Fig. 1. Aircraft model on antenna positioner

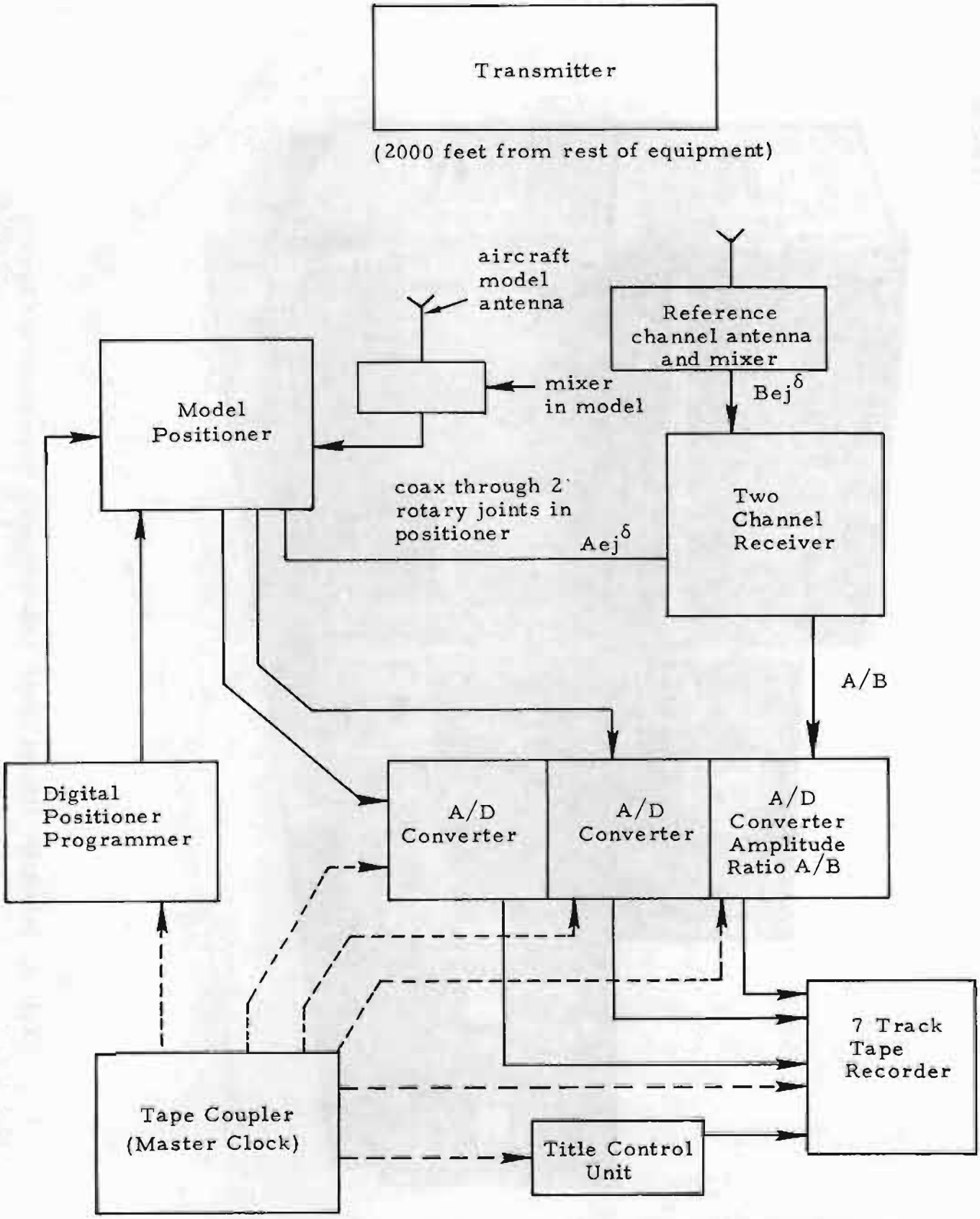

Fig. 2-Simplified Block Diagram of Model 1892 Magnetic Tape Recording System (Scientific Atlanta) and associated equipment.

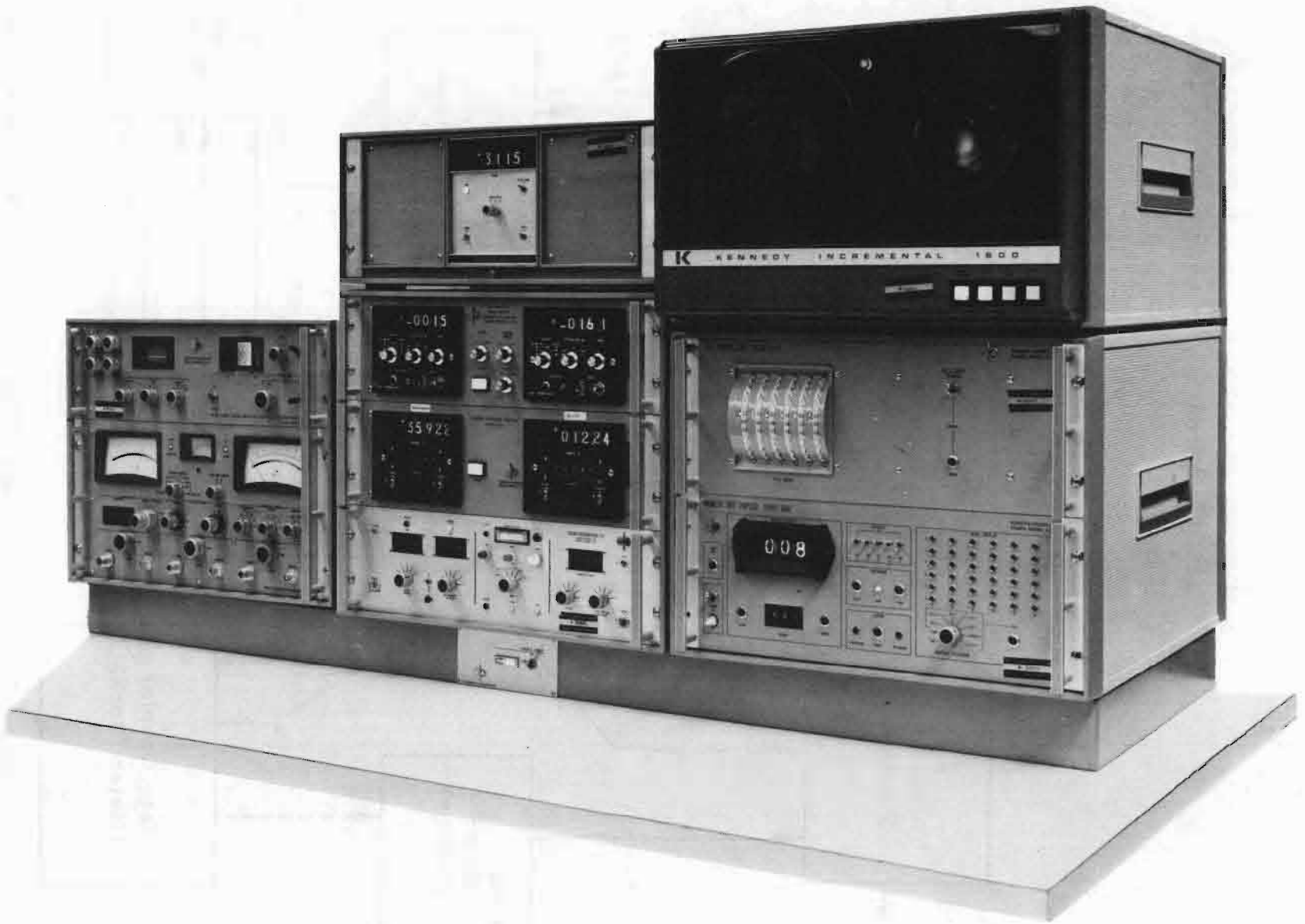

Fig. 3. Scientific Atlanta Model 1892 Magnetic Tape Recorder System

The dual channel or phase amplitude microwave receiver (Scientific-Atlanta Series 1750) has a dynamic range of 60 dB and amplitude accuracy of ±0.25 dB. The output signal is modulated at 1000 Hz. The receiver supplies isolated local oscillator power to two external mixers (in this application one mixer is located in the aircraft model and the receiver accepts 45 MHz IF signals generated in these external mixers.

A description of the coordinate system and the detailed manner in which pattern data are actually measured is shown in Fig. 4. The pole of the spherical coordinate system is the yaw axis of the aircraft. The ϕ coordinate, and angular rotation about the yaw axis, are then measured as indicated.

To record a complete data set, the antenna positioner was set so that $\theta = 1^{\circ}$ and $\phi = 0$. The title word (described later) was first written on the tape. The model was revolved about the yaw axis at a uniform speed and data were sampled every 2 degrees in ϕ. These data consist of θ, ϕ, and amplitude ratio in dB. (This is the ratio of the signal received in the model aircraft antenna to that received in the reference antenna.) Thus, 180 sets of angular and amplitude data are recorded in the initial record. The record word is written just after the title word, before the data were written. At this point the angle ϕ was stopped at zero and the angle θ was advanced to 3°. The new record word was written, followed by 180 sets of data words, and so on until 90 complete records had been recorded. This resulted in $90 \times 180 = 16200$ points in the complete spherical coverage for which data had been measured.

The description just given applies for top mounted antennas. Bottom mounted antennas require that the model be mounted in the inverted position on the antenna positioner. Therefore, the first record on the data file corresponds to $\theta = 179^{\circ}$ and the 90th record corresponds to $\theta = 1^{\circ}$.

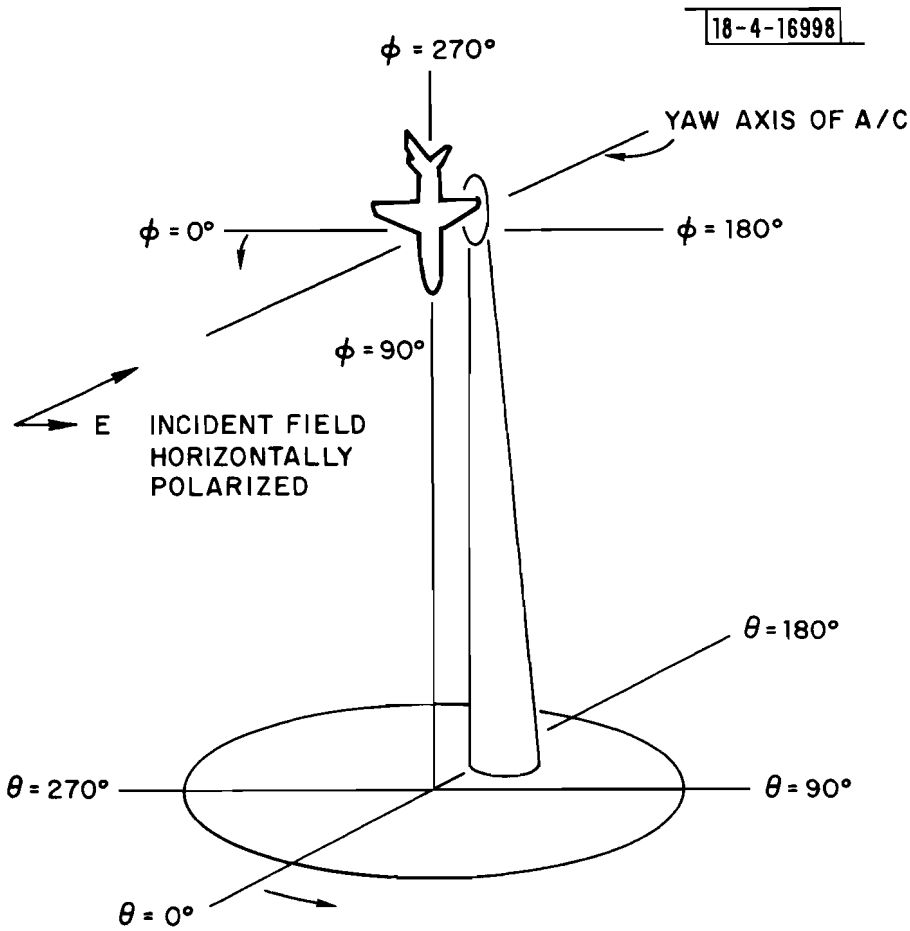

Fig. 4. Model aircraft and tower geometry.

III. DATA NORMALIZATION AND PROCESSING

This process edits out the unnecessary angle data and produces the amplitude data in dB with respect to isotropic on a 9-track tape. Now each file consists of a title word and 16200 words of amplitude data.

The normalizing process is a numerical integration described below: Let X_{mn} be a two-dimensional array containing all of the unnormalized amplitude data at the m^{th} value of ϕ and the n^{th} value of θ. Let there be N equal intervals in the range of θ between 0 and π, and let there be M equal intervals in ϕ between 0 and 2π. Now, if A_{mn} is the corresponding unnormalized power level,

$$A_{mn} = 10^{\frac{X_{mn}}{10}}$$

$$\text{and } \Delta\theta = \frac{\pi}{N} \text{ and } \Delta\phi = \frac{2\pi}{M} \quad .$$

The total radiated power is the sum of all contributions through each elementary unit area ($\sin\theta \, \Delta\theta \, \Delta\phi$)

$$\therefore P_t = \sum_{m=1}^{M} \sum_{n=1}^{N} A_{mn} \sin\left(\frac{n\pi}{N}\right)\left(\frac{\pi}{N}\right)\left(\frac{2\pi}{M}\right)$$

$$= \left(\frac{2\pi^2}{NM}\right) \sum_{m=1}^{M} \sum_{n=1}^{N} A_{mn} \sin\left(\frac{n\pi}{N}\right)$$

and to determine the average power radiated per steradian of surface we divide by 4π

$$\therefore \; <P> = \left(\frac{\pi}{2NM}\right) \sum_{m=1}^{M} \sum_{n=1}^{N} A_{mn} \sin\left(\frac{n\pi}{N}\right) \; .$$

This is the isotropic level of the antenna radiation and in our case where N = 90 and M = 180

$$<P> = \left(\frac{\pi}{2x16,200}\right) \sum_{m=1}^{180} \sum_{n=1}^{90} A_{mn} \sin\left(\frac{n\pi}{90}\right) .$$

Note that when the $A_{mn's}$ are all unity, $<P>$ = unity also, as it must for an isotropic radiator.

Now if $\overline{X_{mn}}$ mn represents the "normalized" amplitude data expressed in dB and X_{mn} the unnormalized data,

$$\overline{X_{mn}} \; mn = X_{mn} - 10 \log_{10} <P> \; dBi.$$

The production of principal plane "omnidirectional" H plane, and E plane cuts is clearly a very simple process when the normalized 9-track data are available (see Fig. 5a). It is important to take note of whether it is a top mounted or bottom mounted antenna; then the omnidirectional data required are either from the 45th or 46th record, i.e., at $\theta = 89^{\circ}$ or $\theta = 91^{\circ}$. In the complete file this corresponds to data words from 2700 to 2880 or from 2880 to 3060, respectively. The E plane patterns are only slightly more involved. All data for which $\phi = 0.0^{\circ}$ and $\phi = 180.0^{\circ}$ are required for the E-plane cut

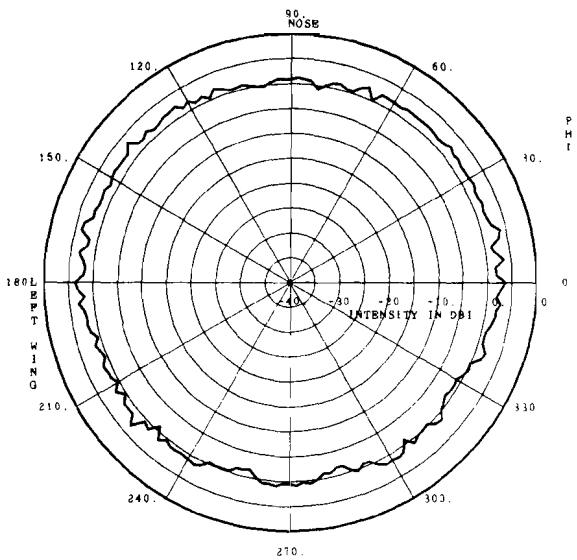

(a) horizontal plane

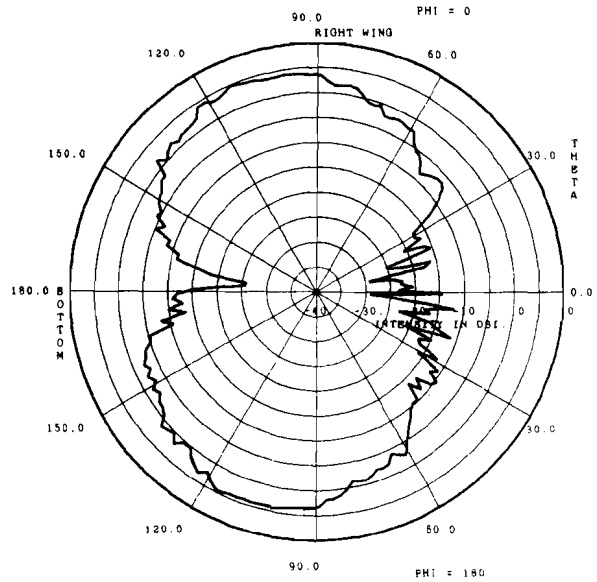

(b) wing to wing

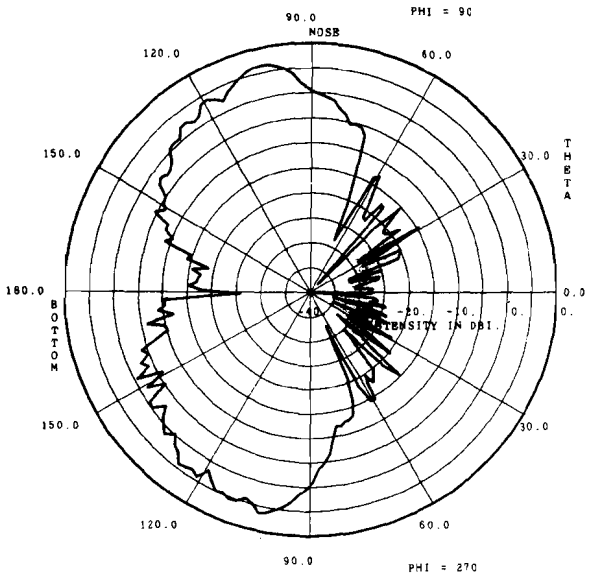

(c) nose to tail

ATC-47(5)

Fig. 5. Lear jet bottom-mounted front, flaps down, wheels up

containing the wings (see Fig. 5b), and all data for which $\phi = 90^{o}$ and $\phi = 270.0^{o}$ are required for the E-plane cut containing the nose and tail (see Fig. 5c). A complete set of principal plane patterns for those aircraft that were actually measured (the measurements program was about 75% completed before being stopped) is given in Appendix B.

Radiation density and contour plots are, in principle at least, quite straightforward. There are available computer routines which, given data measured at various points in a plane, can linearly interpolate and draw in the contours of constant intensity. Such a program was used but, due to the very large amount of data, the computing time was considered to be excessive and unwarranted, considering the limited interest in this type of data presentation. A very much simpler and cruder approximation to an accurate contour plot is obtained by quantizing the data and printing out on a rectangular grid the resulting data, going from left to right on each scan line and printing a symbol only if the radiation level has shifted to some other quantized level. While this is simple and required very little computer time, it does require a great deal of patience and time to draw in the contour by hand later on. An example of this process is given in Fig. 6.

Other applications of the data involving arbitrary maneuvers of the aircraft and the effective antenna gain to vertically-polarized radiation from a beacon interrogator on the ground clearly involve coordinate transformation and, since roll and pitch angles are permissible for the aircraft, cross-polarization losses must be accounted for. The cross-polarization correction and coordinate transformations required are described in Appendix C.

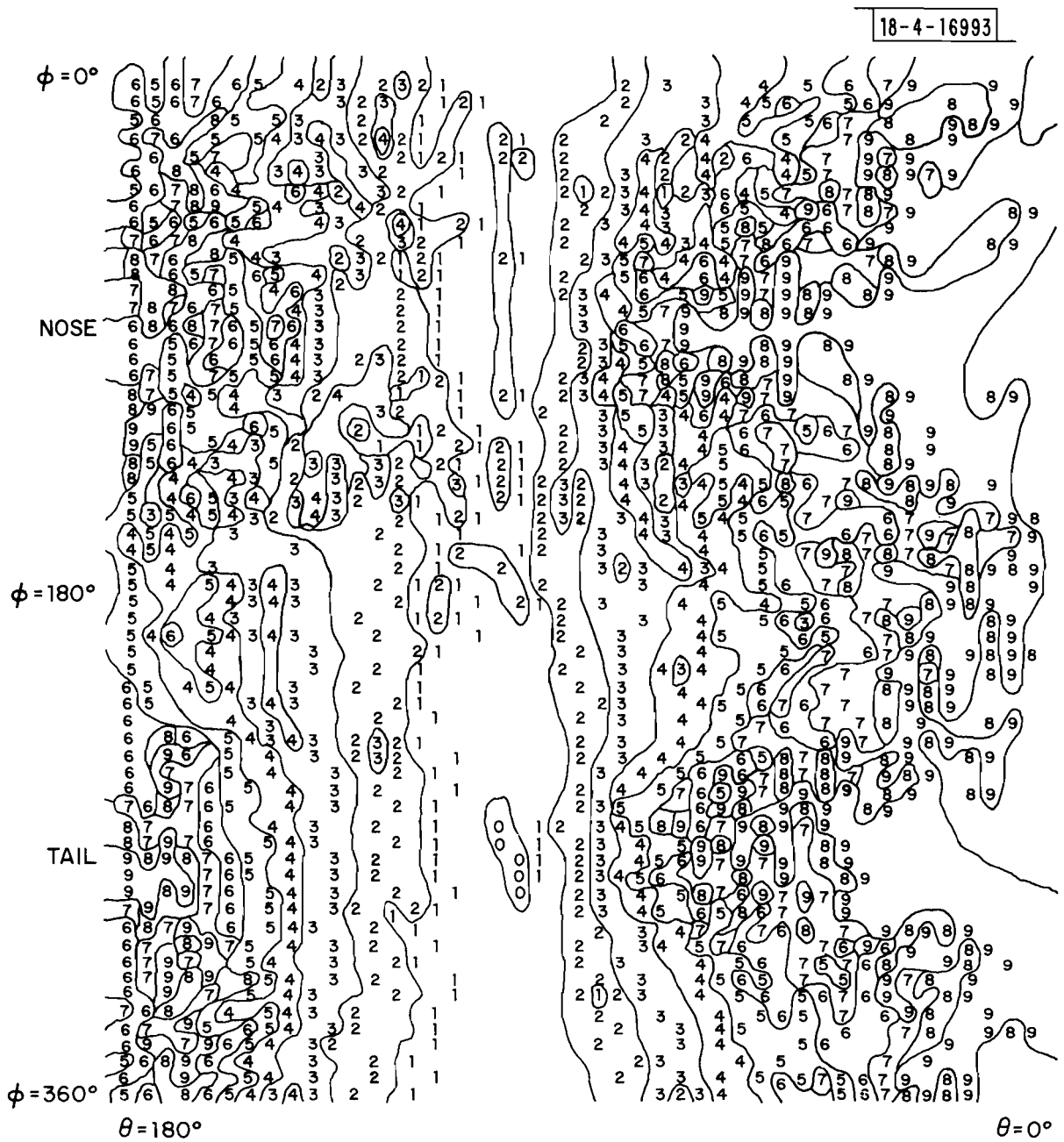

Fig. 6. Radiation density contours for the Lear Jet with wheels up and flaps down and antenna in bottom front position.

Thus, when some situation is defined with aircraft coordinates relative to a ground located radar, and aircraft velocity and roll angles are known, the first step requires that θ and ϕ be found and the corresponding antenna data must then be located. The cross-polarized correction is then added to obtain the aircraft antenna gain for that particular set of conditions.

With the aid of the coordinate conversion, cross polarization correction and data lockup subroutines, it is a relatively simple process to obtain the effective aircraft antenna gain under any assumed set of conditions. It is assumed, of course, that the aircraft antenna is well matched to the receiver or, if not, that allowance will be made for the mismatch. Ground reflections complicate the overall picture of the transmission channel and in the following multipath signals are ignored in the interest of simplicity. However, any assumed multipath model could be incorporated in the procedure with the resulting increased complexity and computing time.

A useful application of the data could be a plot of the conditioned probability that the antenna gain will be at least as great as x dBi versus x dBi under a set of assumed conditions. For example, if the angle of elevation of a given aircraft is fixed at a given value, the roll angle is equally probable between given limits and the heading is also equally probable anywhere from zero to 360°; then such a graph of the cumulation probability can be plotted and it will have considerable value in the assessment of the relative merit of possible antenna locations and perhaps indicate whether or not antenna diversity is needed. Figure 7 is such a result. Further applications and reduction of the recorded data are described in Ref. 3.

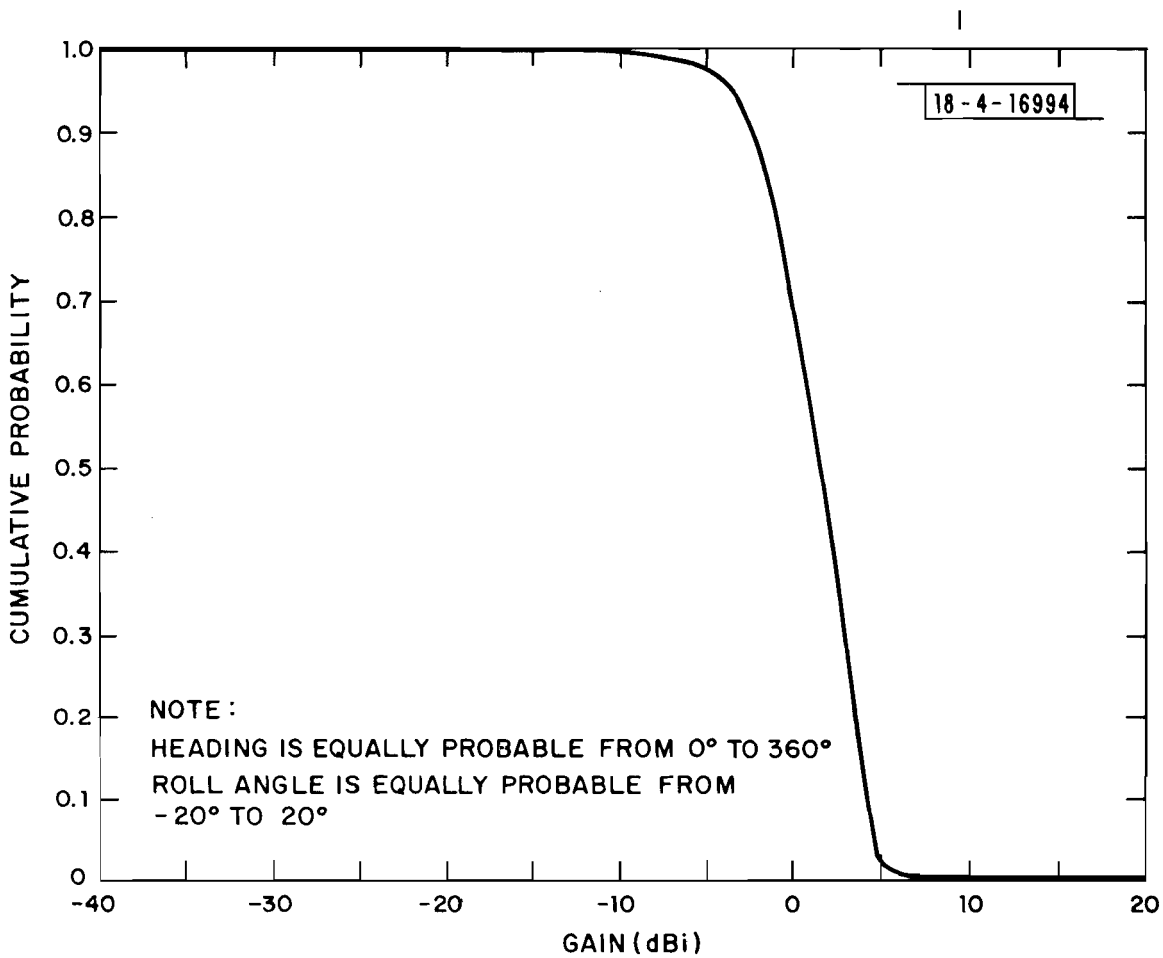

Fig. 7. Typical probability distribution function for antenna gain.

APPENDIX A

AIRCRAFT MODELS AND ANTENNA POSITIONS

Fig. A. 1a. Lear jet (3/4 view).

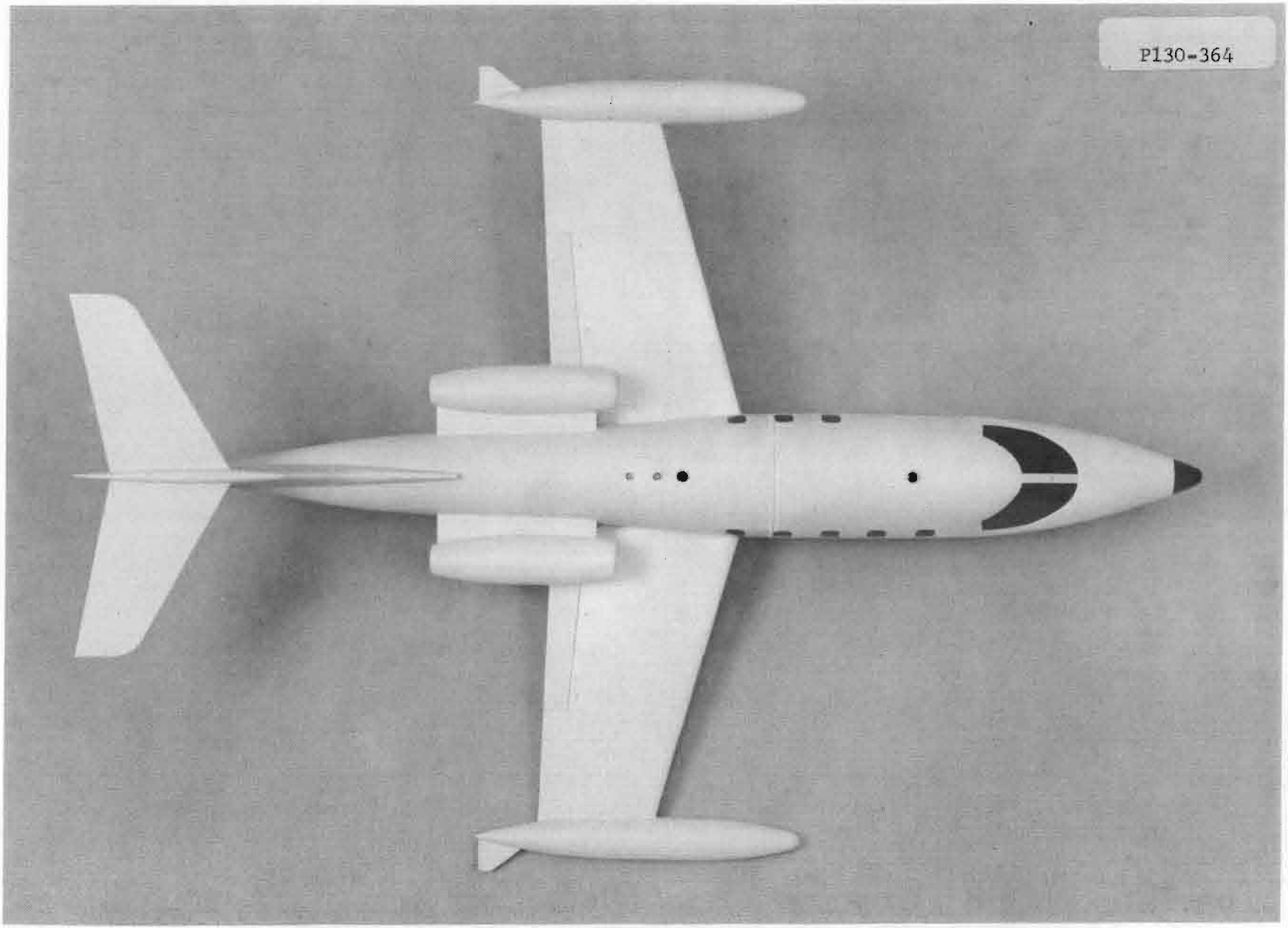

Fig. A. 1b. Lear jet (top view).

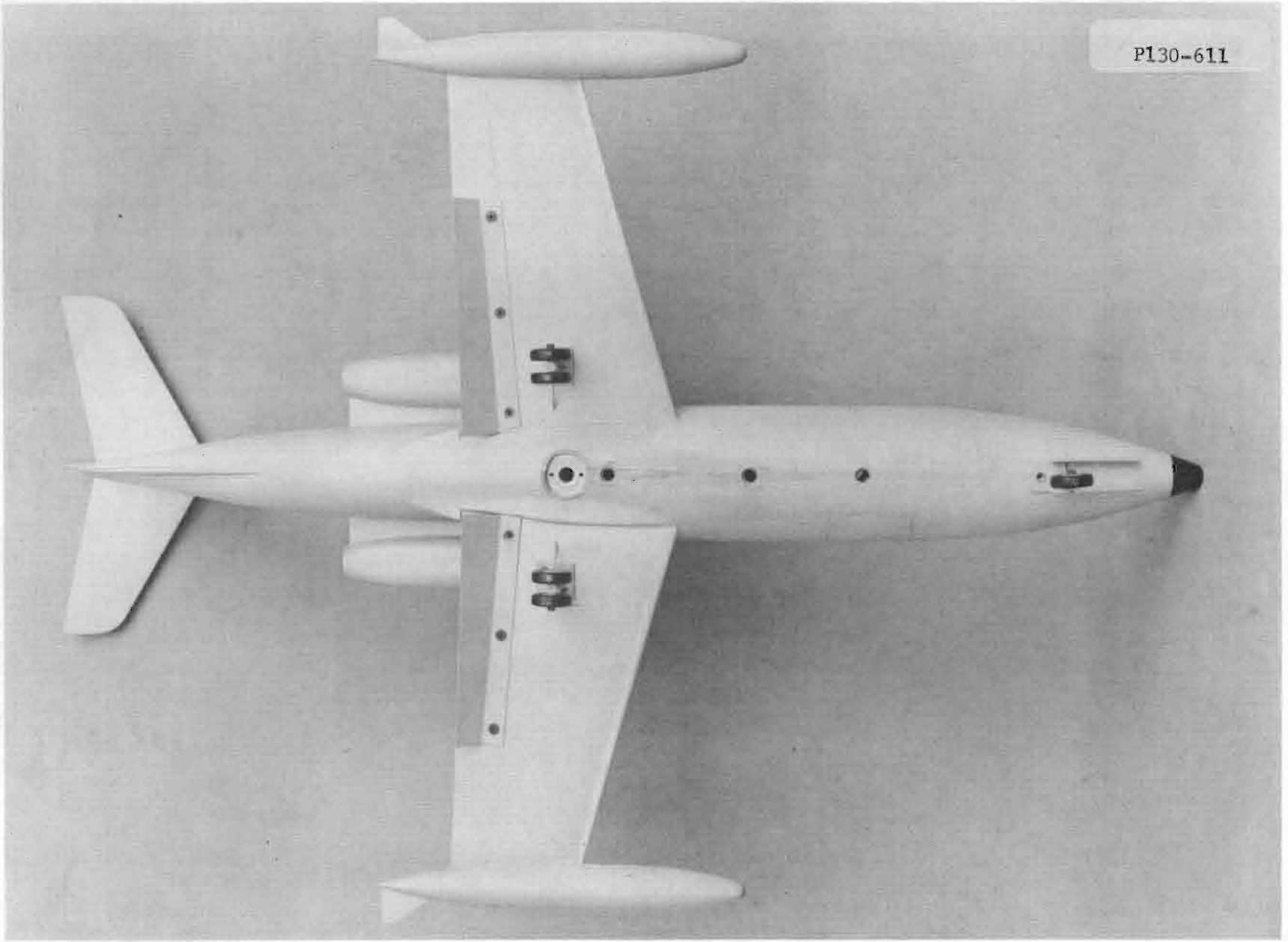

Fig. A. 1c. Lear jet (bottom view).

Fig. A. 2a. Cessna 150 (3/4 view).

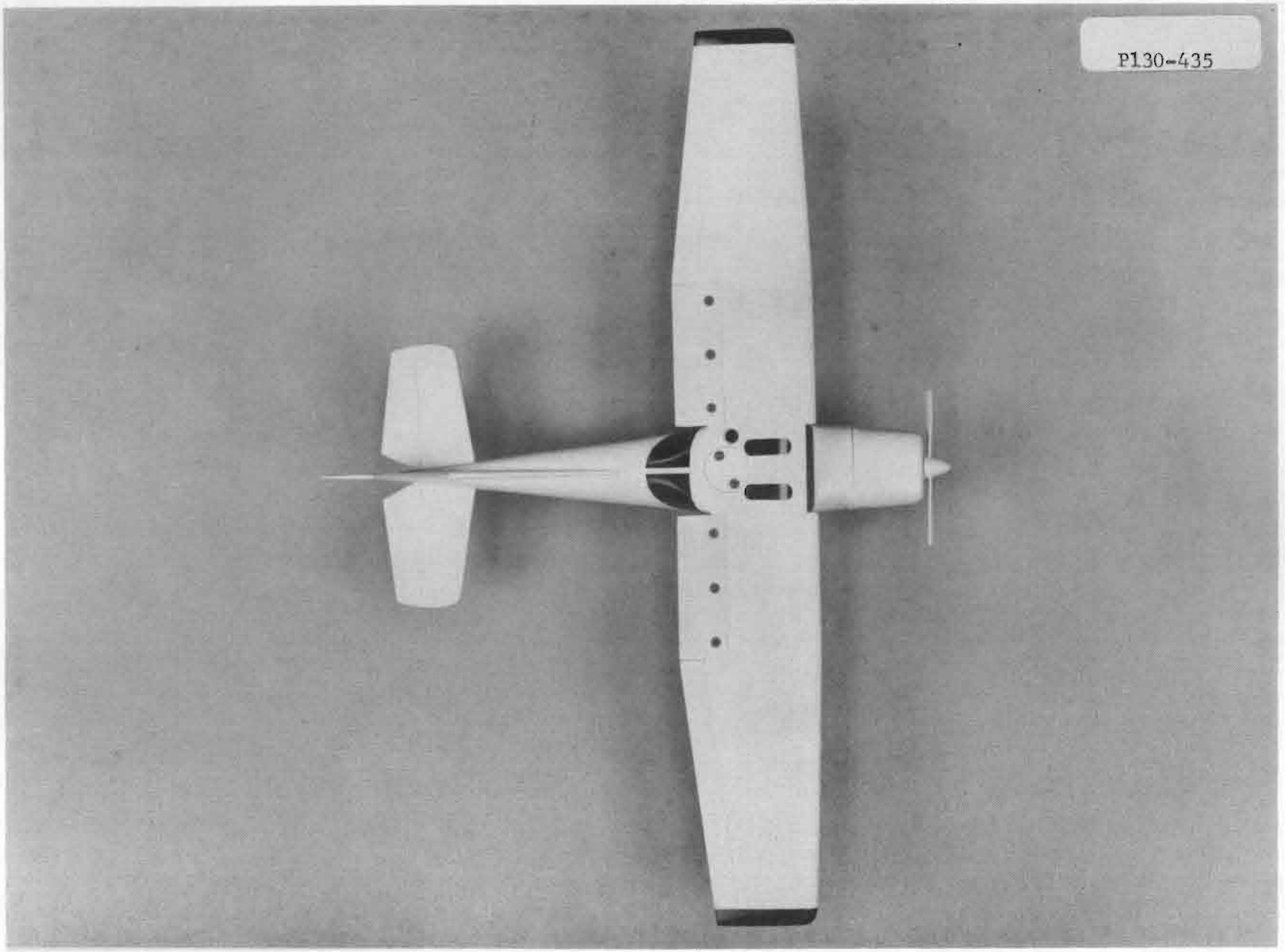

Fig. A.2b. Cessna 150 (top view).

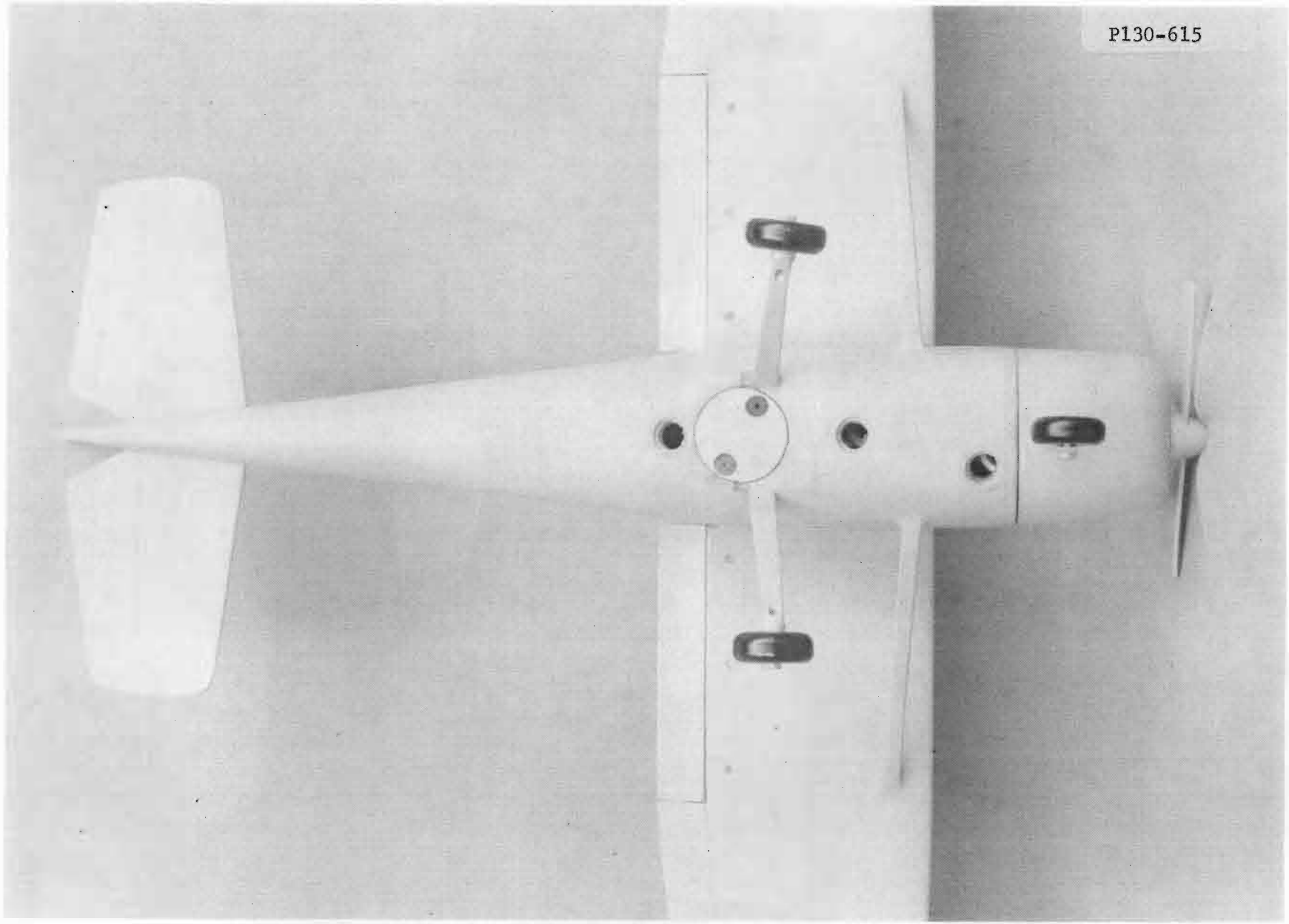

Fig. A. 2c. Cessna 150 (bottom view).

Fig. A. 3a. Piper Cherokee (3/4 view).

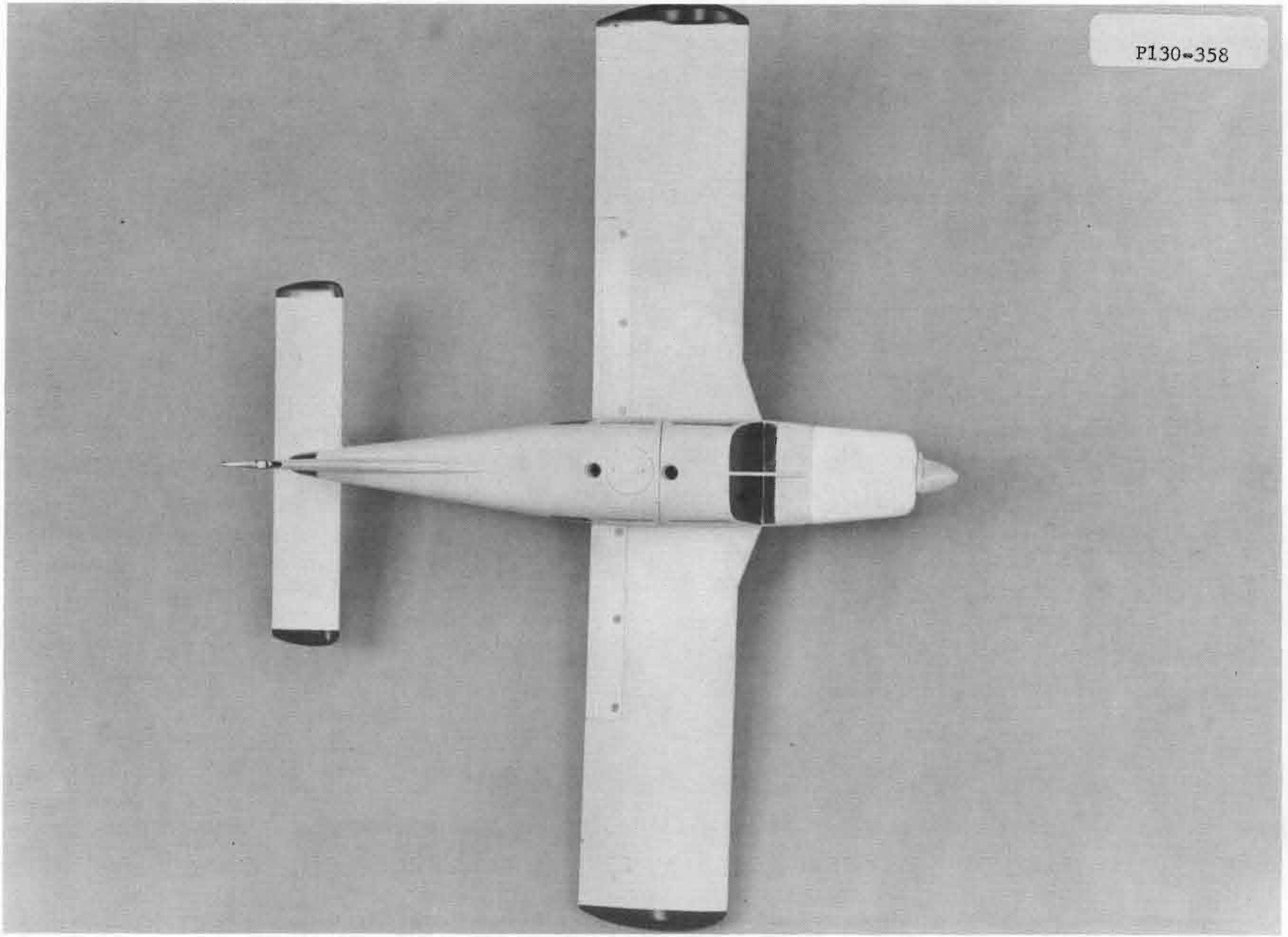

Fig. A, 3b. Piper Cherokee (top view).

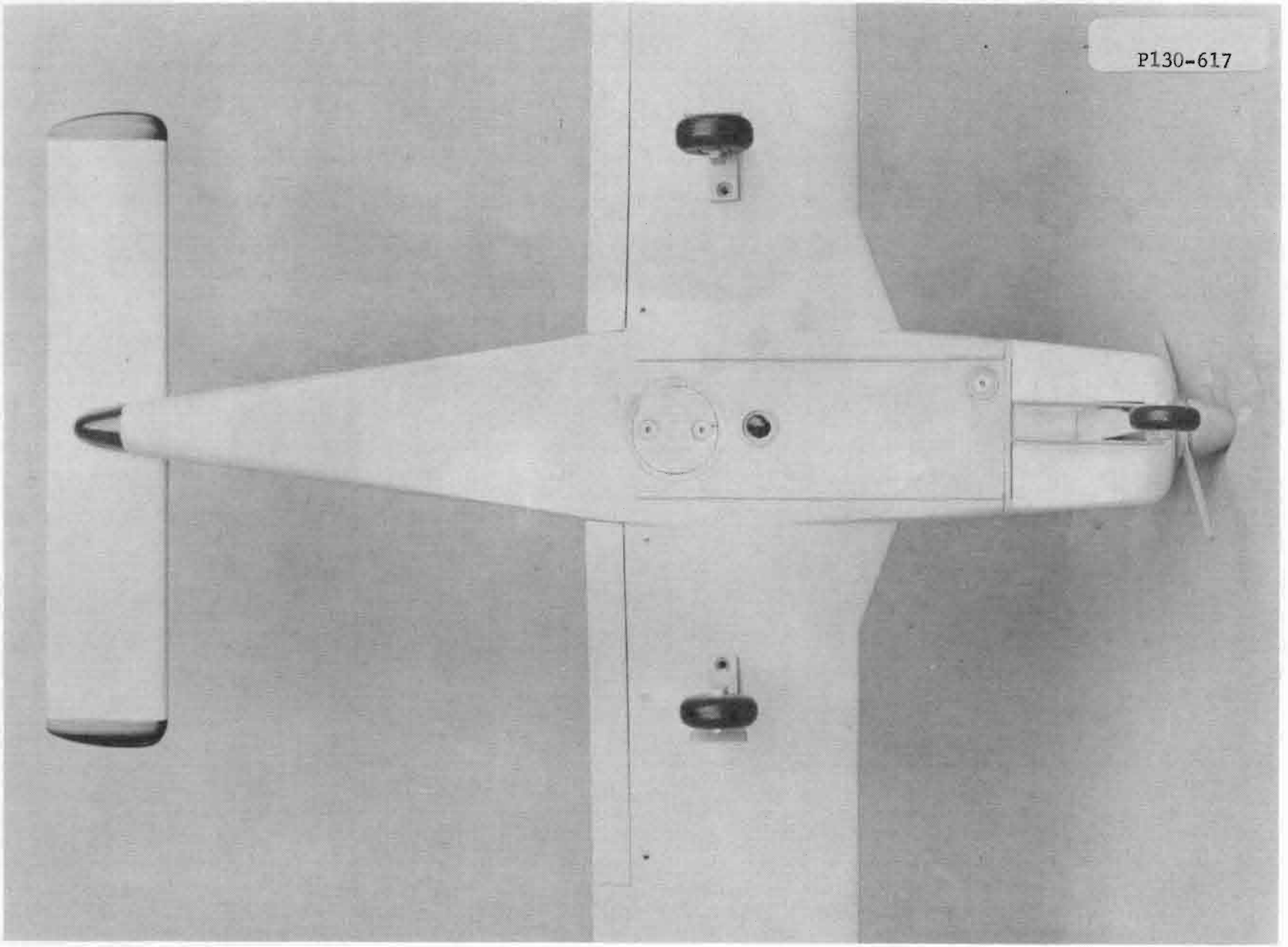

Fig. A. 3c. Piper Cherokee (bottom view).

Fig. A. 4a. Grumman Gulfstream II (3/4 view).

Fig. A. 4b. Grumman Gulfstream II (top view).

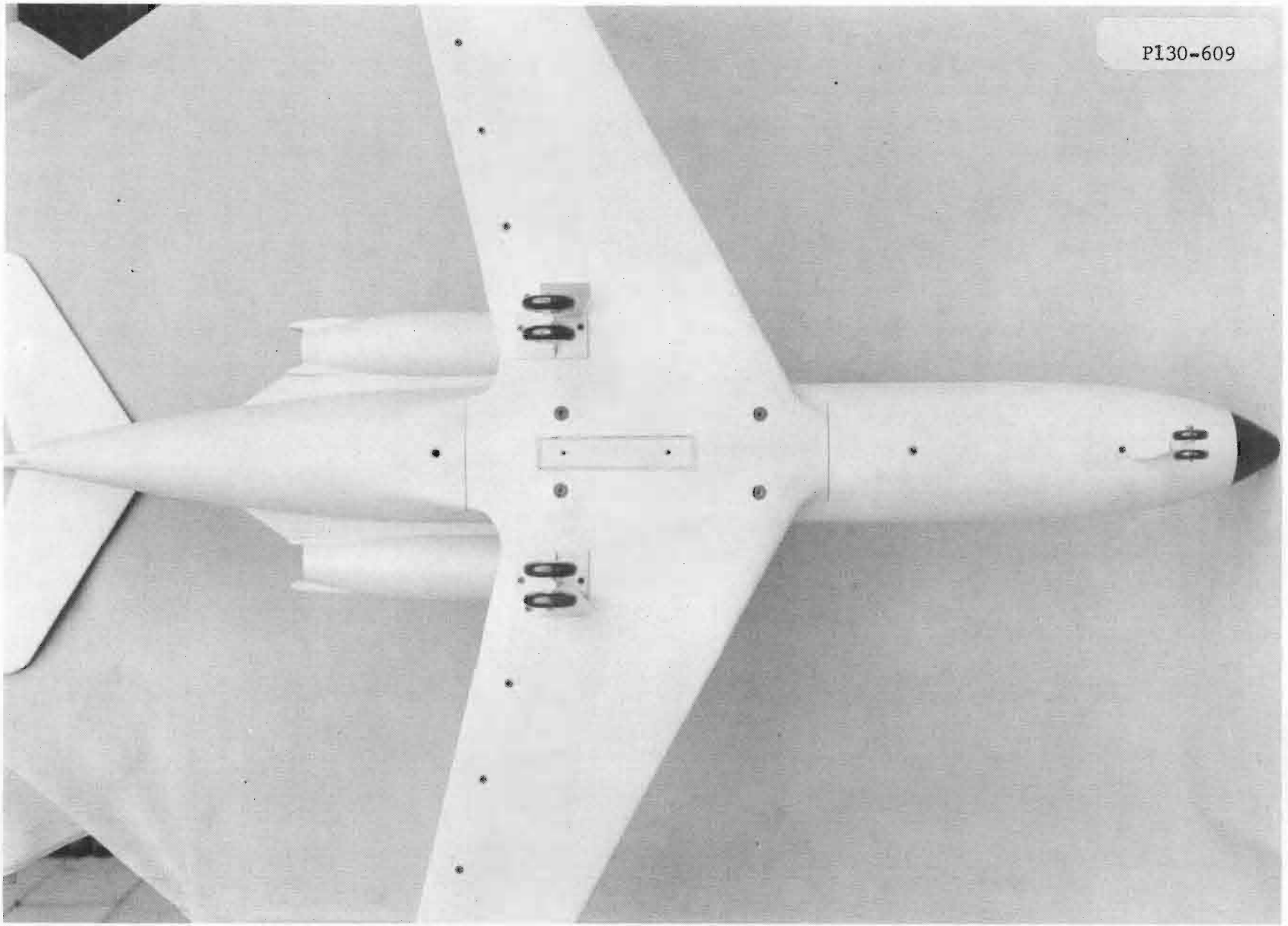

Fig. A. 4c. Grumman Gulfstream II (bottom view).

Fig. A. 5a. Helio V10D (3/4 view).

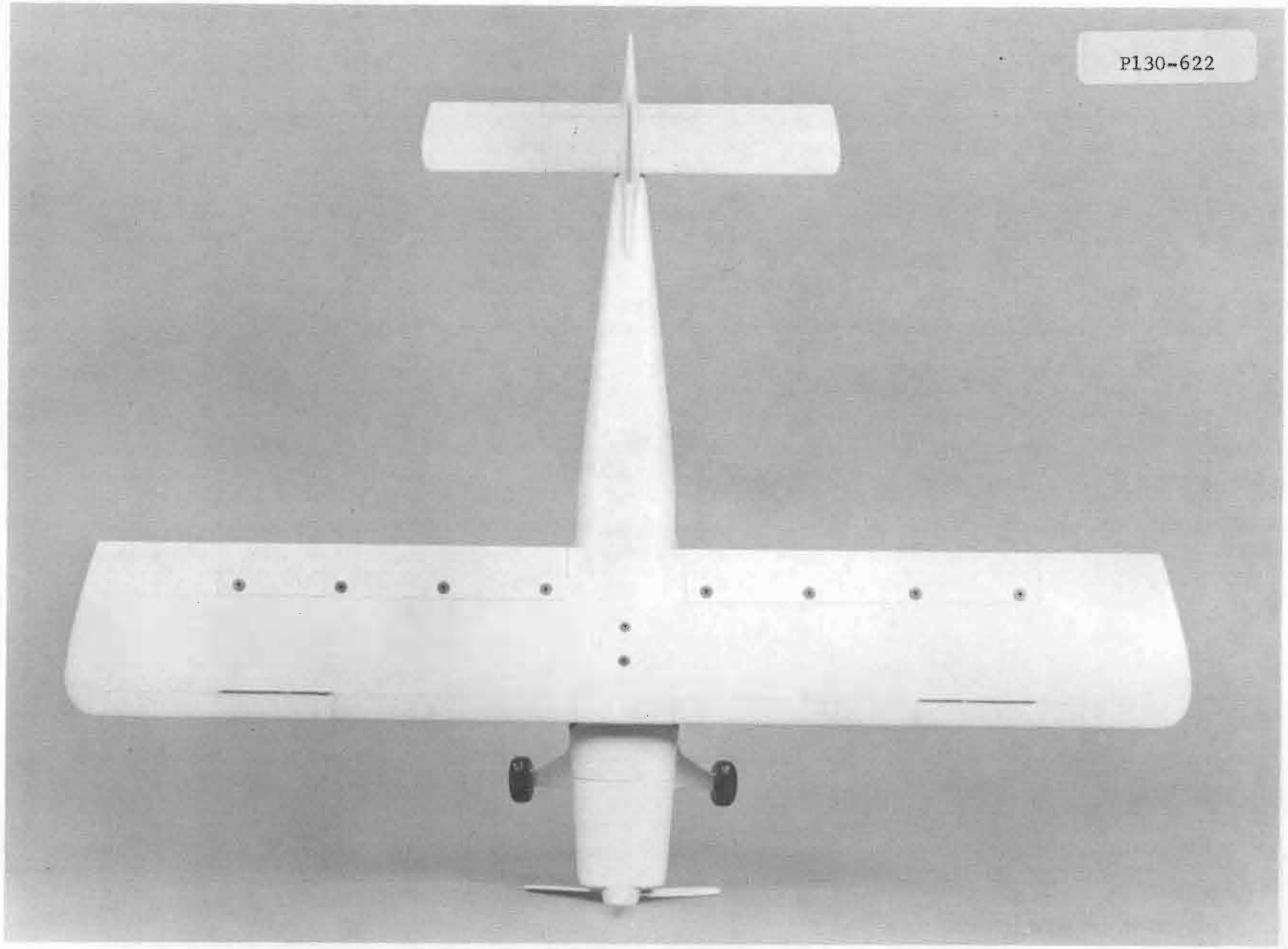

Fig. A. 5b. Helio V10D (top view).

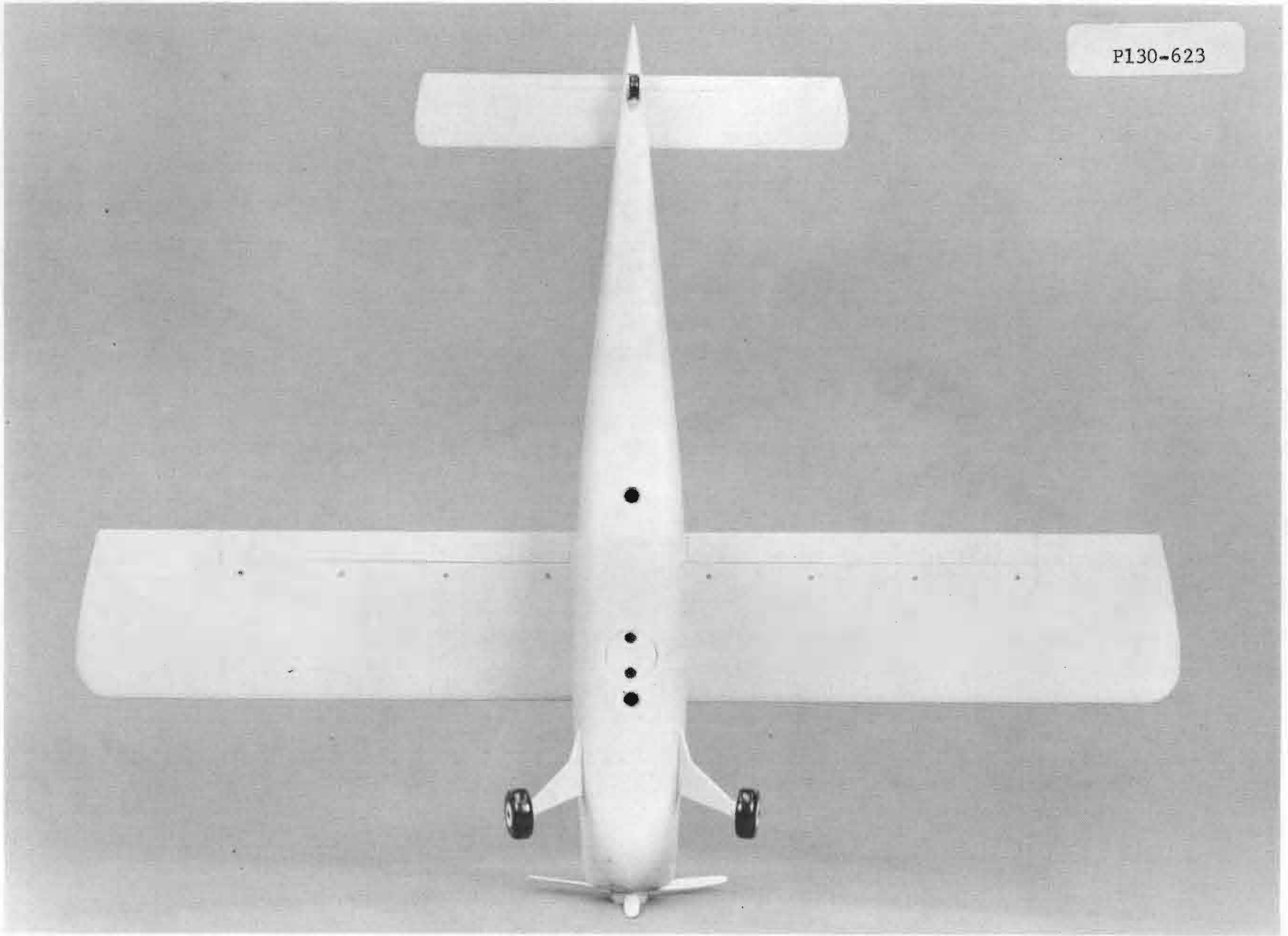

Fig. A. 5c. Helio V10D (bottom view).

Fig. A. 6a. Twin Otter (3/4 view).

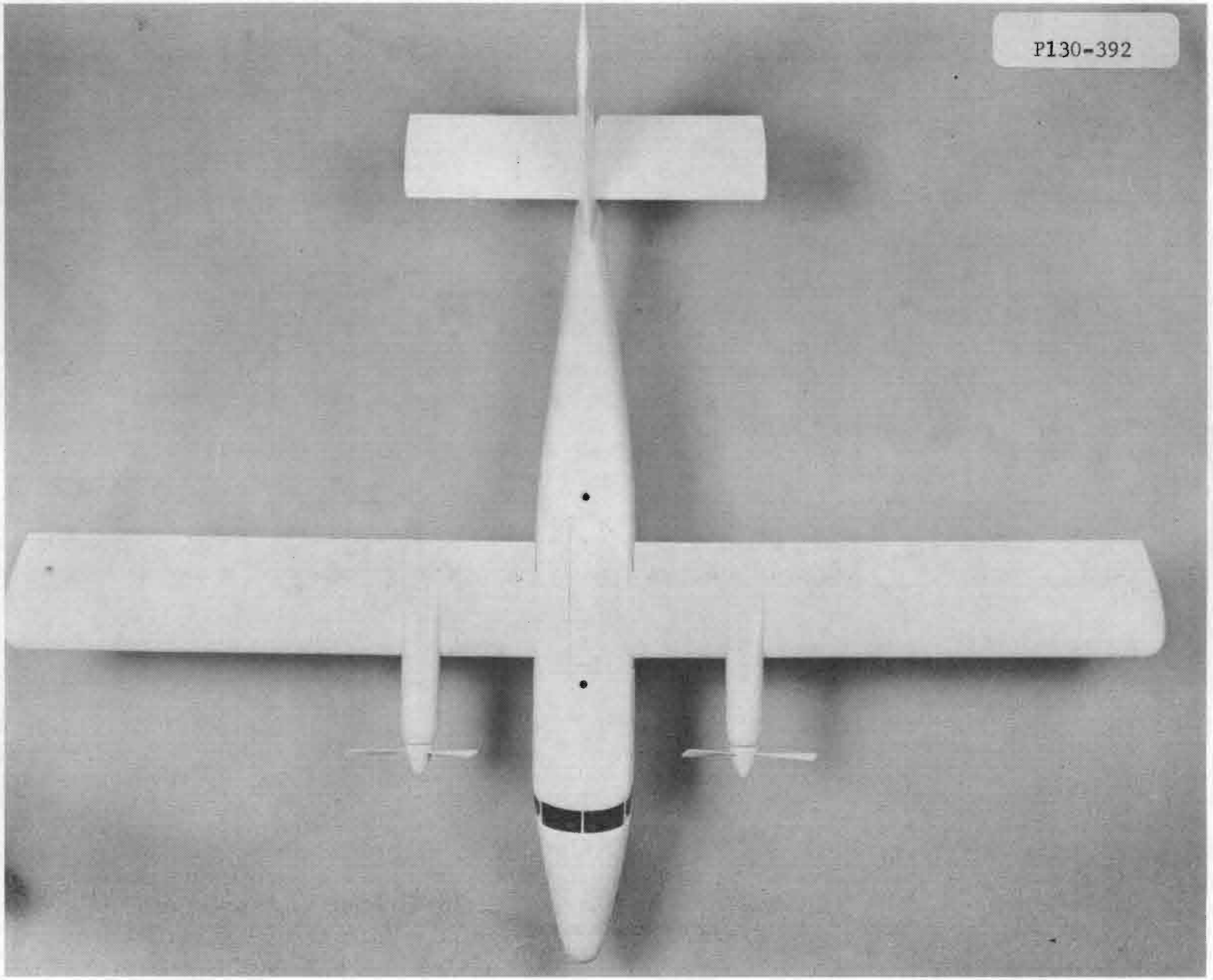

Fig. A. 6b. Twin Otter (top view).

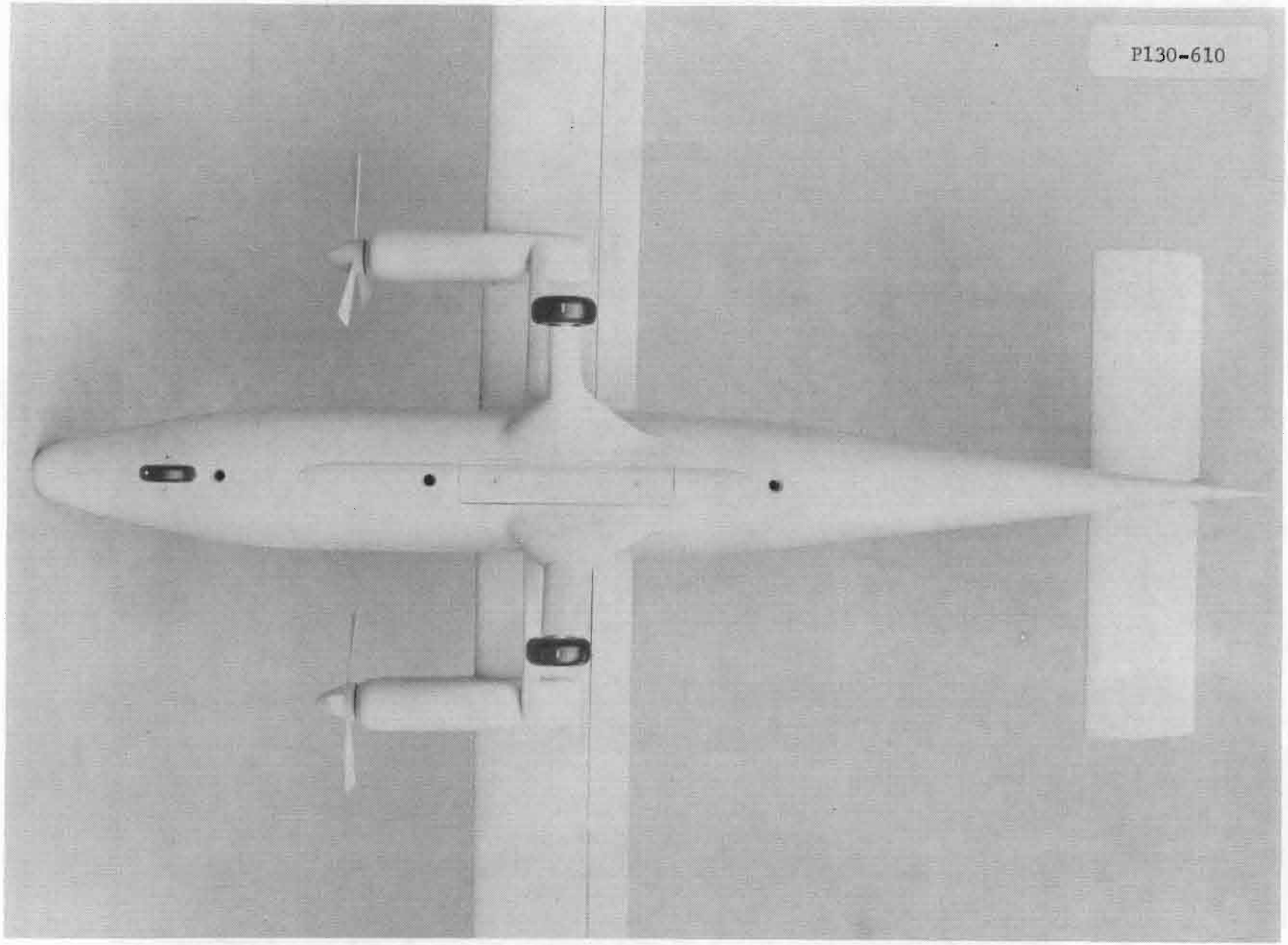

Fig. A. 6c. Twin Otter (bottom view).

Fig. A. 7a. Beech B-99 (3/4 view).

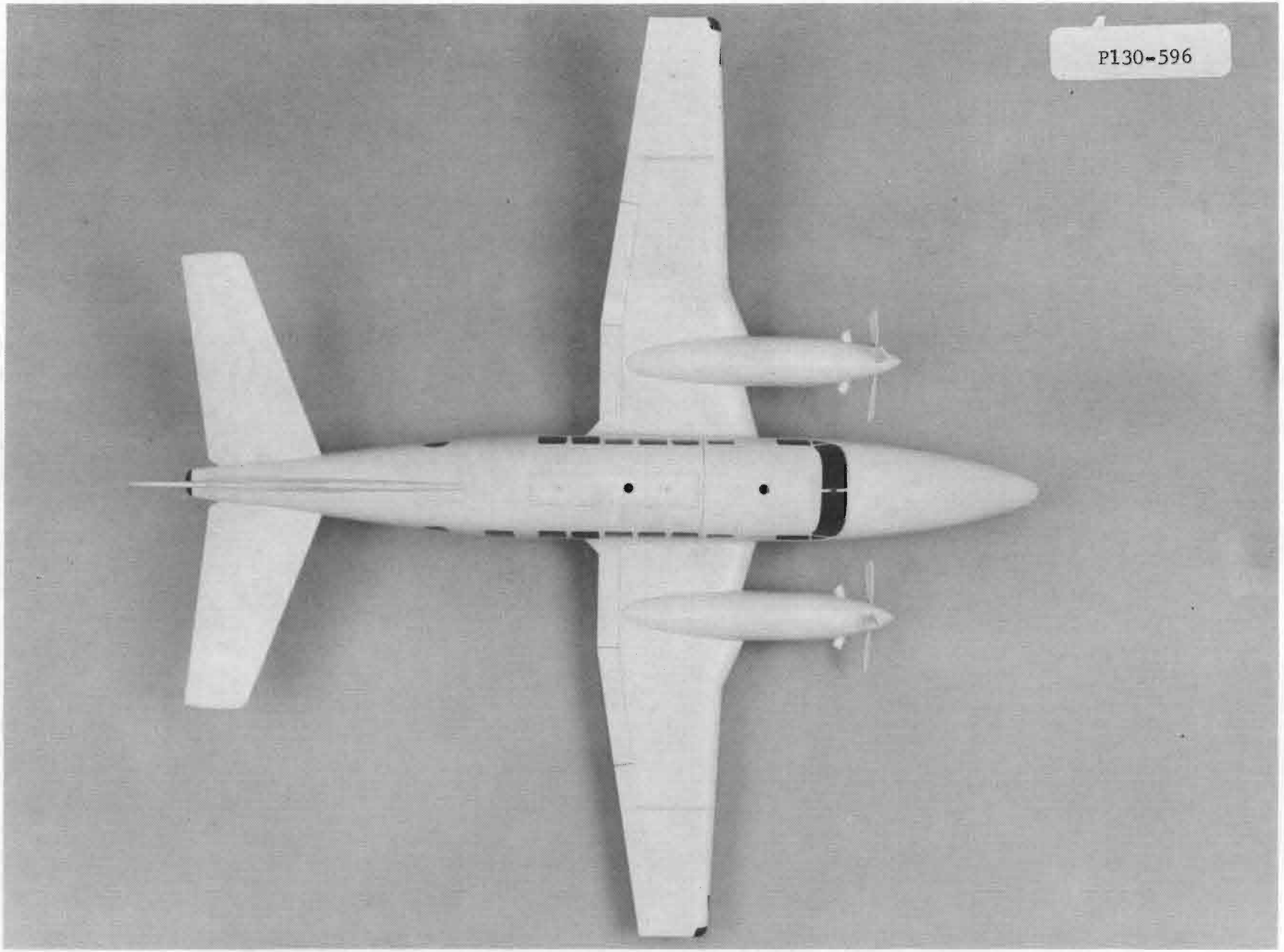

Fig. A. 7b. Beech B-99 (top view).

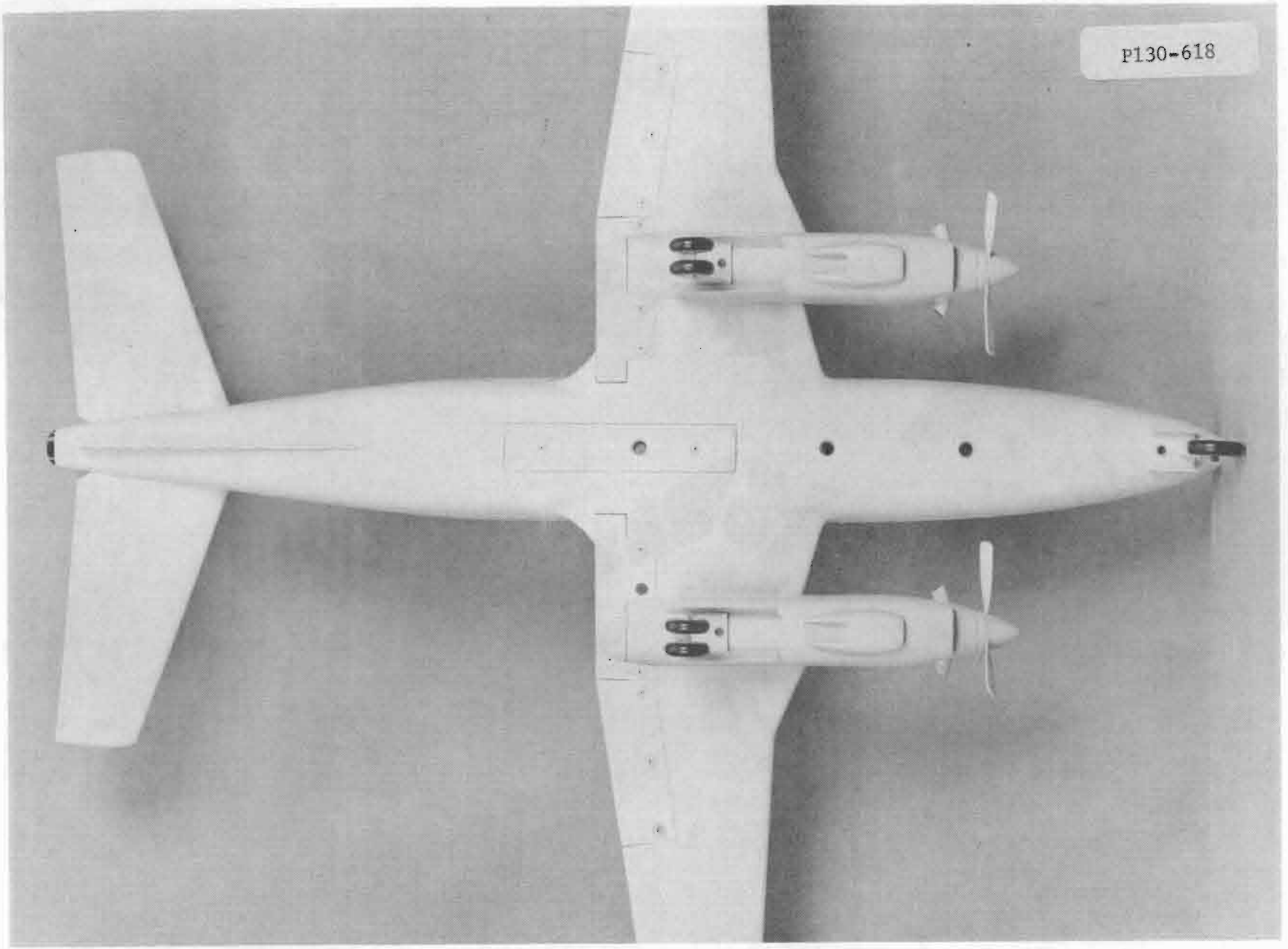

Fig. A. 7c. Beech B-99 (bottom view).

Fig. A. 8a. Beech Baron (3/4 view).

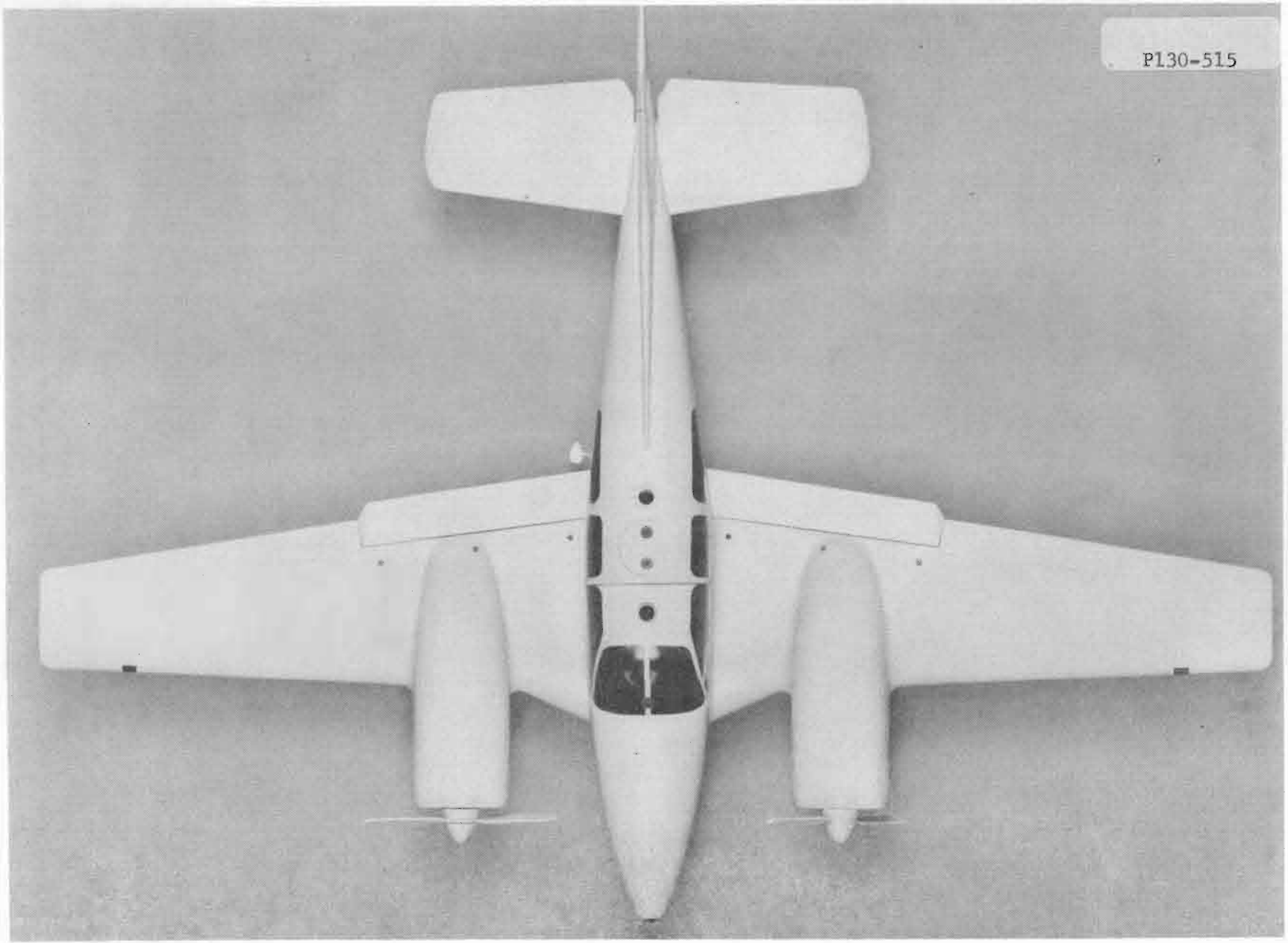

Fig. A. 8b. Beech Baron (top view).

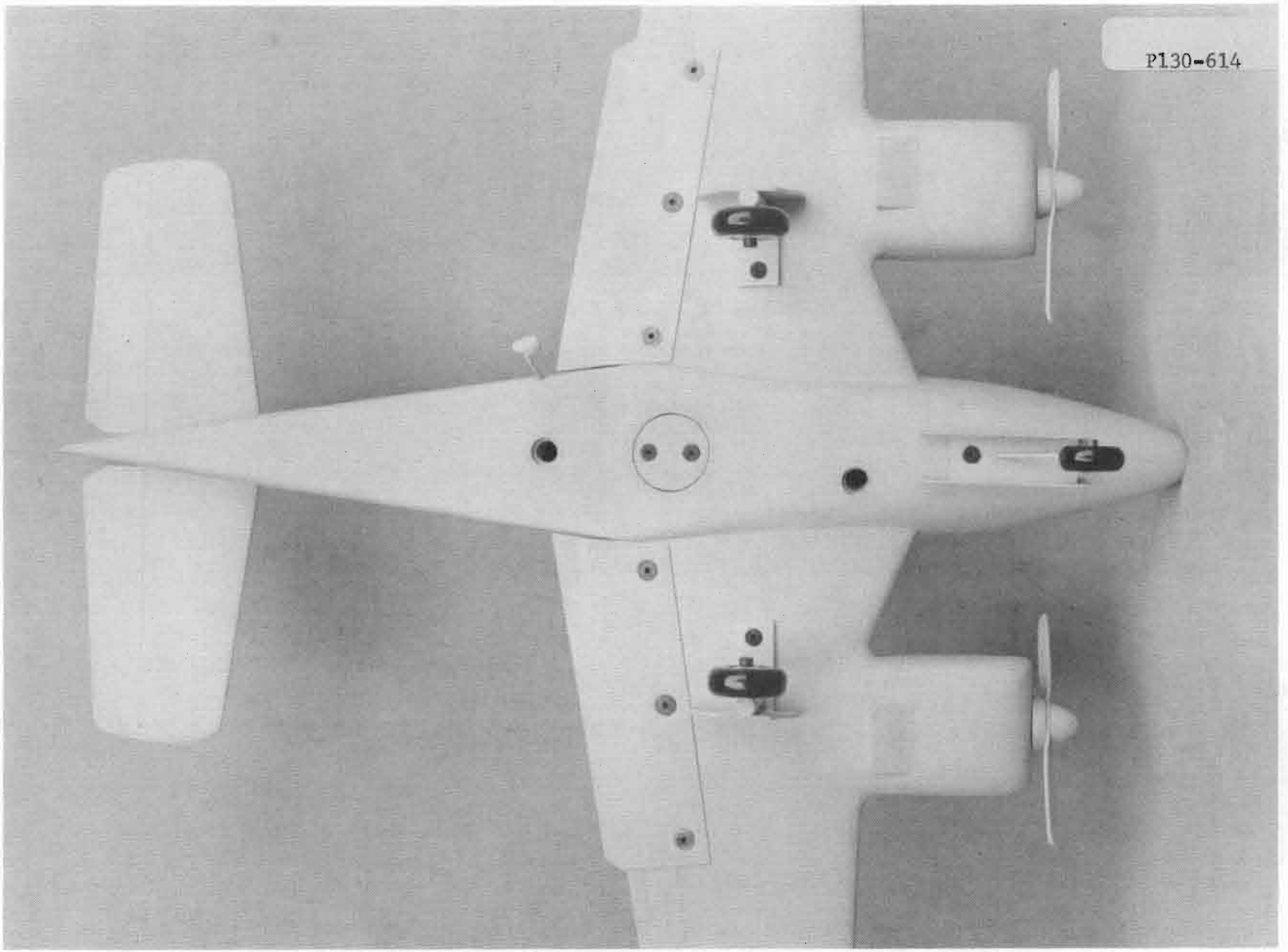

Fig. A. 8c. Beech Baron (bottom view).

Fig. A. 9a. Cessna H52 B (3/4 view).

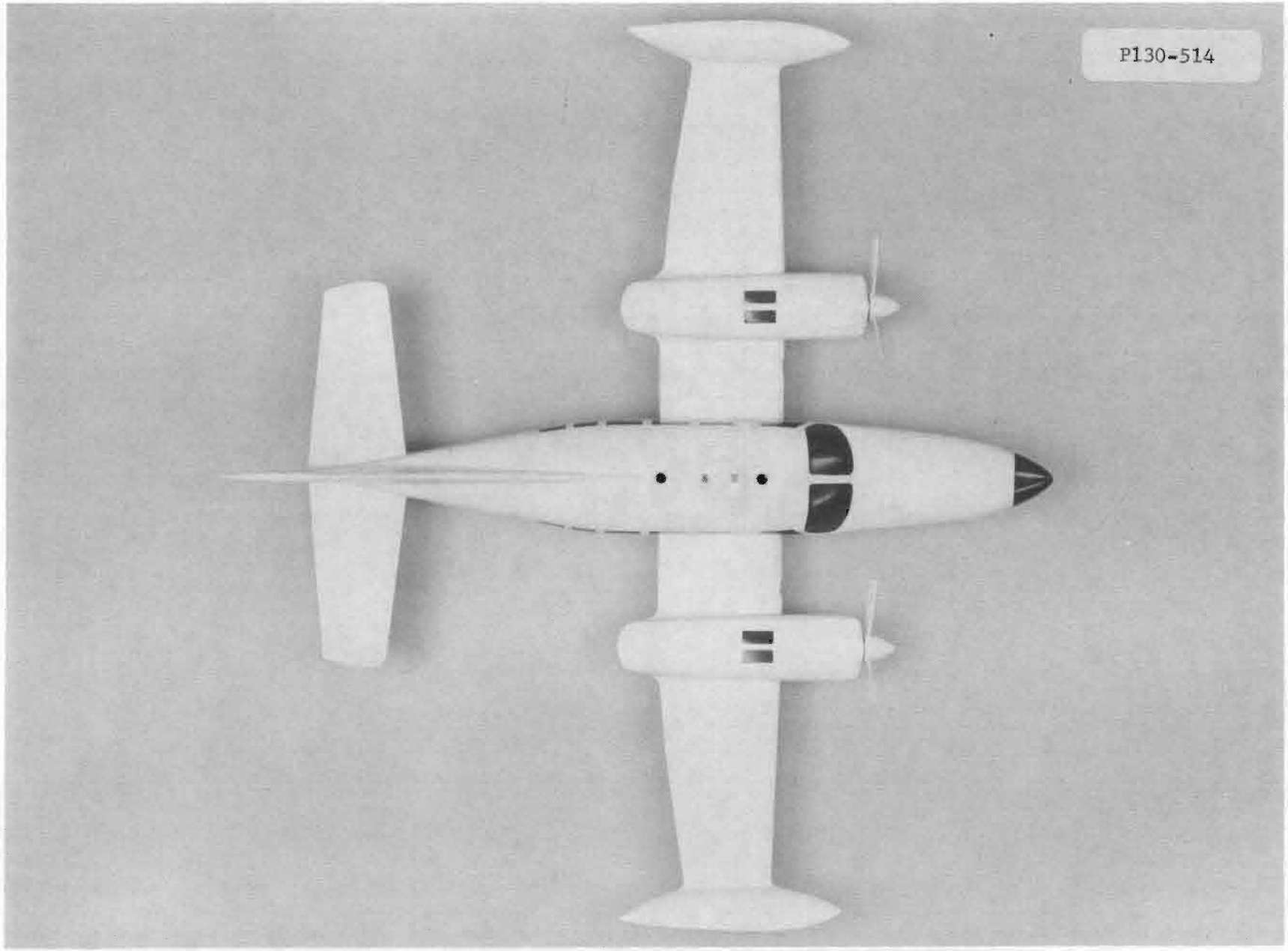

Fig. A.9b. Cessna H52 B (top view).

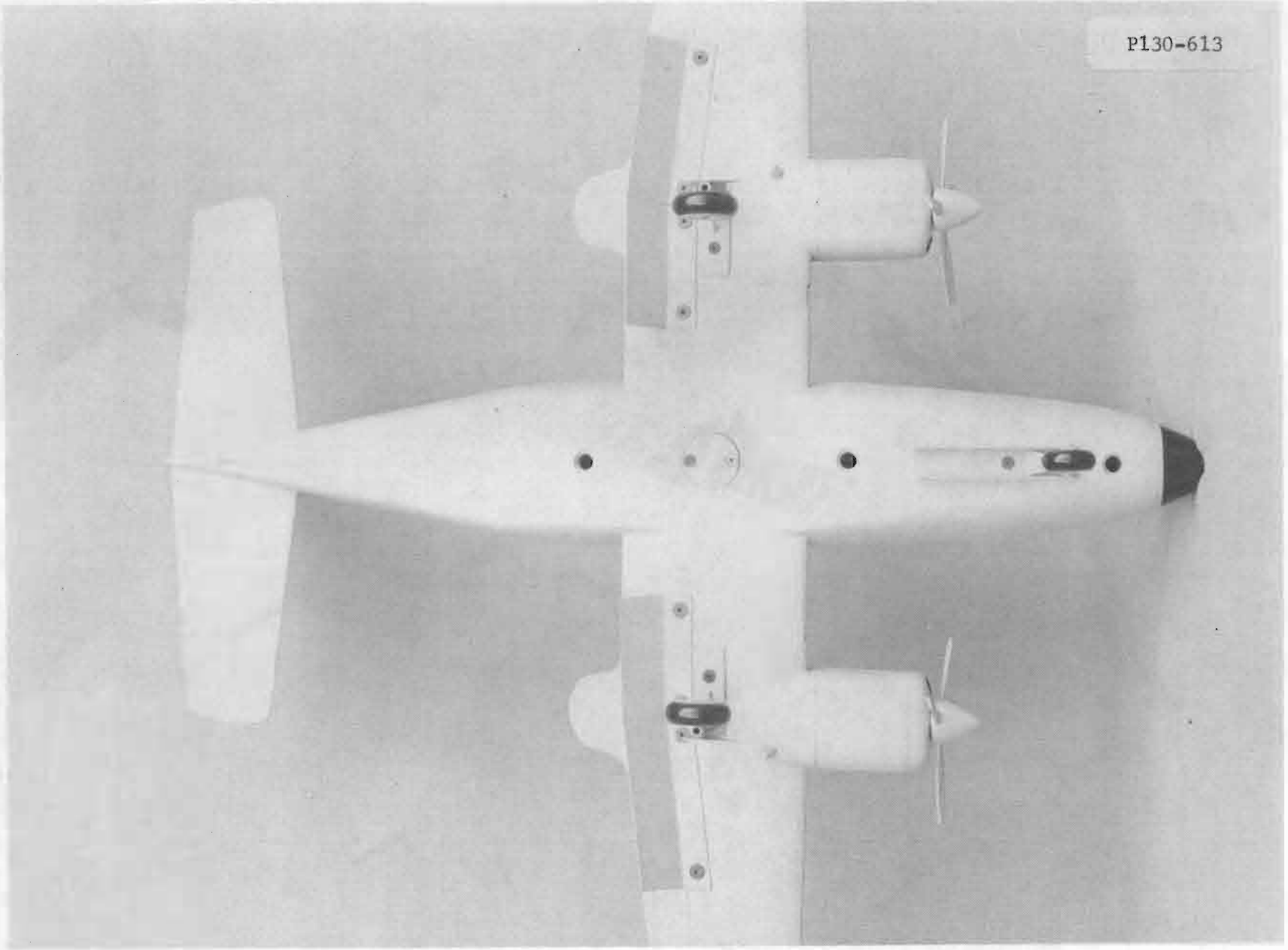

Fig. A.9c. Cessna H52 B (bottom view).

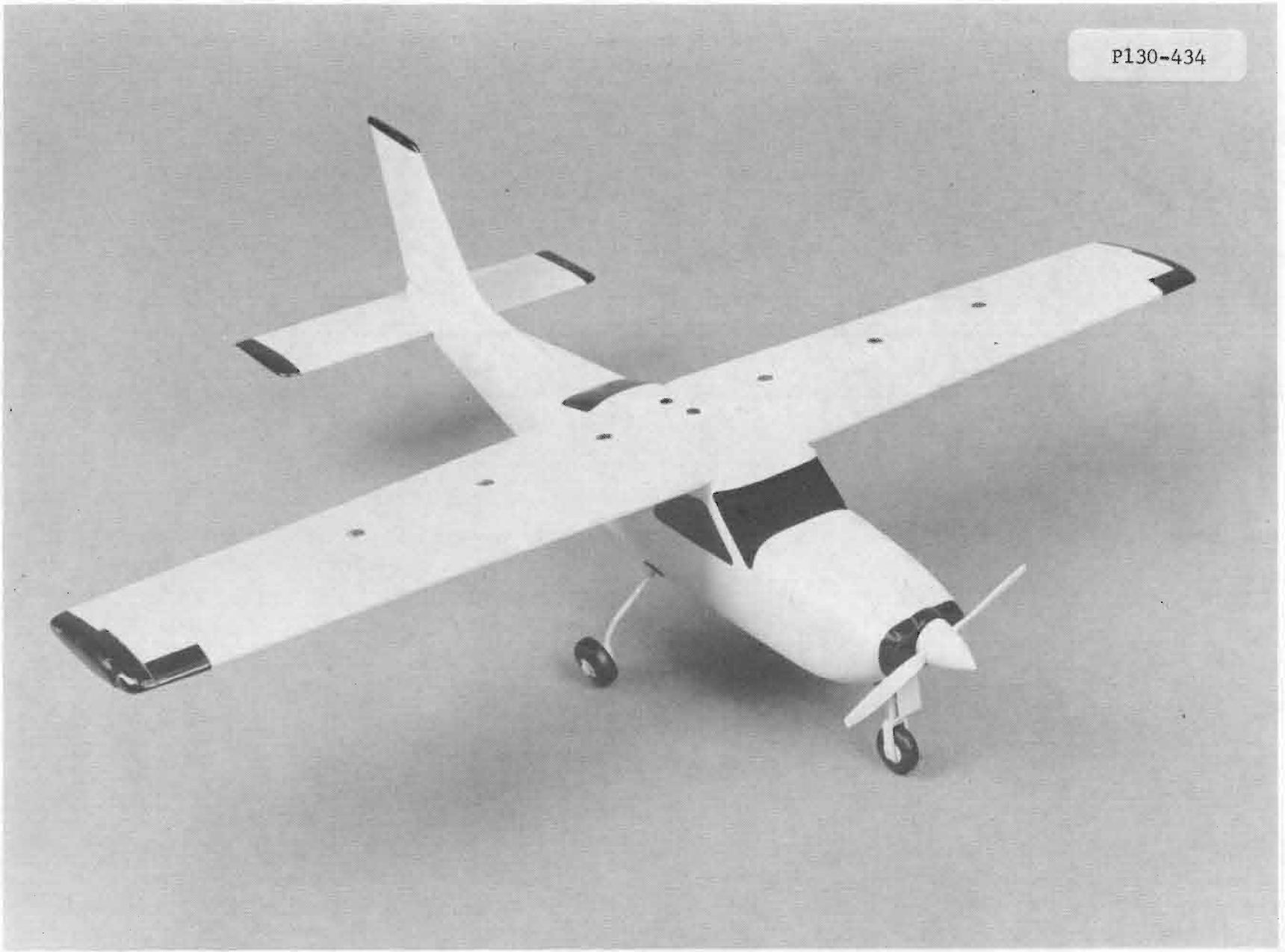

Fig. A.10a. Cessna Cardinal (3/4 view).

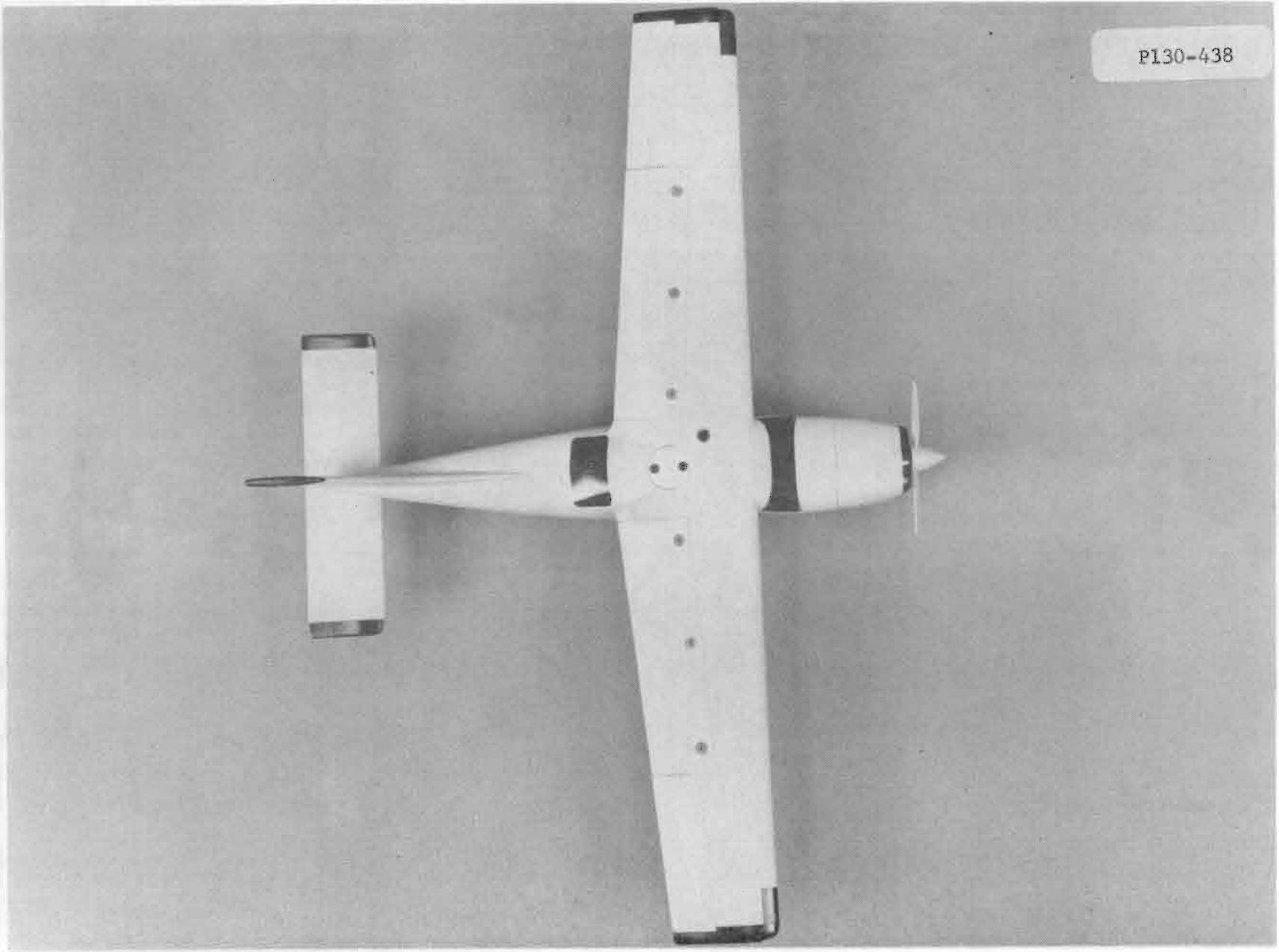

Fig. A.10b. Cessna Cardinal (top view).

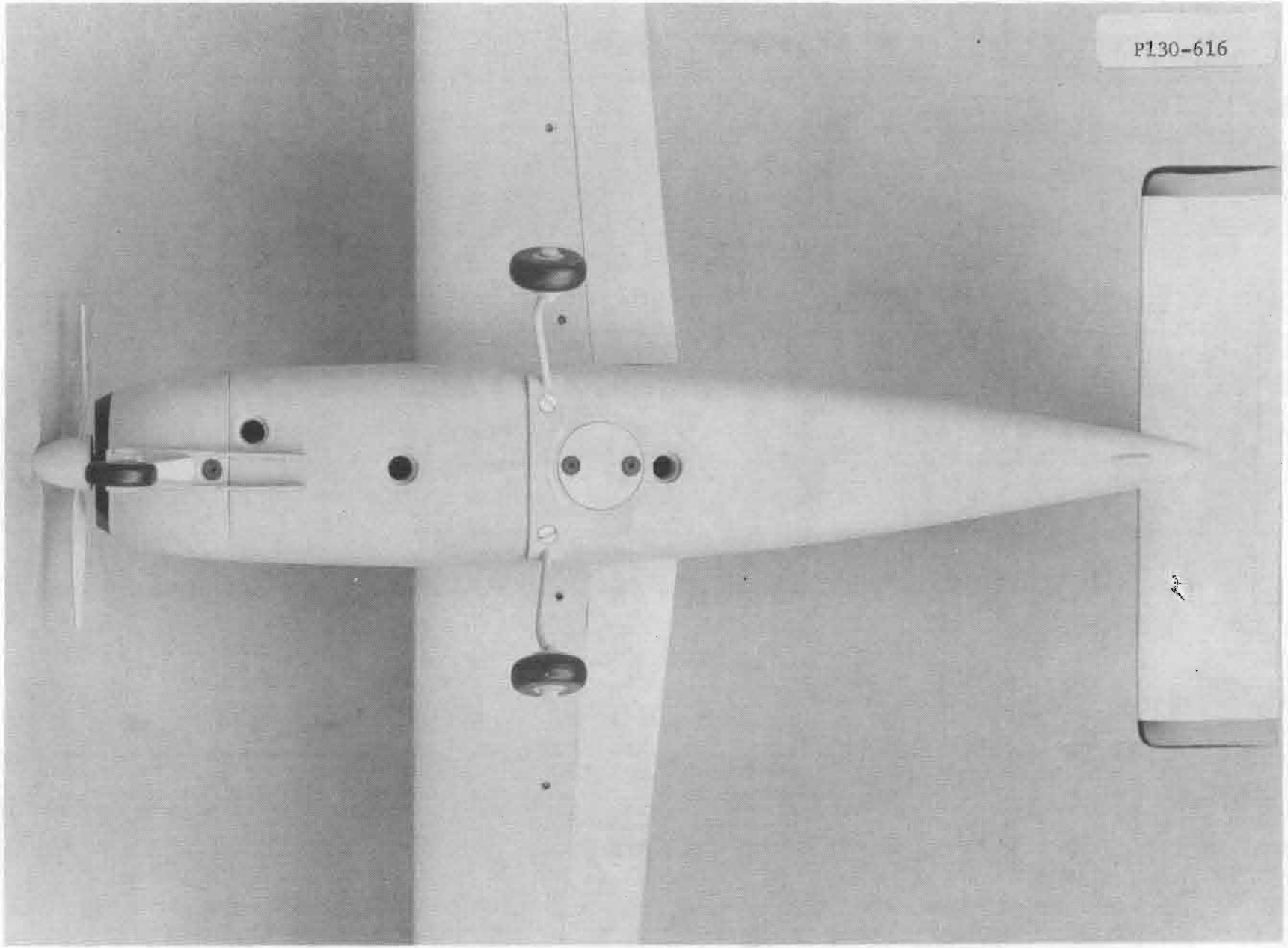

Fig. A.10c. Cessna Cardinal (bottom view).

Fig. A.11a. Shrike Commander (3/4 view).

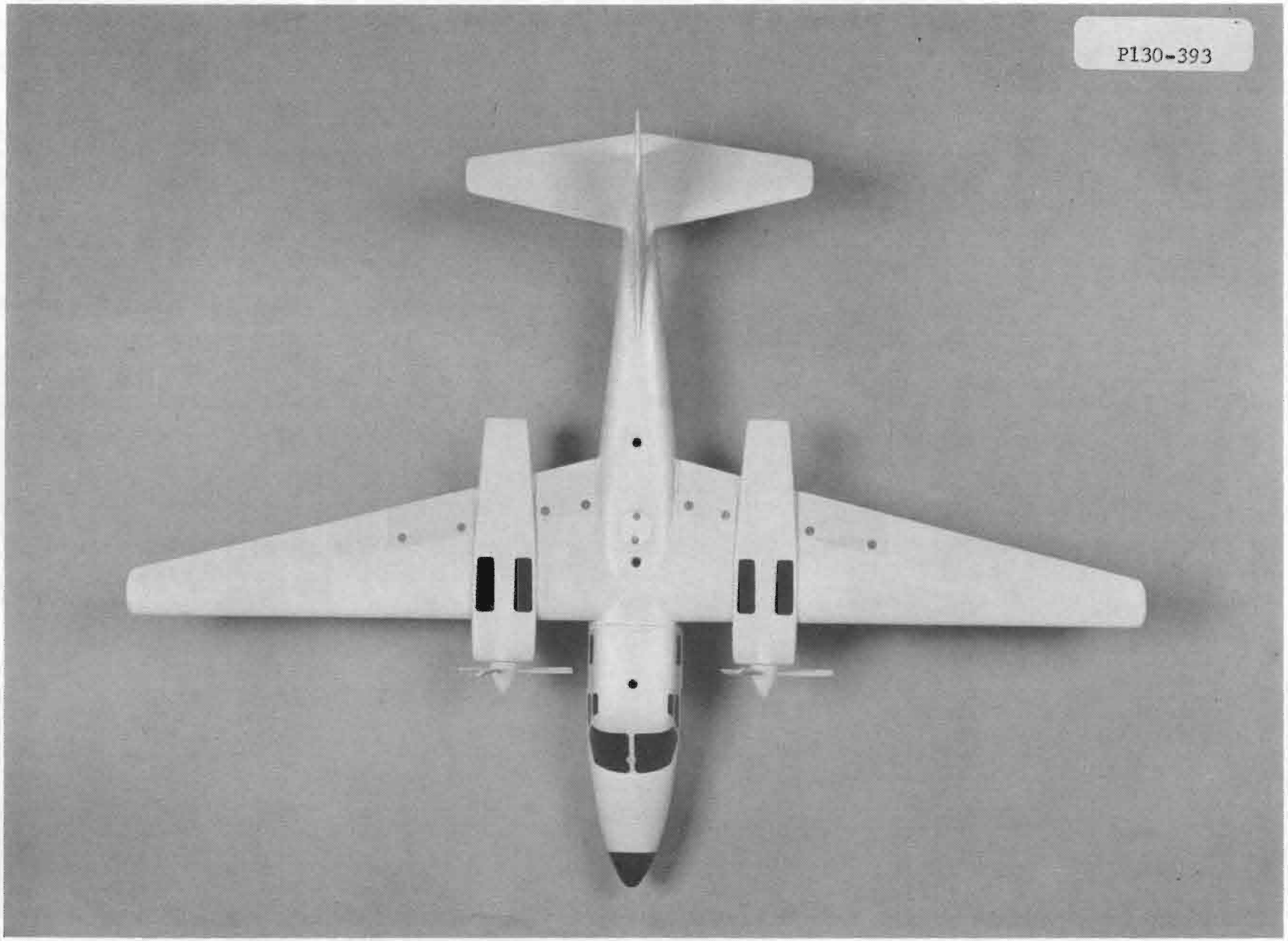

Fig. A. 11b. Shrike Commander (top view).

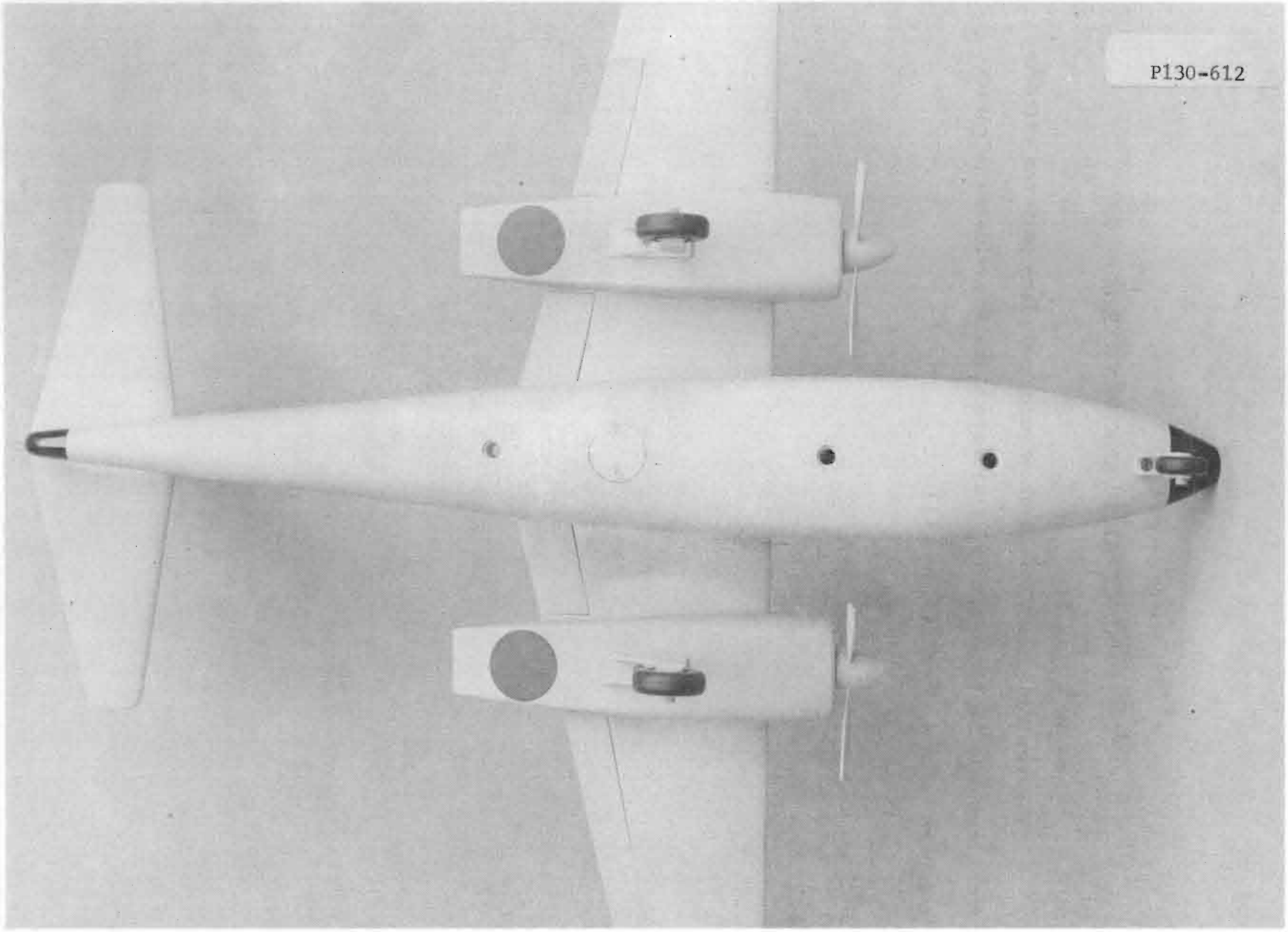

Fig. A.11c. Shrike Commander (bottom view).

APPENDIX B

PRINCIPAL PLANE PATTERNS

Figures B.1-1 to B.11-11 show principal plane patterns extracted from tape data for those aircraft that were actually evaluated (aircraft numbers 1, 2, 4, 7, 8, 10, and 11).

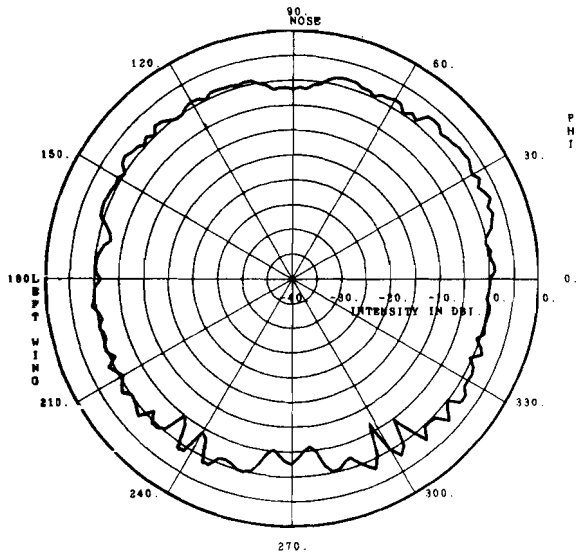

(a) horizontal plane

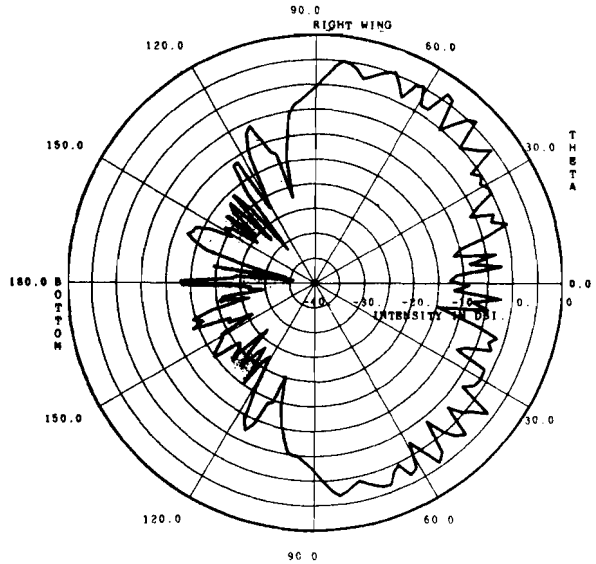

(b) wing to wing

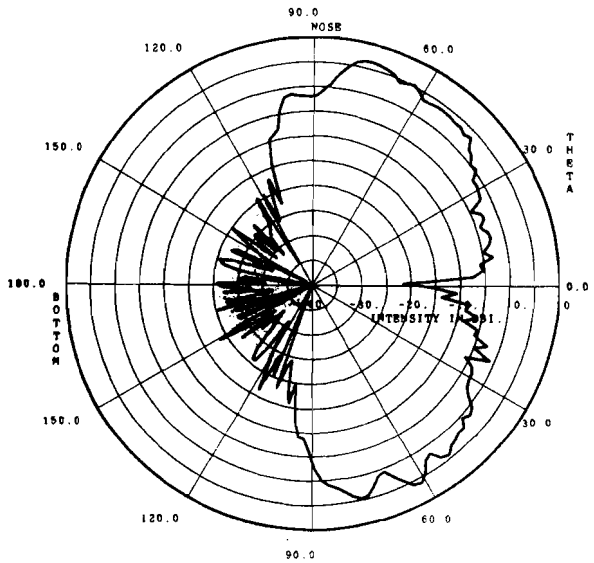

(c) nose to tail

ATC-47(B.1-1)

Fig. B.1-1. Lear jet, top-mounted rear, flaps up, wheels down

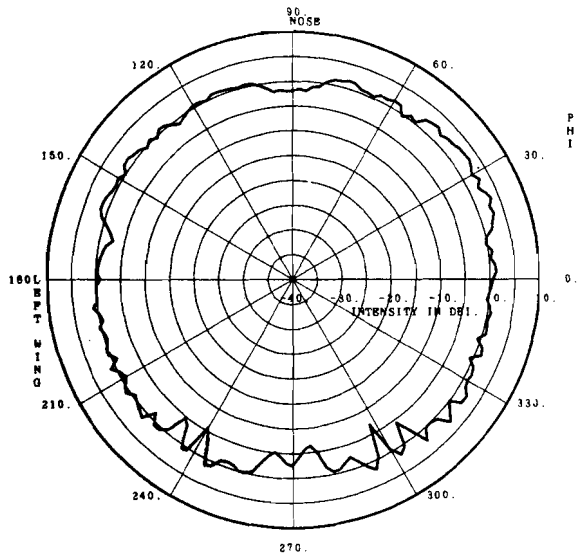

(a) horizontal plane

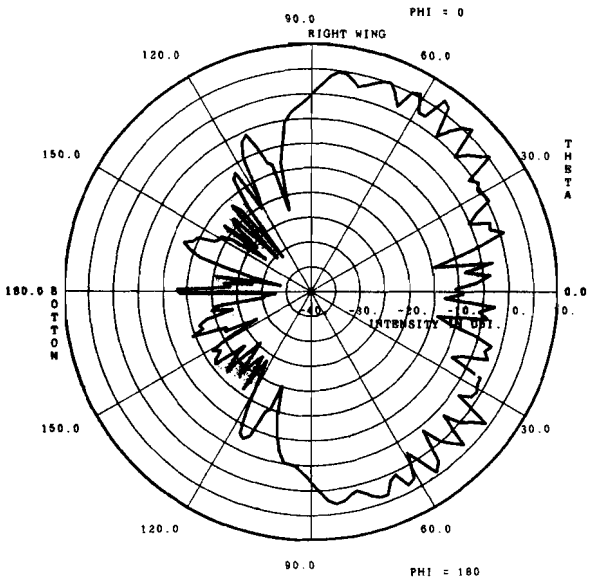

(b) wing to wing

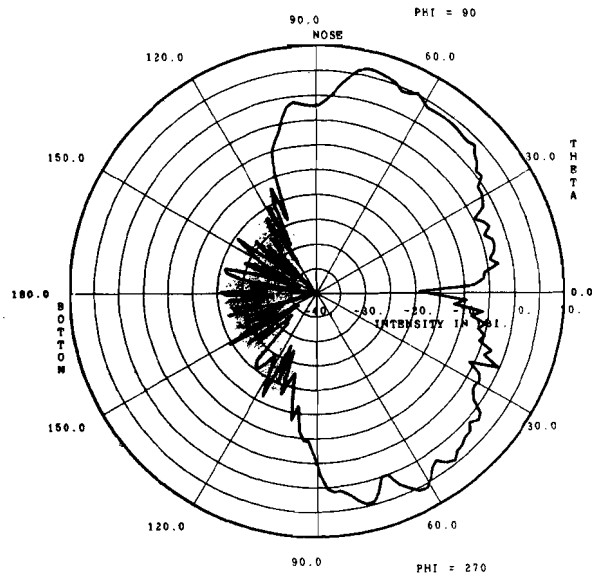

(c) nose to tail

ATC-47(B.1-2)

Fig. B.1-2. Lear jet, top-mounted rear, flaps down, wheels down

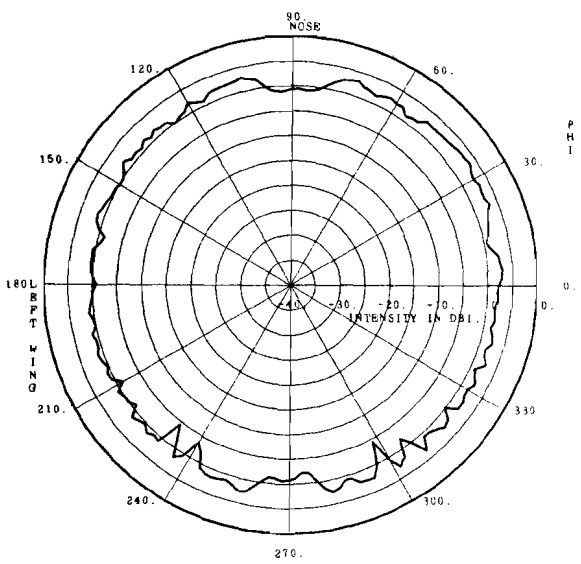

(a) horizontal plane

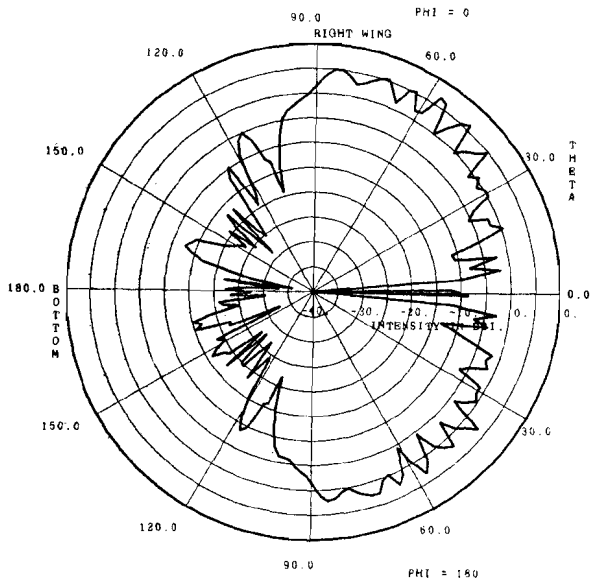

(b) wing to wing

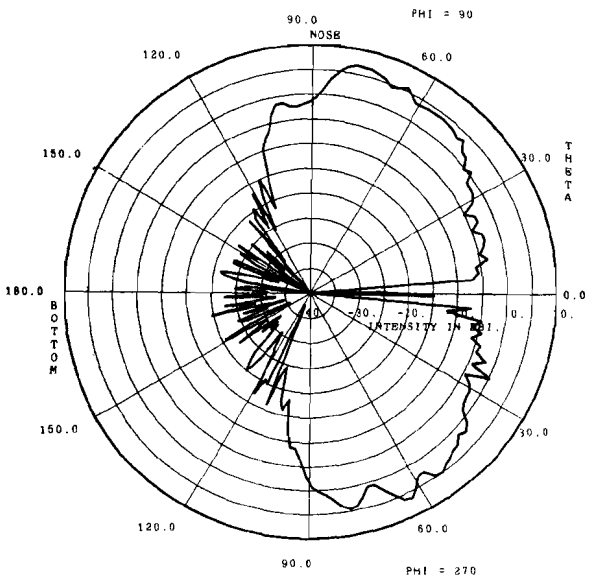

(c) nose to tail

ATC-47(B.1-3)

Fig. B.1-3. Lear jet, top-mounted rear, flaps up, wheels up

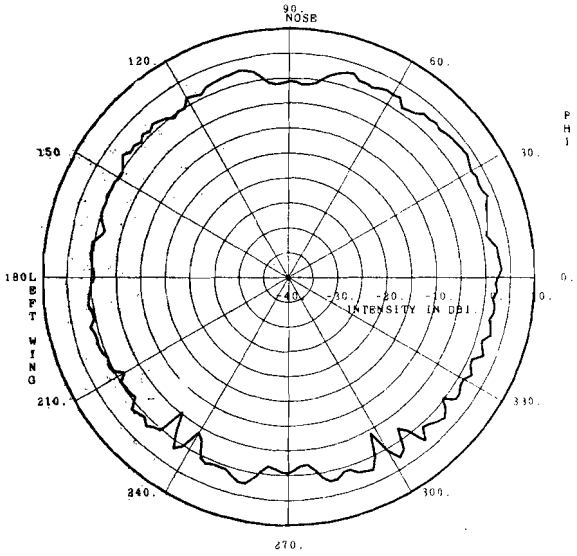

(a) horizontal plane

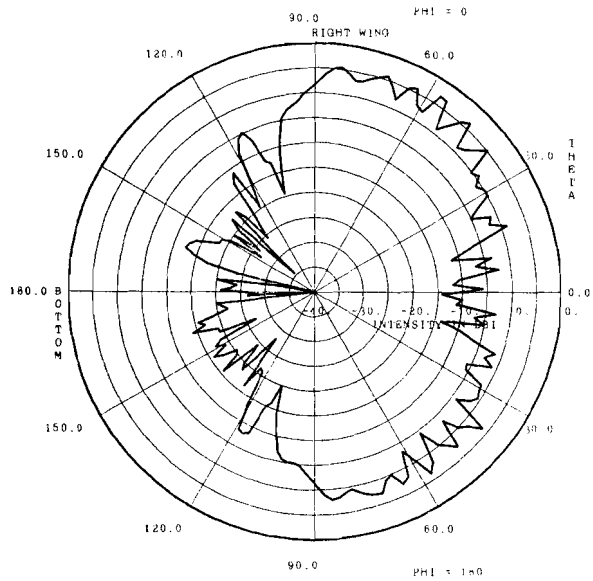

(b) wing to wing

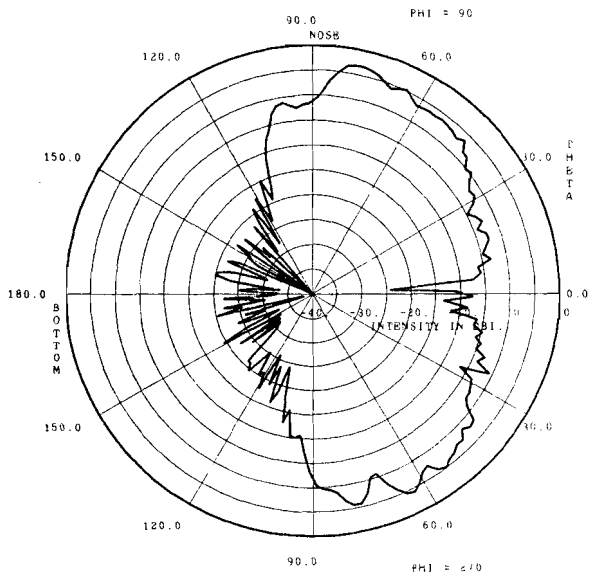

(c) nose to tail

ATC-47(B.1-4)

Fig. B.1-4. Lear jet, top-mounted rear, flaps down, wheels up

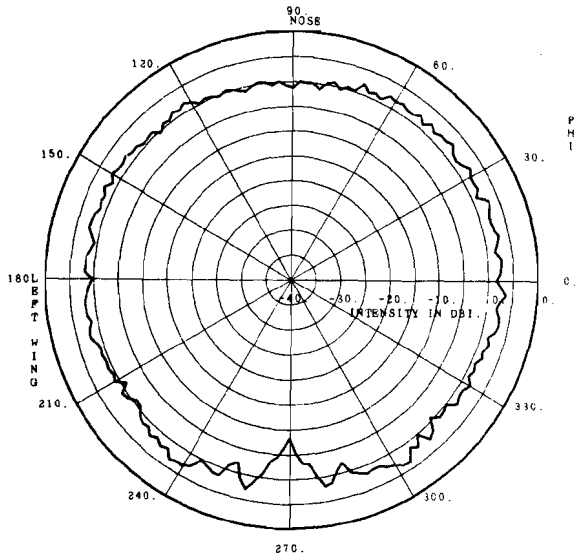

(a) horizontal plane

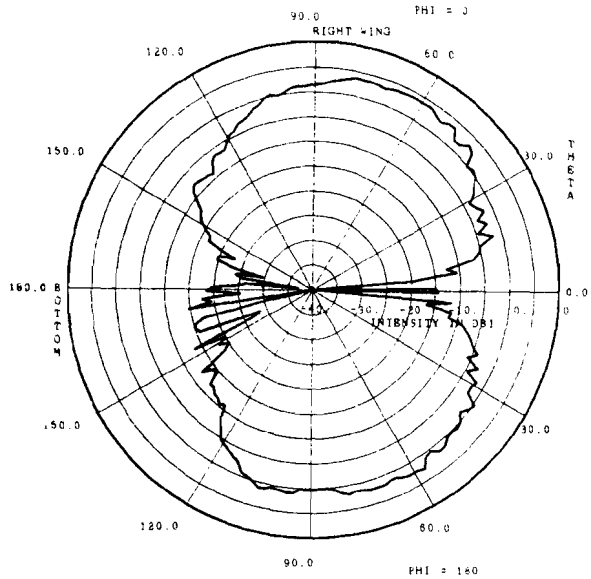

(b) wing to wing

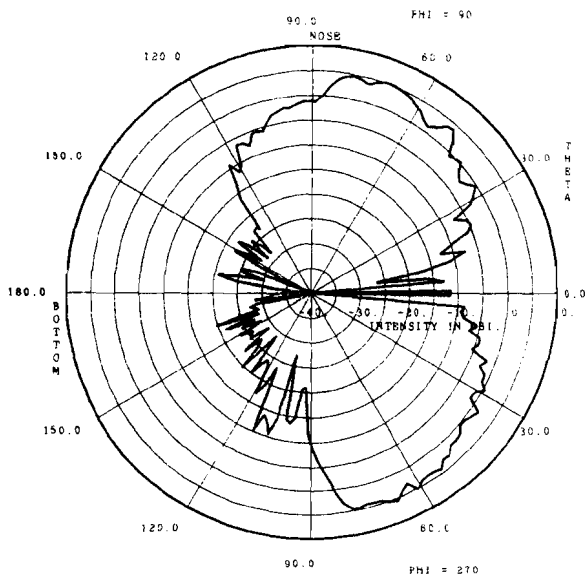

(c) nose to tail

ATC-47(B.1-5)

Fig. B.1-5. Lear jet, top-mounted front, flaps up, wheels down

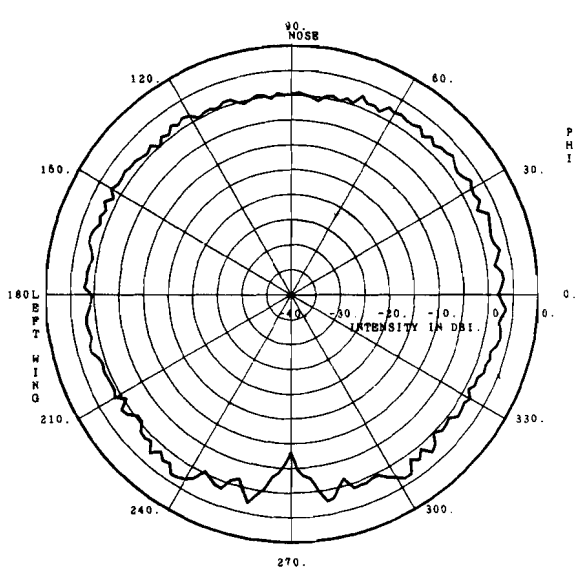

(a) horizontal plane

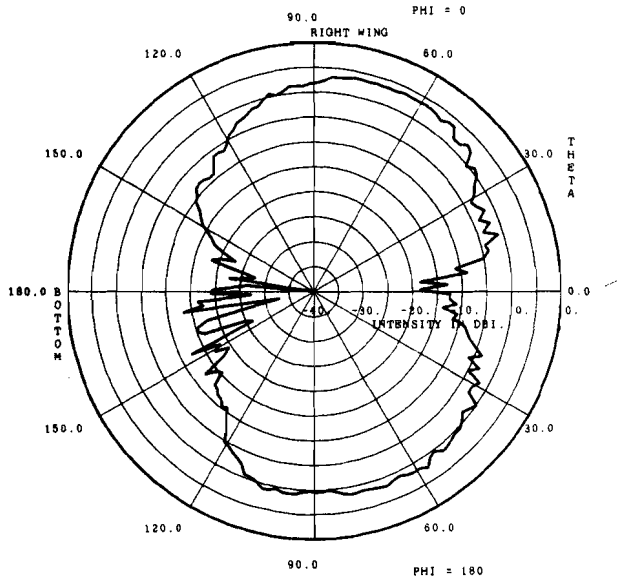

(b) wing to wing

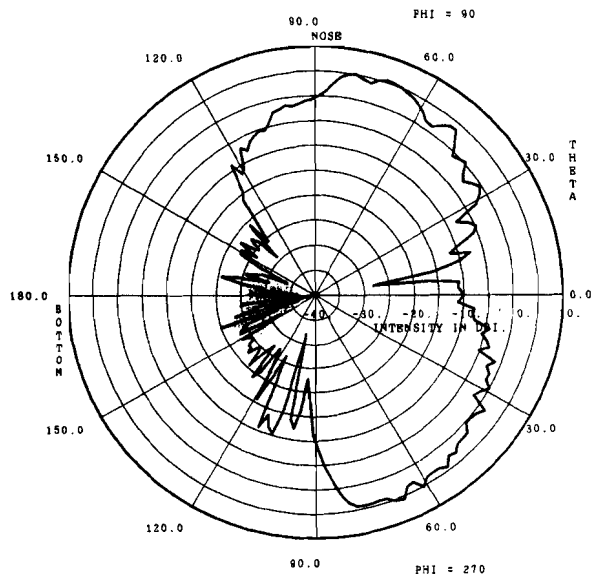

(c) nose to tail

ATC-47(B.1-6)

Fig. B.1-6. Lear jet top-mounted front, flaps down, wheels down

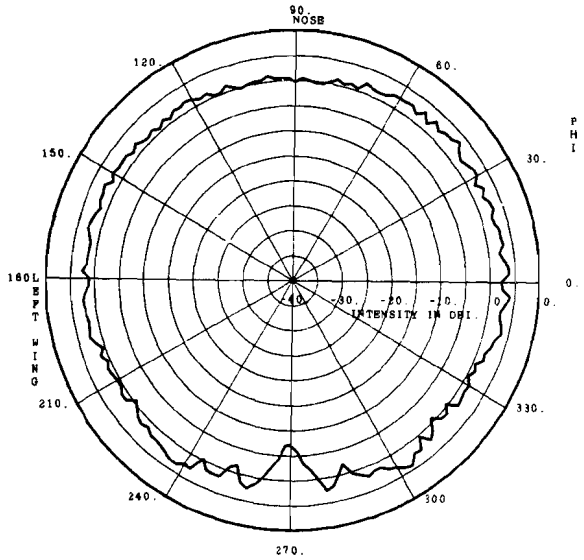

(a) horizontal plane

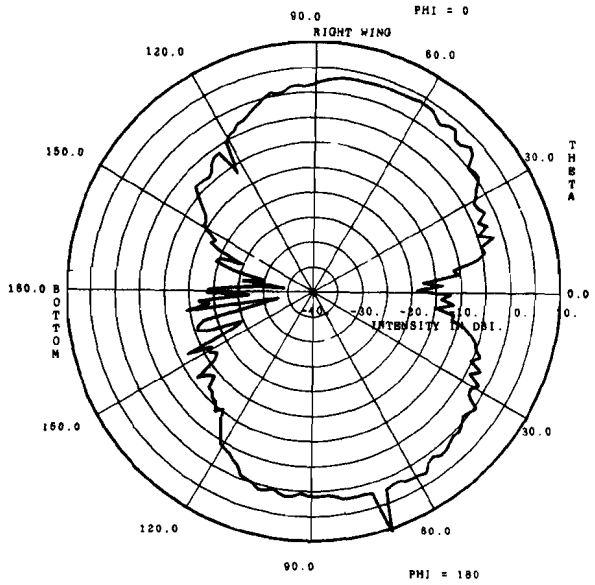

(b) wing to wing

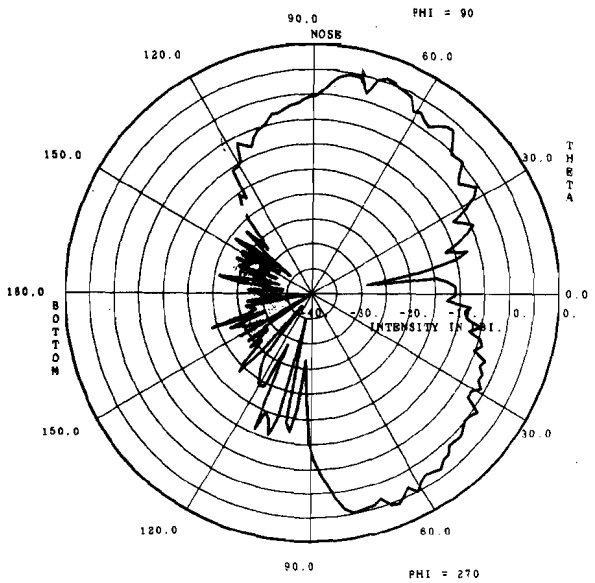

(c) nose to tail

ATC-47(B.1-7)

Fig. B. 1-7. Lear jet top-mounted front, flaps up, wheels down

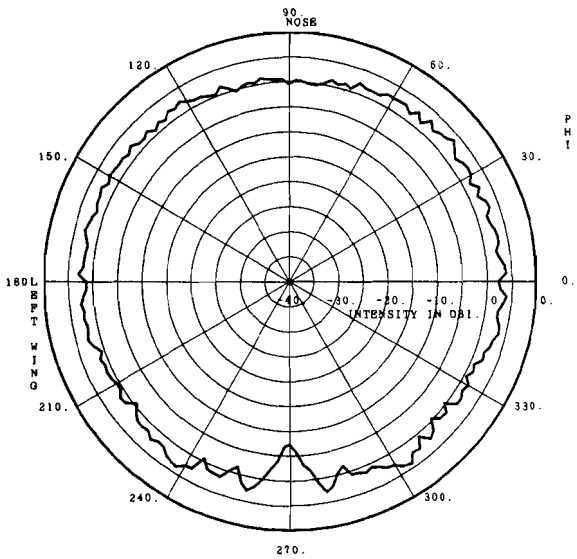

(a) horizontal plane

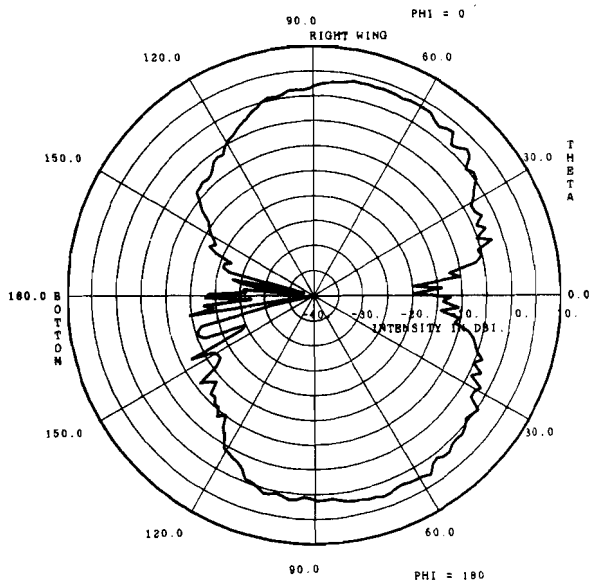

(b) wing to wing

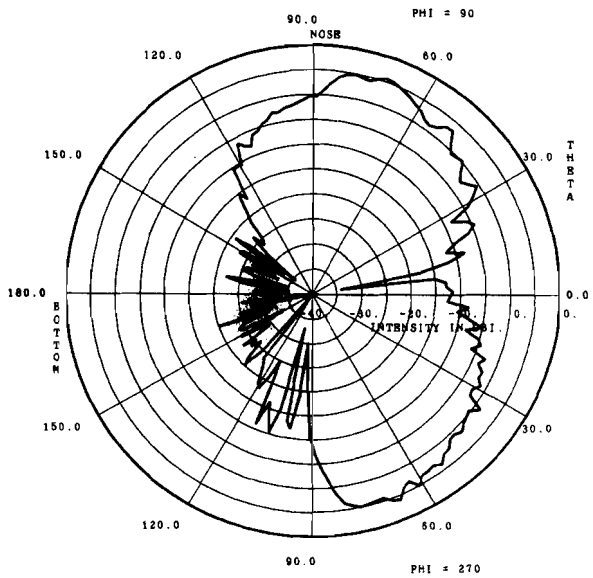

(c) nose to tail

ATC-47(B.1-8)

Fig. B.1-8. Lear jet top-mounted front, flaps down, wheels up

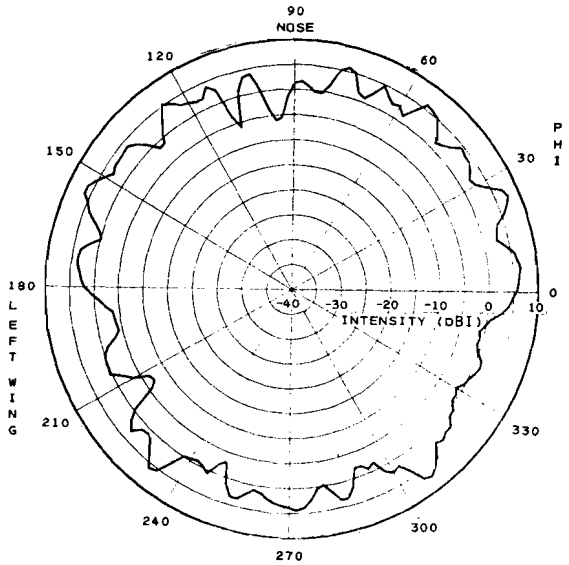

(a) horizontal plane

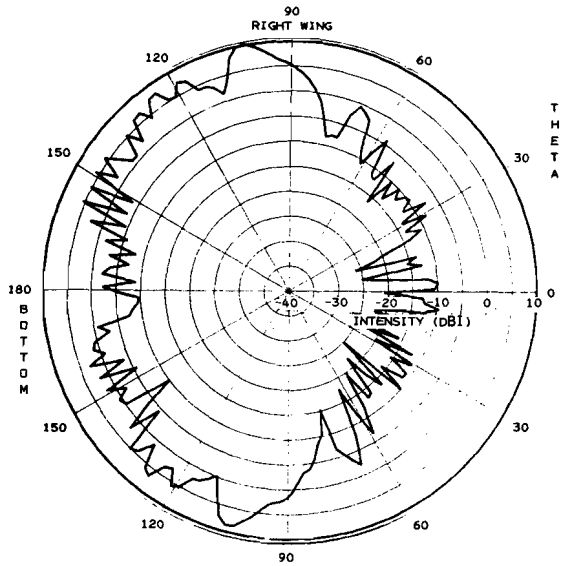

(b) wing to wing

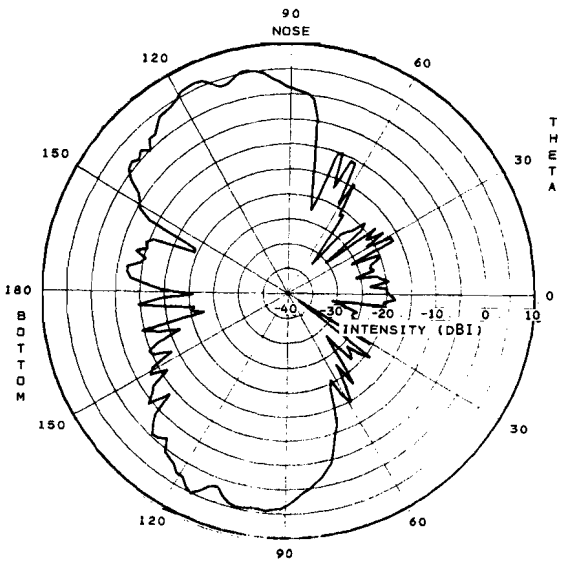

(c) nose to tail

ATC-47(B.1-9)

Fig. B.1-9. Lear jet bottom-mounted rear, flaps up, wheels down

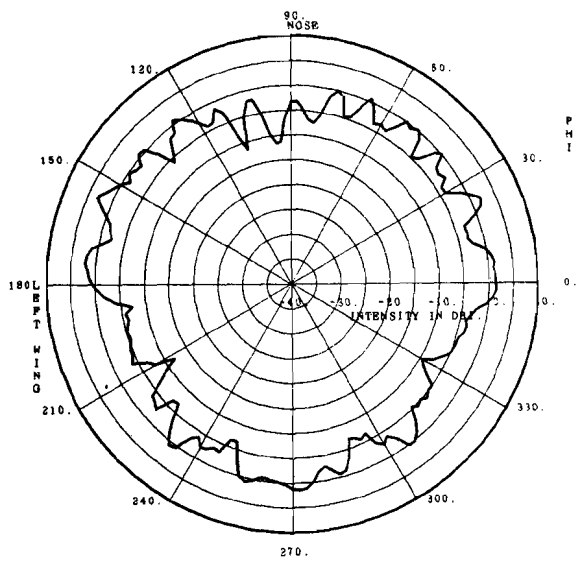

(a) horizontal plane

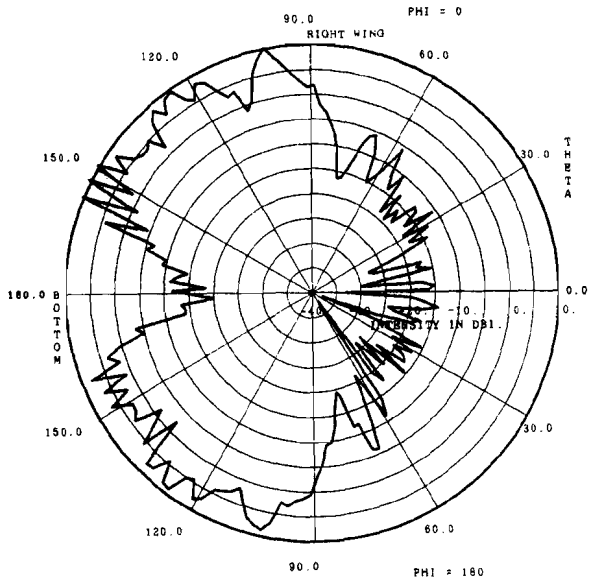

(b) wing to wing

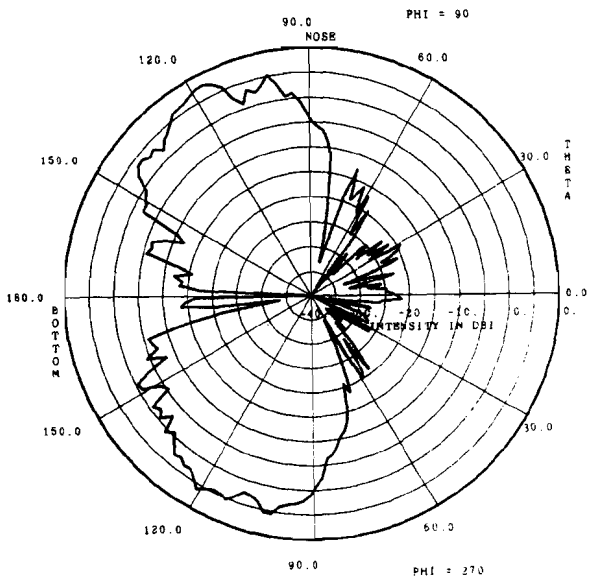

(c) nose to tail

ATC-47(B.1-10)

Fig. B.1-10. Lear jet bottom-mounted rear, flaps down, wheels down

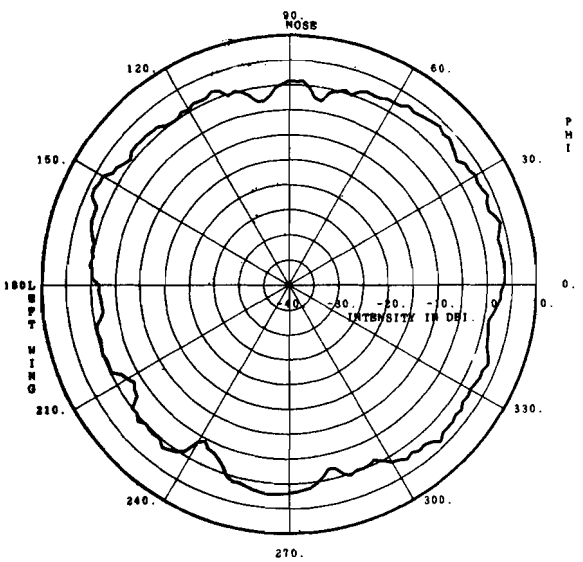

(a) horizontal plane

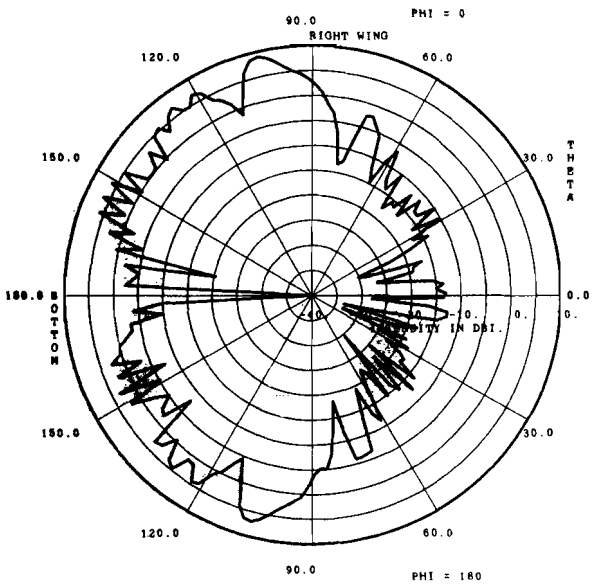

(b) wing to wing

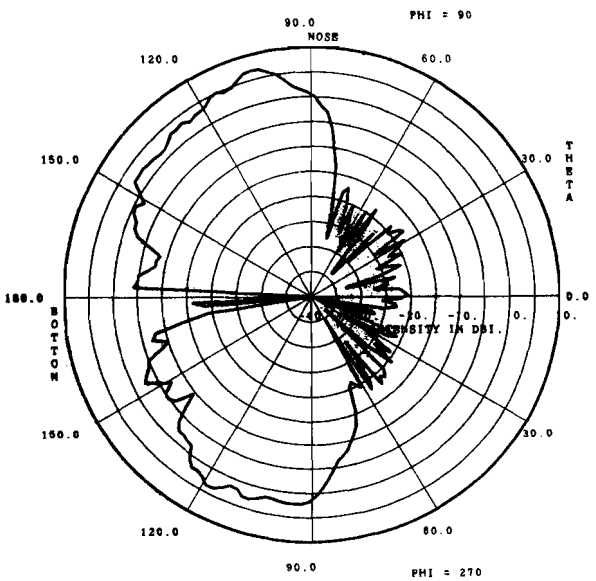

(c) nose to tail

ATC-47(B.1-11)

Fig. B.1-11. Lear jet bottom-mounted rear, flaps up, wheels up

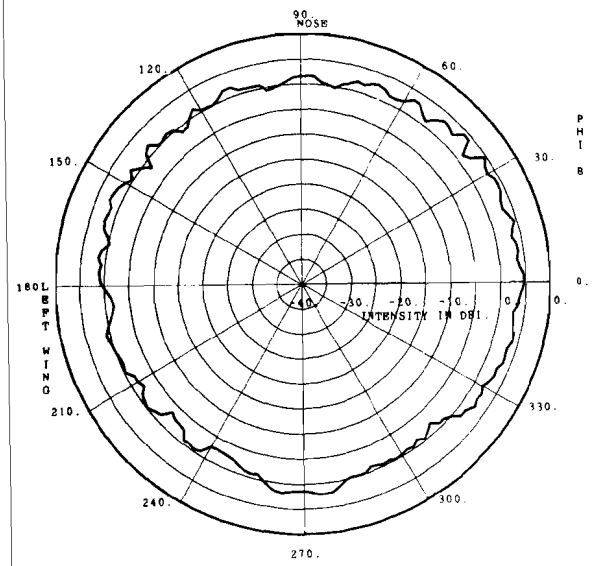

(a) horizontal plane

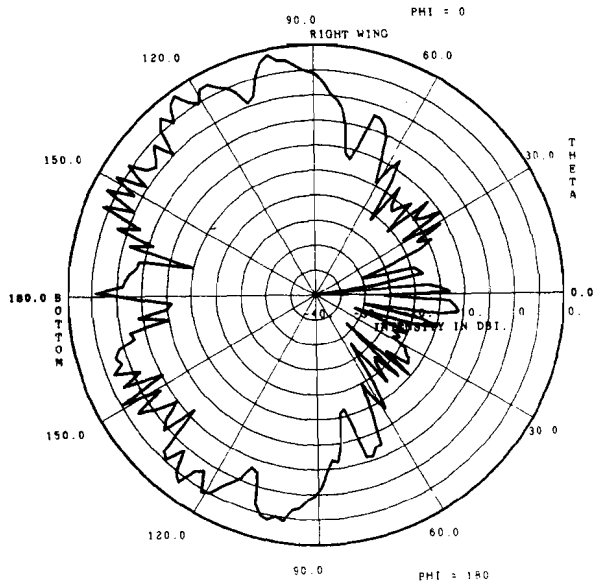

(b) wing to wing

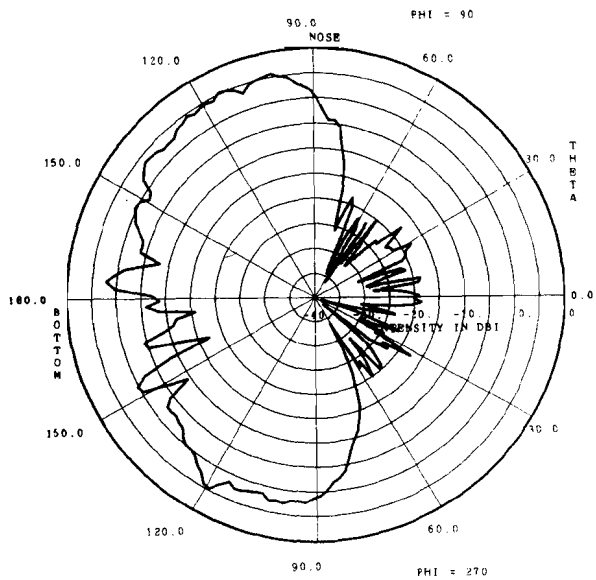

(c) nose to tail

ATC-47(B.1-12)

Fig. B.1-12. Lear jet bottom-mounted rear, flaps down, wheels up

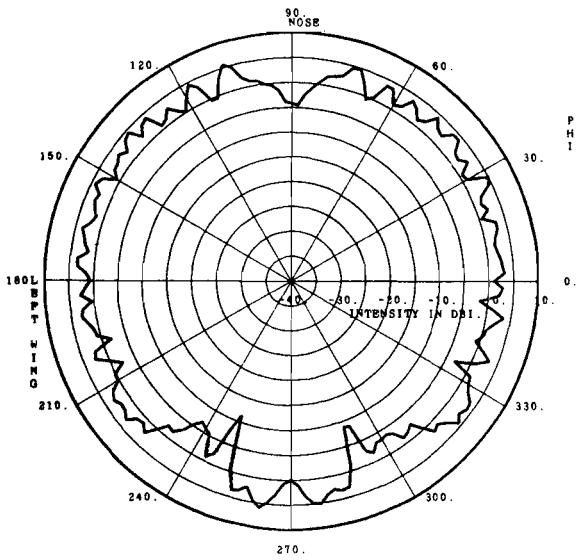

(a) horizontal plane

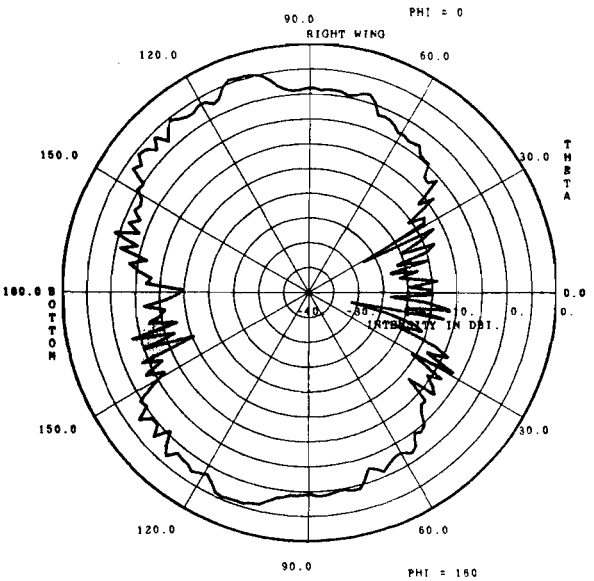

(b) wing to wing

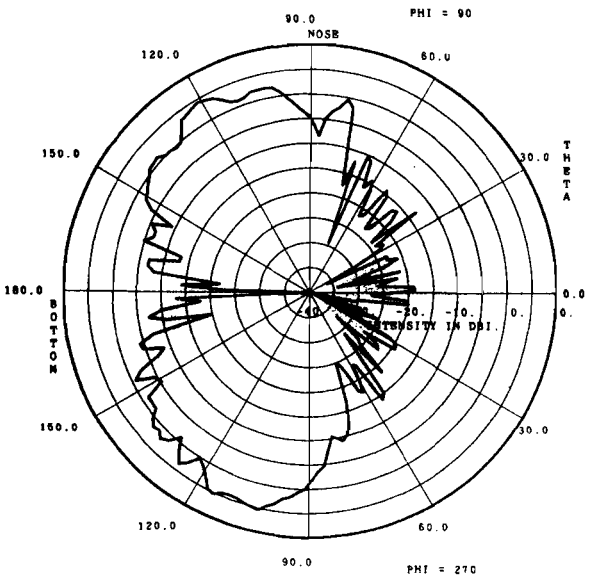

(c) nose to tail

ATC-47(B.1-13)

Fig. B.1-13. Lear jet bottom-mounted center, flaps up, wheels down

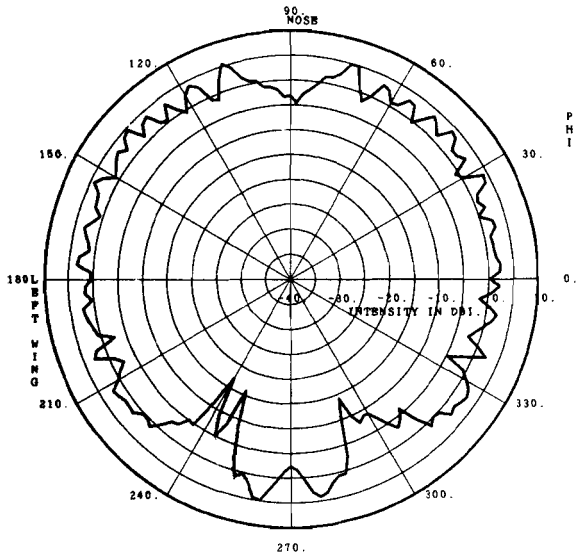

(a) horizontal plane

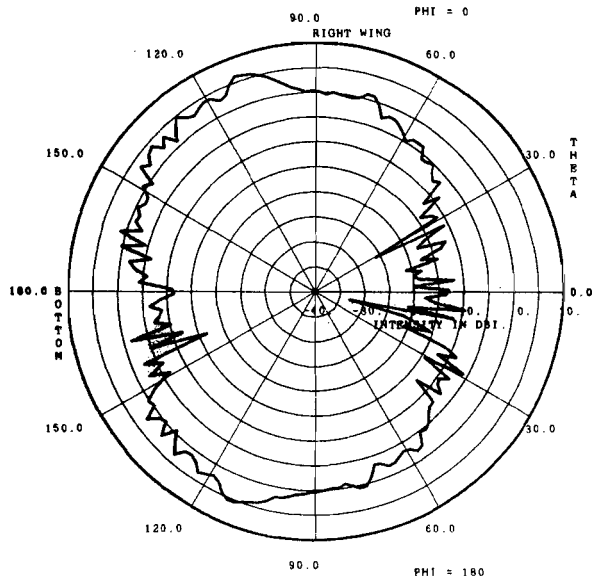

(b) wing to wing

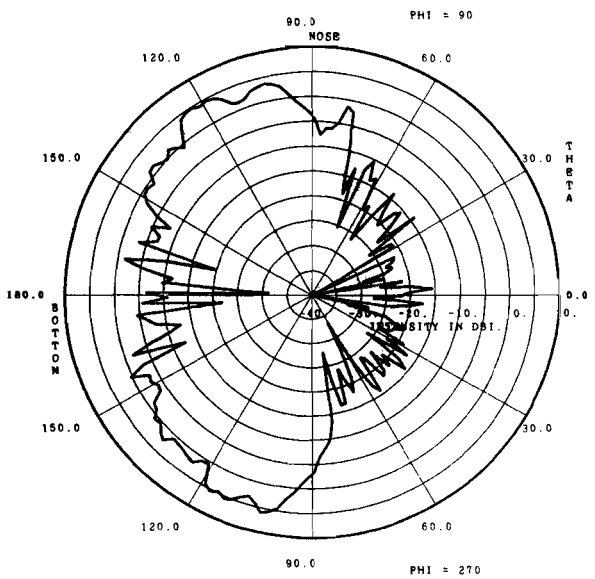

(c) nose to tail

ATC-47(B.1-14)

Fig. B.1-14. Lear jet bottom-mounted center, flaps down, wheels down

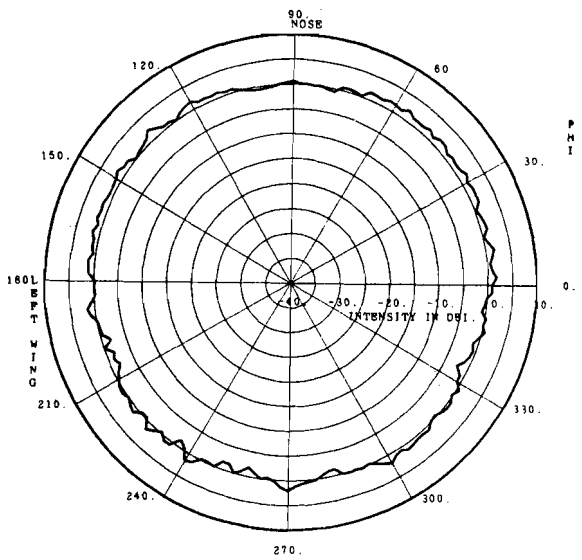

(a) horizontal plane

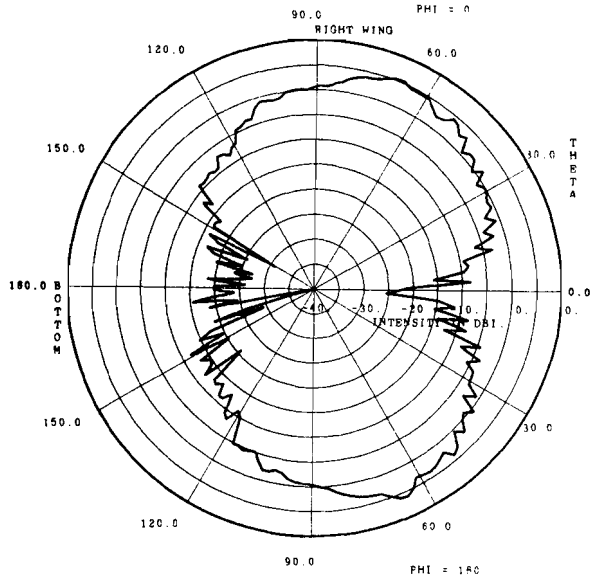

(b) wing to wing

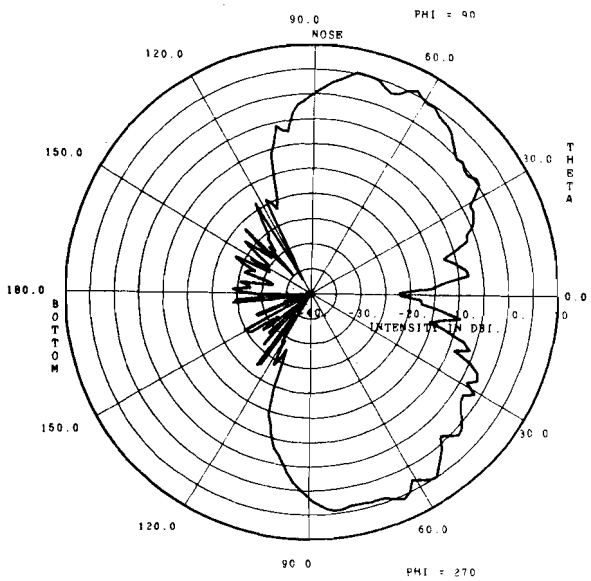

(c) nose to tail

ATC-47(B.1-15)

Fig. B.1-15. Lear jet bottom-mounted center, flaps up, wheels up

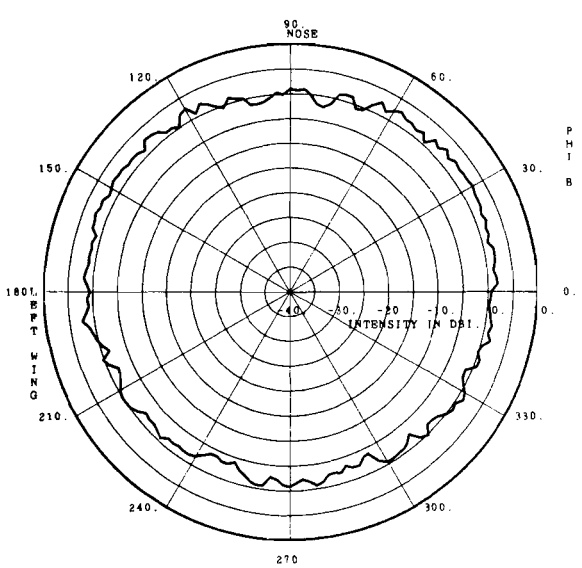

(a) horizontal plane

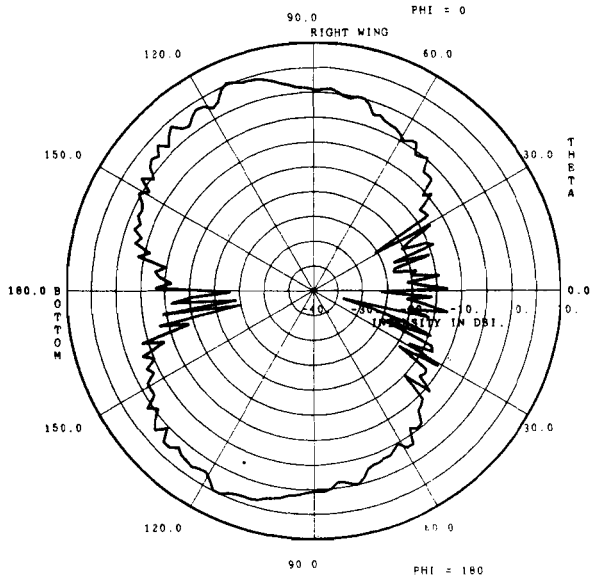

(b) wing to wing

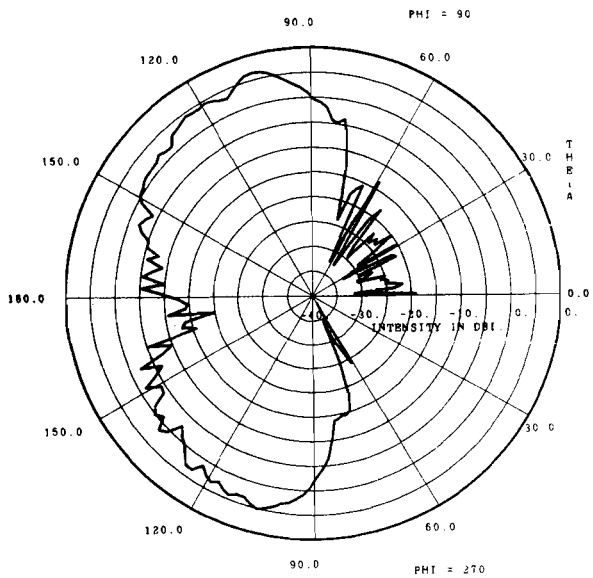

(c) nose to tail

ATC-47(B.1-16)

Fig. B.1-16. Lear jet bottom-mounted center, flaps down, wheels up

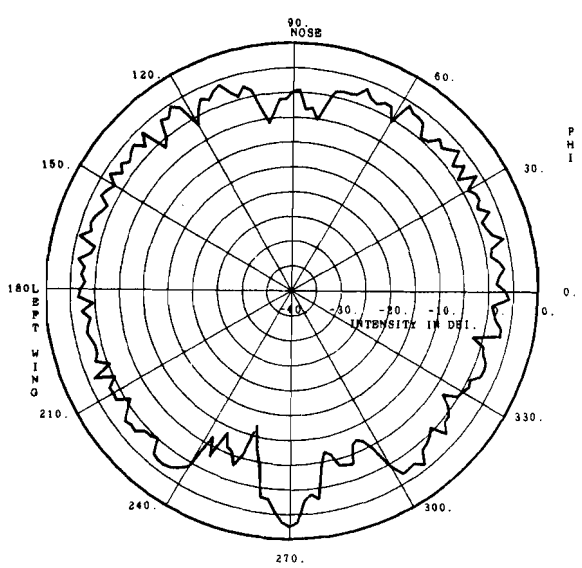

(a) horizontal plane

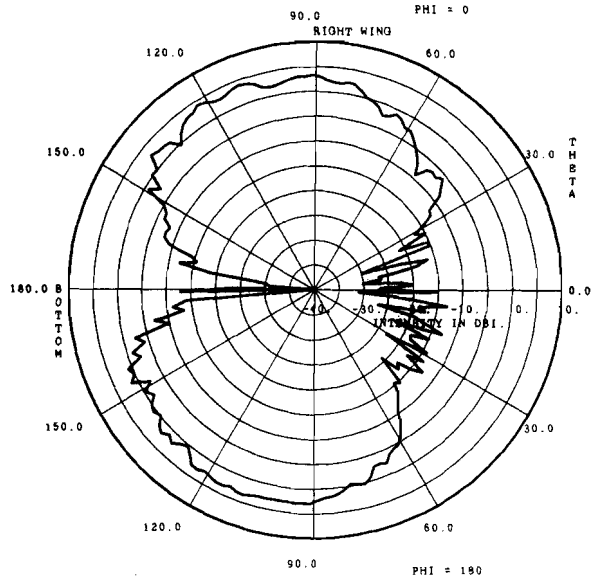

(b) wing to wing

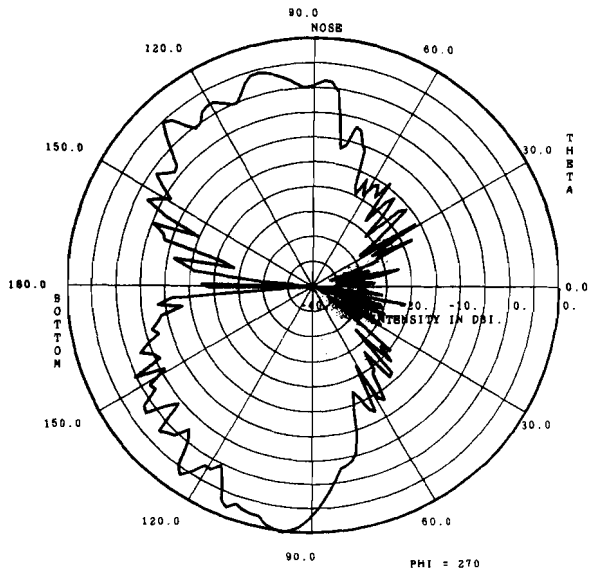

(c) nose to tail

ATC-47(B.1-17)

Fig. B.1-17. Lear jet bottom-mounted front, flaps up, wheels down

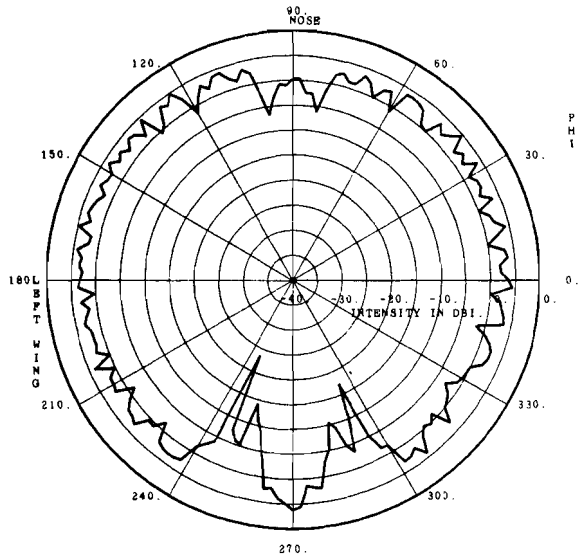

(a) horizontal plane

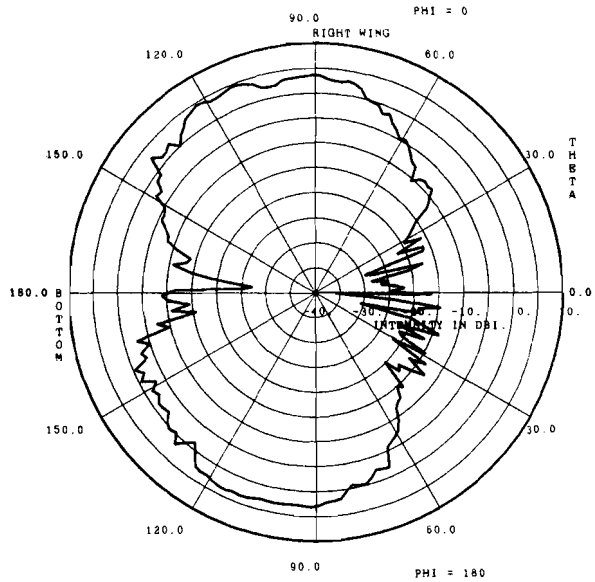

(b) wing to wing

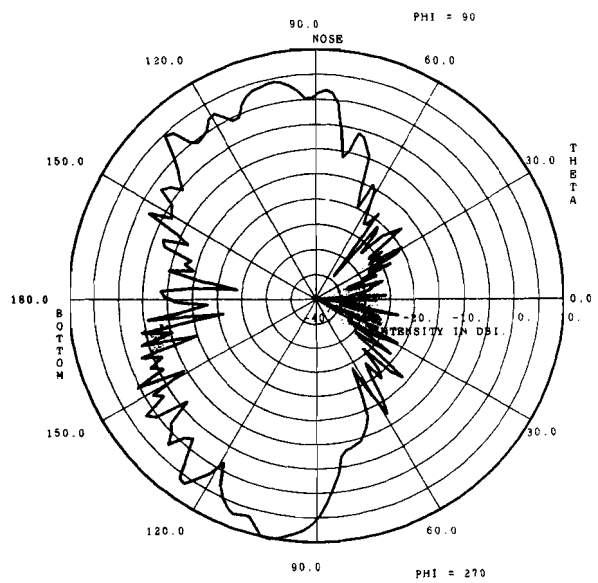

(c) nose to tail

ATC-47(B.1-18)

Fig. B.1-18. Lear jet bottom-mounted front, flaps down, wheels down

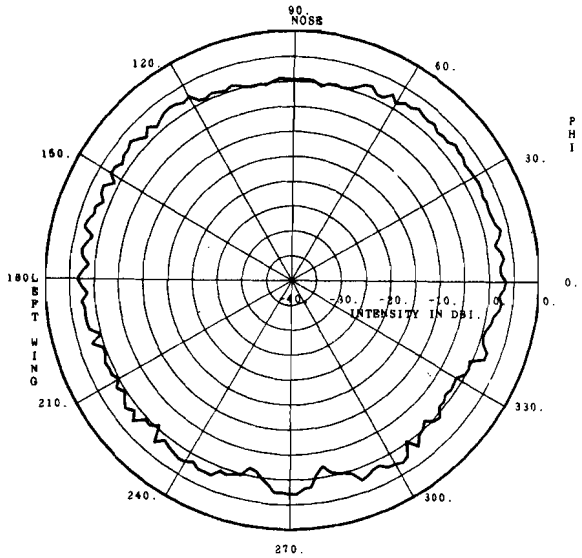

(a) horizontal plane

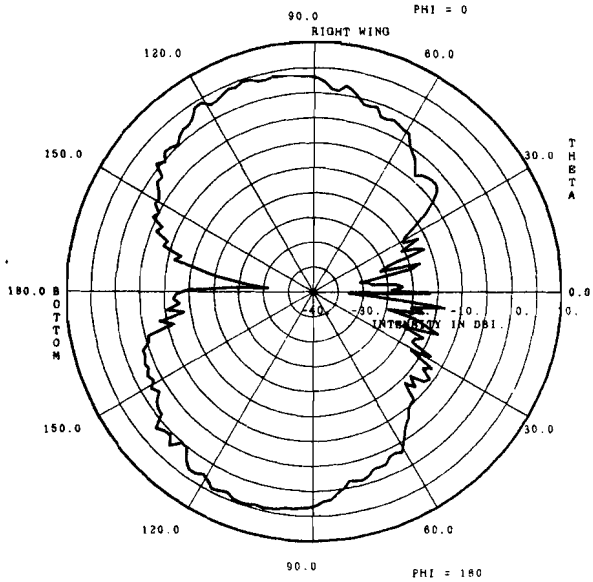

(b) wing to wing

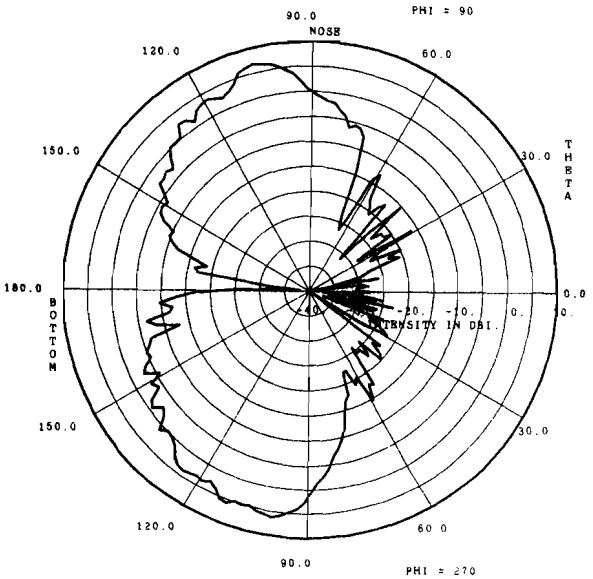

(c) nose to tail

ATC-47(B.1-19)

Fig. B.1-19. Lear jet bottom-mounted front, flaps up, wheels up

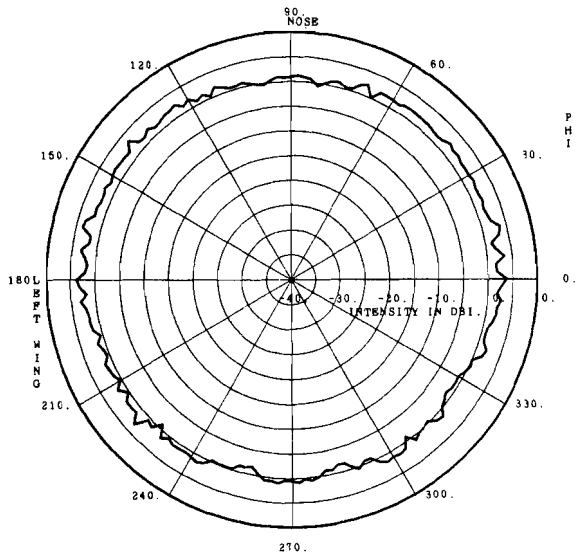

(a) horizontal plane

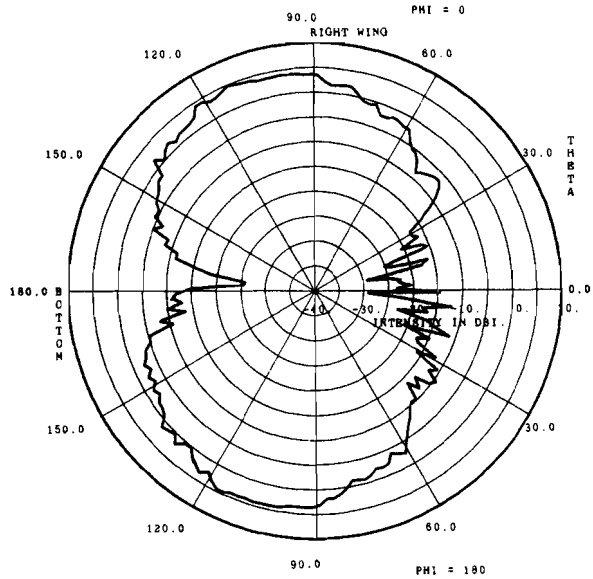

(b) wing to wing

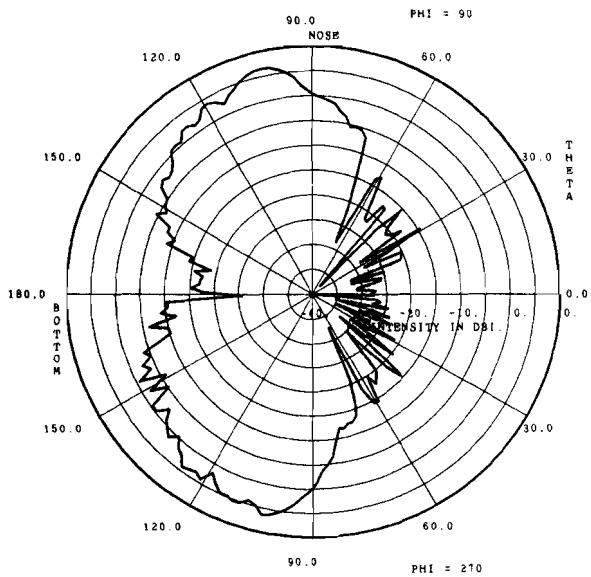

(c) nose to tail

ATC-47(B.1-20)

Fig. B.1-20. Lear jet bottom-mounted front, flaps down, wheels up

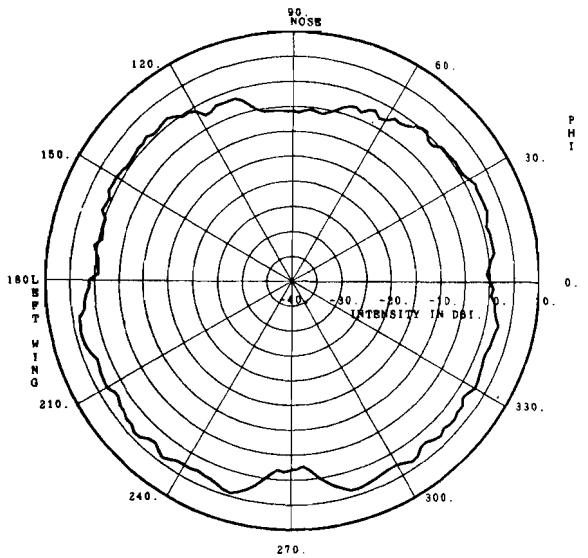

(a) horizontal plane

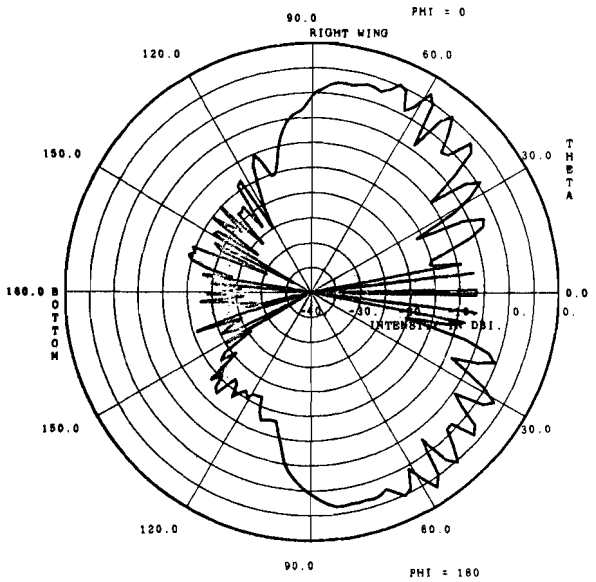

(b) wing to wing

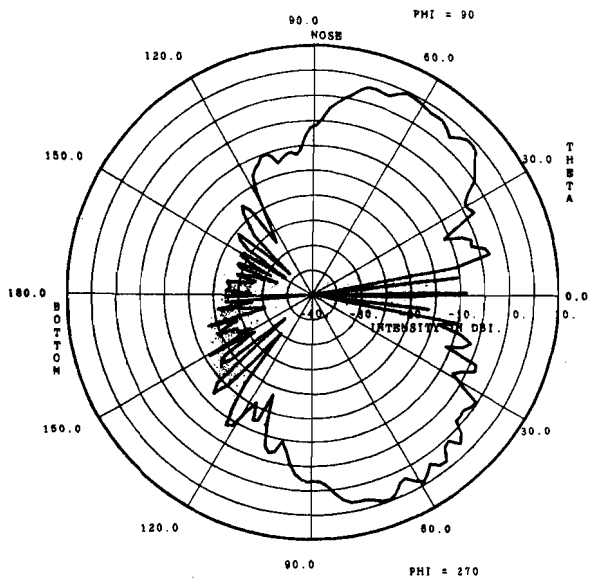

(c) nose to tail

ATC-47(B.2-1)

Fig. B.2-1. Piper Cherokee top-mounted rear, flaps up, wheels down

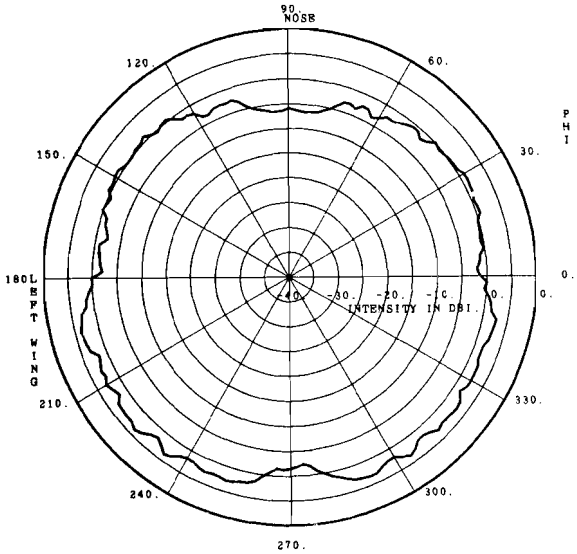

(a) horizontal plane

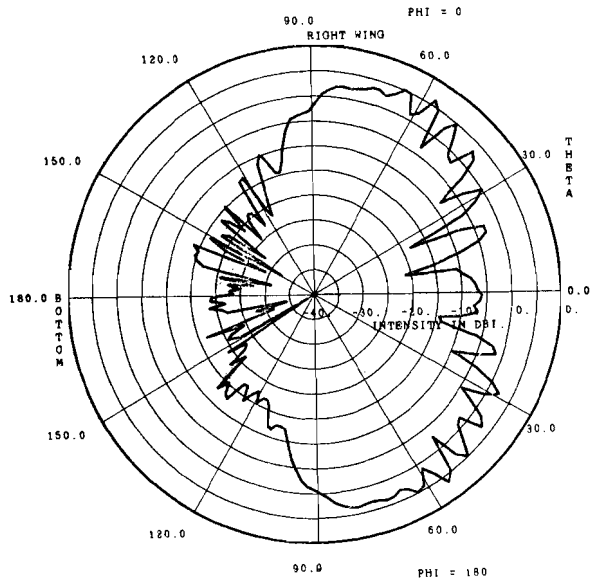

(b) wing to wing

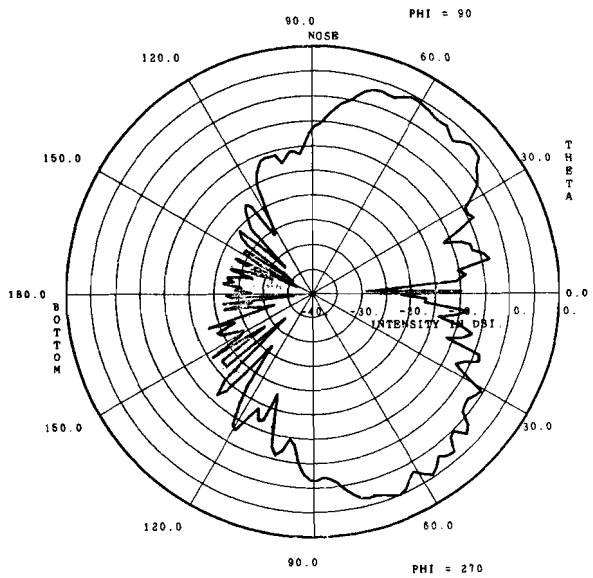

(c) nose to tail

ATC-47(B.2-2)

Fig. B.2-2. Piper Cherokee top-mounted rear, flaps down, wheels down

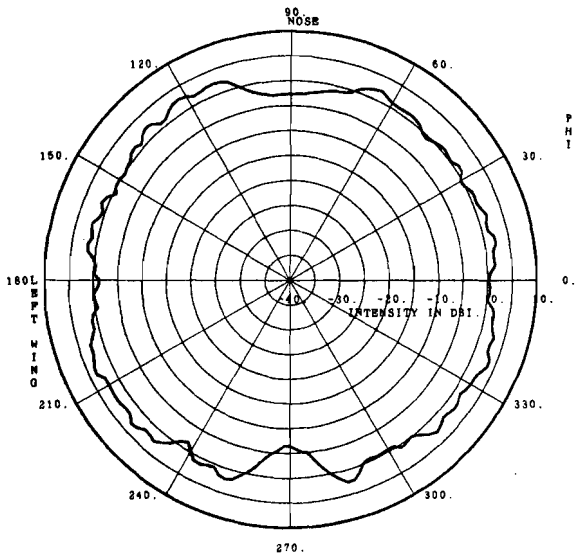

(a) horizontal plane

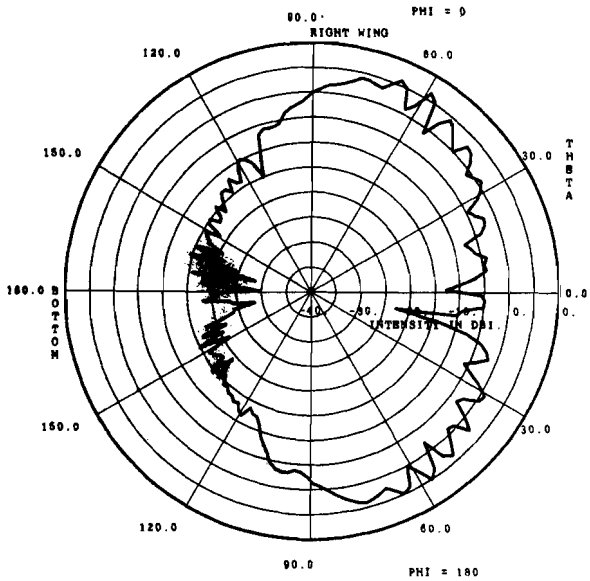

(b) wing to wing

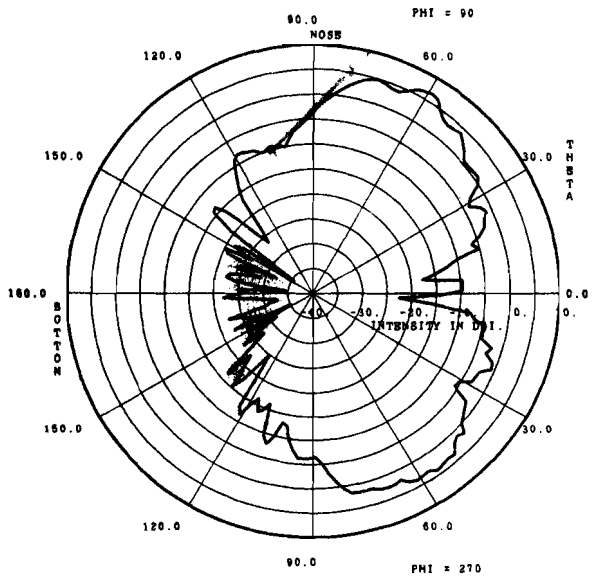

(c) nose to tail

ATC-47(B.2-3)

Fig. B. 2-3. Piper Cherokee top-mounted front, flaps up, wheels down

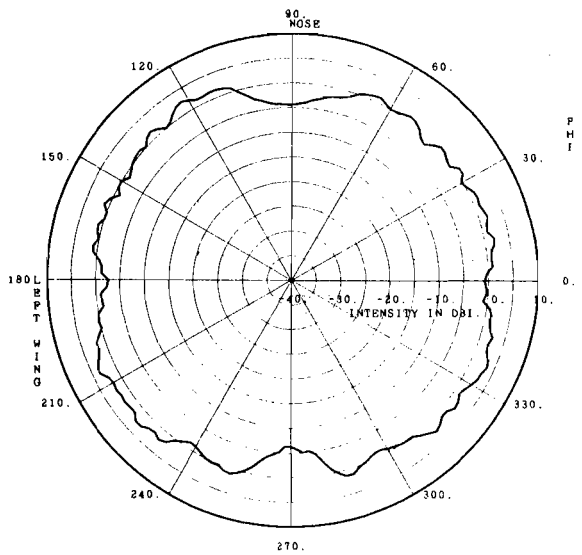

(a) horizontal plane

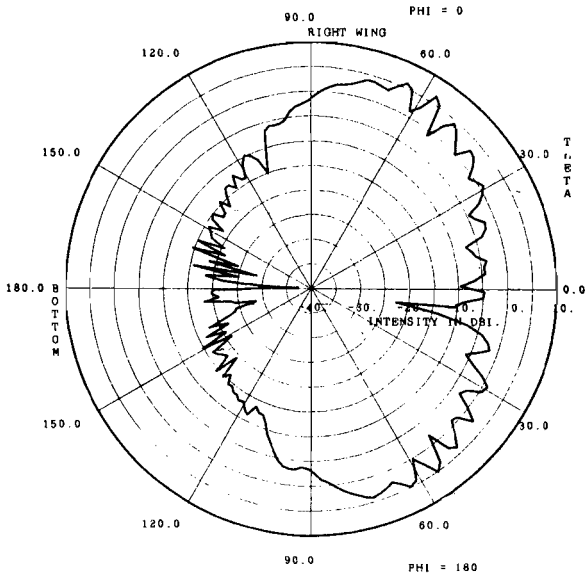

(b) wing to wing

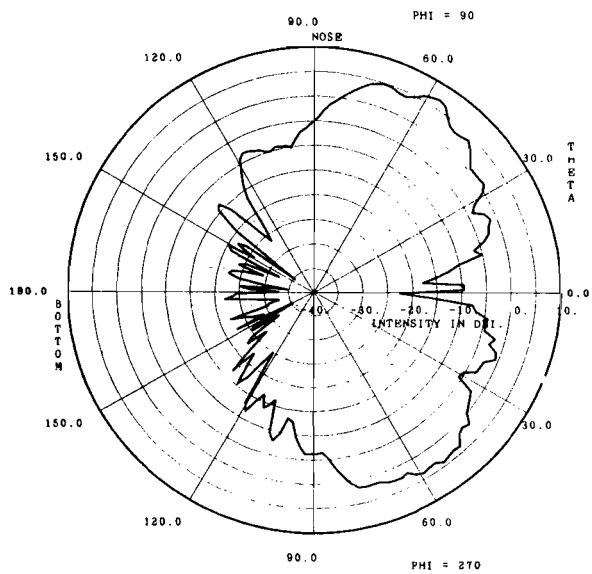

(c) nose to tail

ATC-47(B.2-4)

Fig. B.2-4. Piper Cherokee top-mounted front, flaps up, wheels down

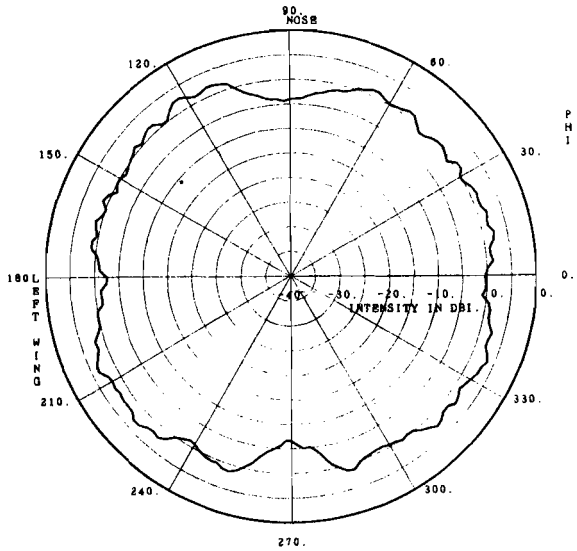

(a) horizontal plane

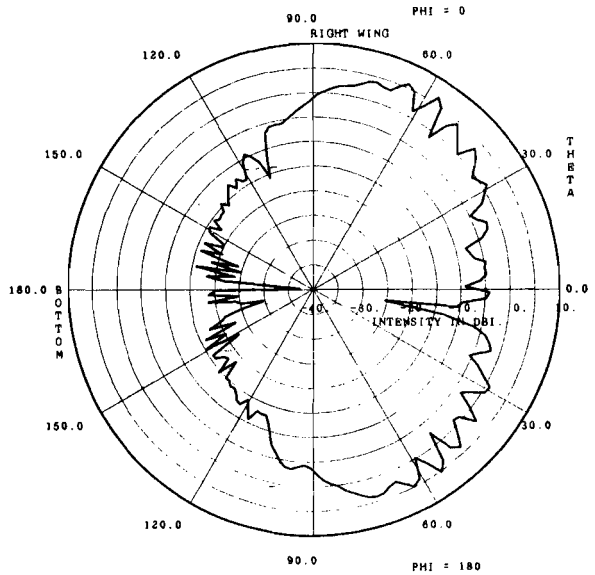

(b) wing to wing

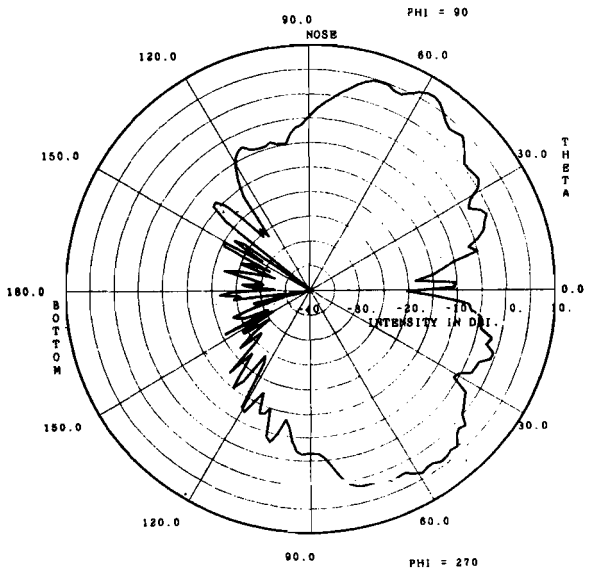

(c) nose to tail

ATC-47(B.2-5)

Fig. B.2-5. Piper Cherokee top-mounted front, flaps down, wheels down

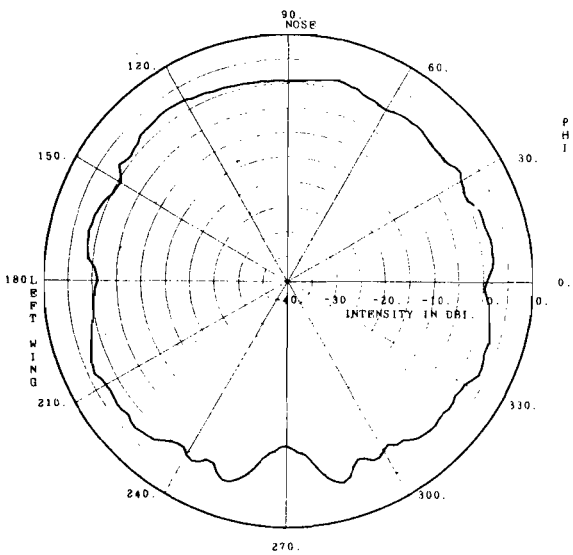

(a) horizontal plane

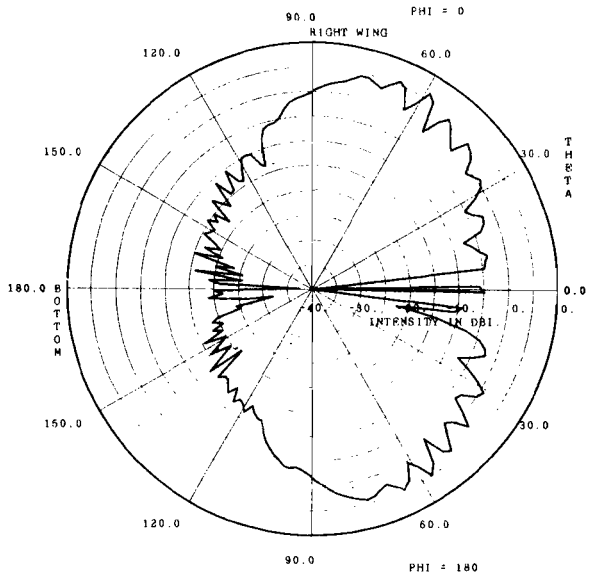

(b) wing to wing

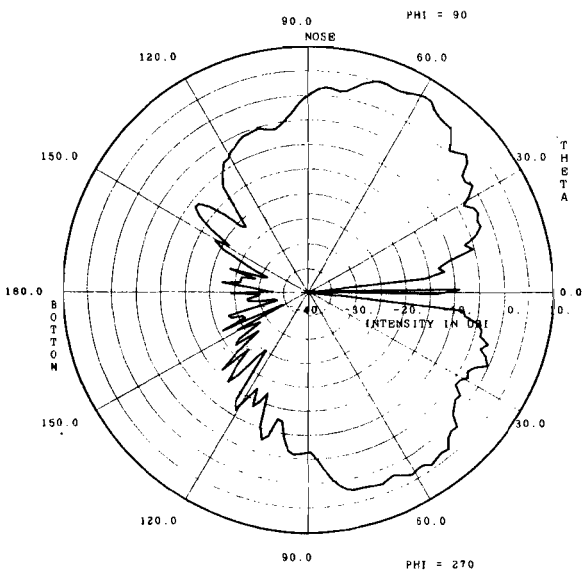

(c) nose to tail

ATC-47(B.2-6)

Fig. B. 2-6. Piper Cherokee top-mounted front, flaps up, wheels up

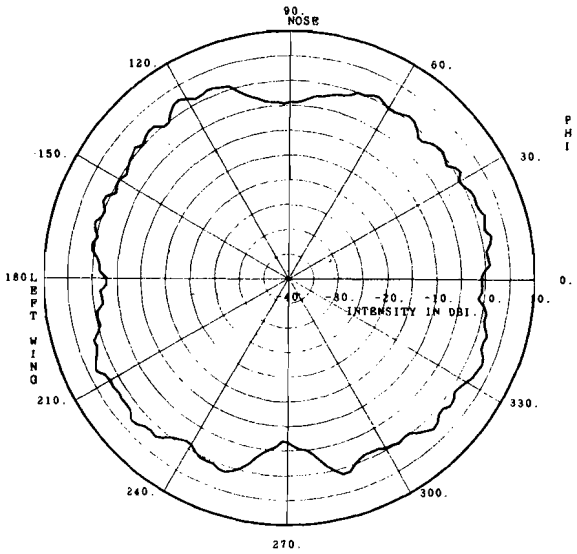

(a) horizontal plane

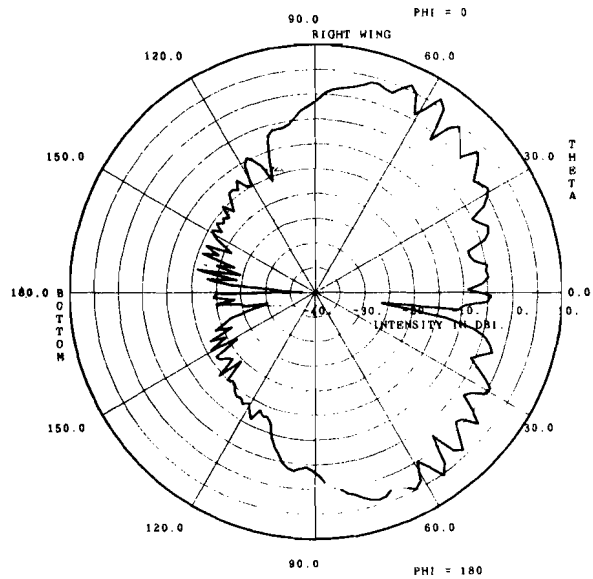

(b) wing to wing

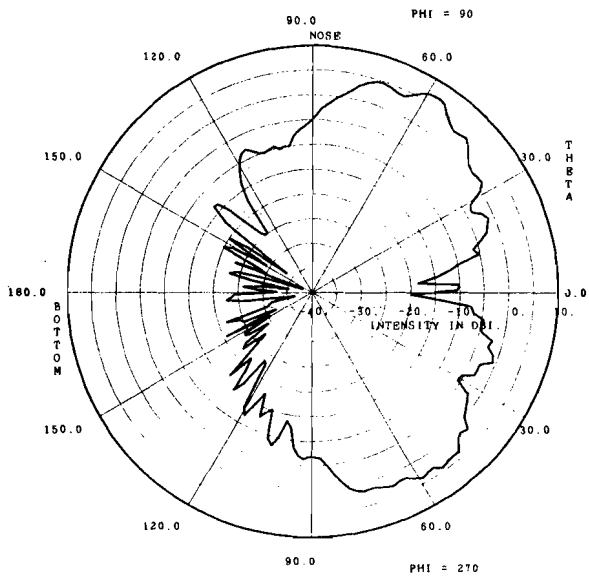

(c) nose to tail

ATC-47(B.2-7)

Fig. B.2-7. Piper Cherokee top-mounted front, flaps down, wheels up

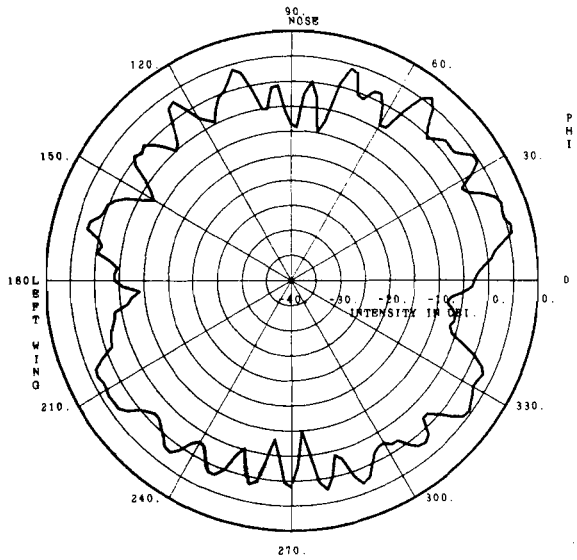

(a) horizontal plane

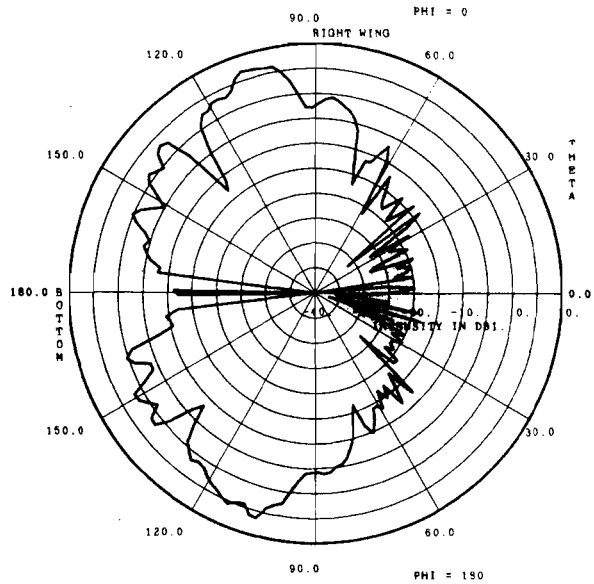

(b) wing to wing

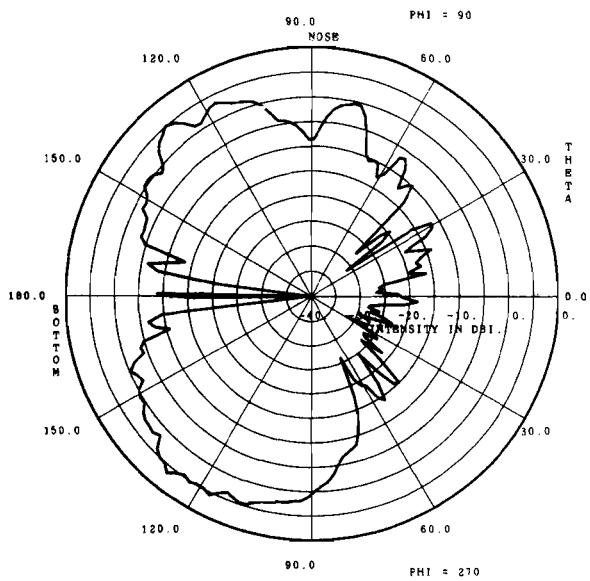

(c) nose to tail

ATC-47(B.2-8)

Fig. B.2-8. Piper Cherokee bottom-mounted rear, flaps up, wheels down

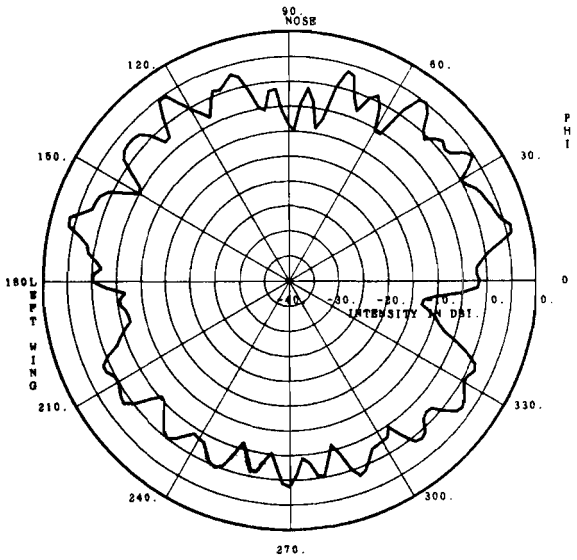

(a) horizontal plane

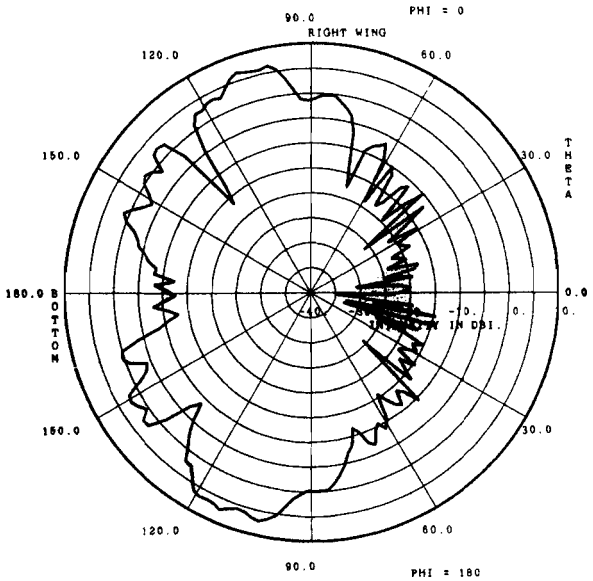

(b) wing to wing

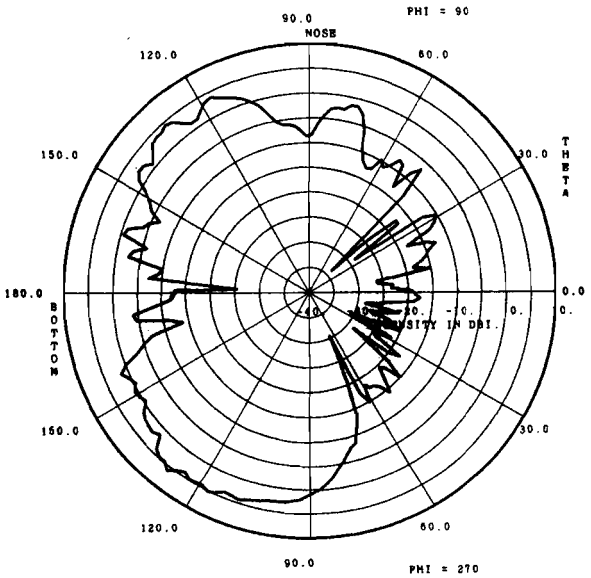

(c) nose to tail

ATC-47(B,2-9)

Fig. B. 2-9. Piper Cherokee bottom-mounted rear, flaps down, wheels down

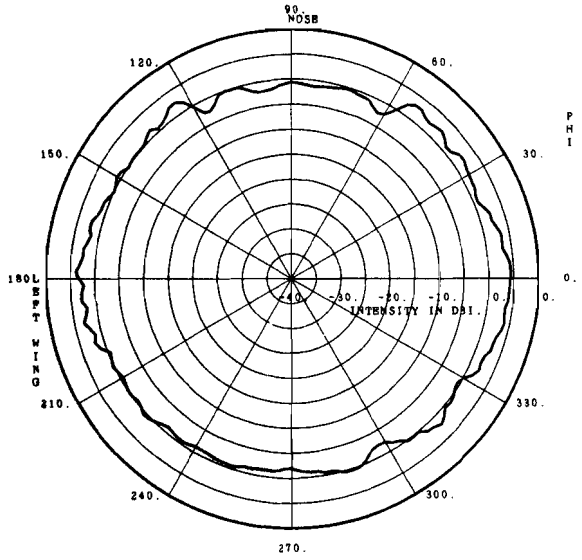

(a) horizontal plane

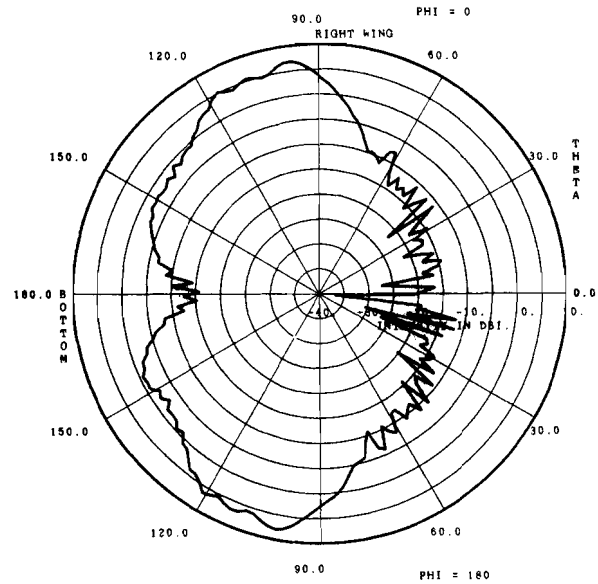

(b) wing to wing

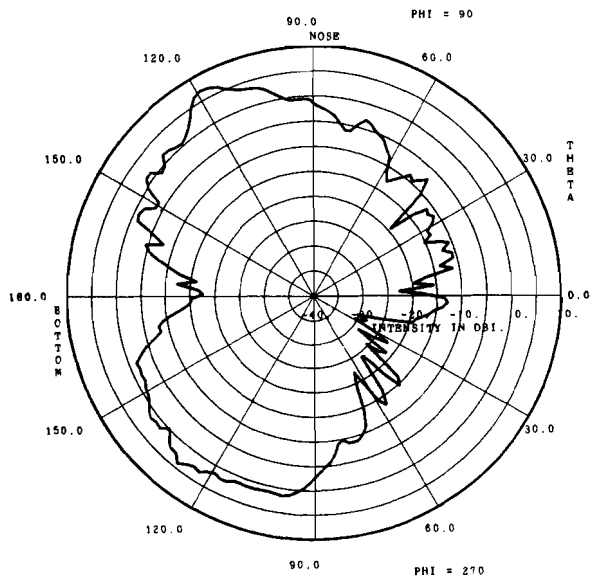

(c) nose to tail

ATC-47(B.2-10)

Fig. B.2-10. Piper Cherokee bottom-mounted rear, flaps up, wheels down

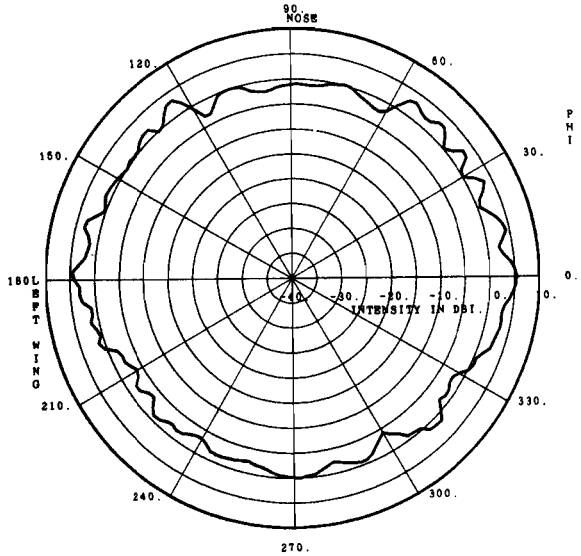

(a) horizontal plane

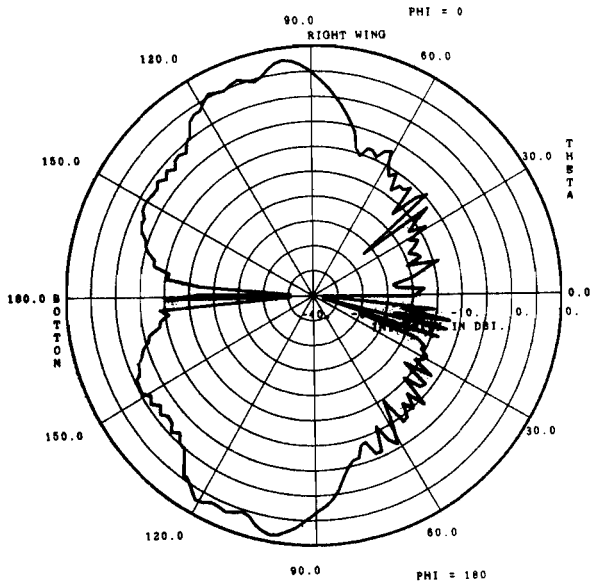

(b) wing to wing

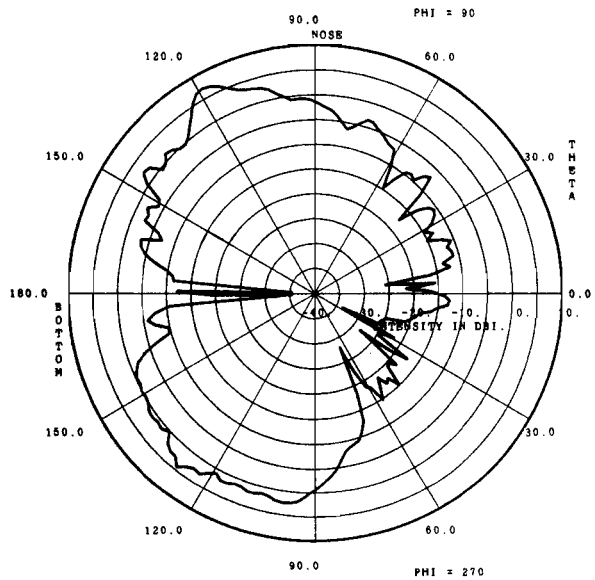

(c) nose to tail

ATC-47(B.2-11)

Fig. B.2-11. Piper Cherokee bottom-mounted rear, flaps down, wheels up

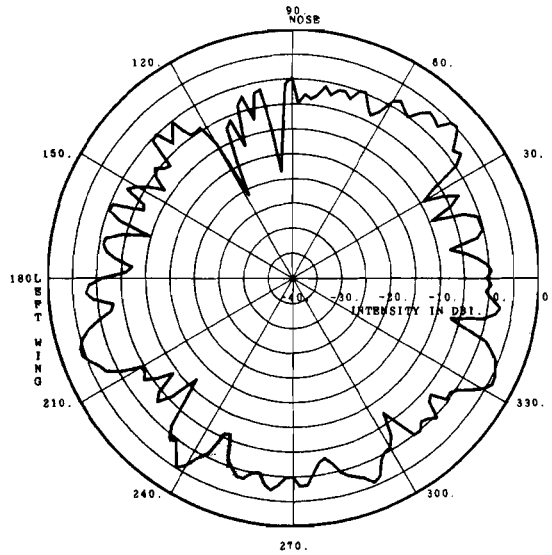

(a) horizontal plane

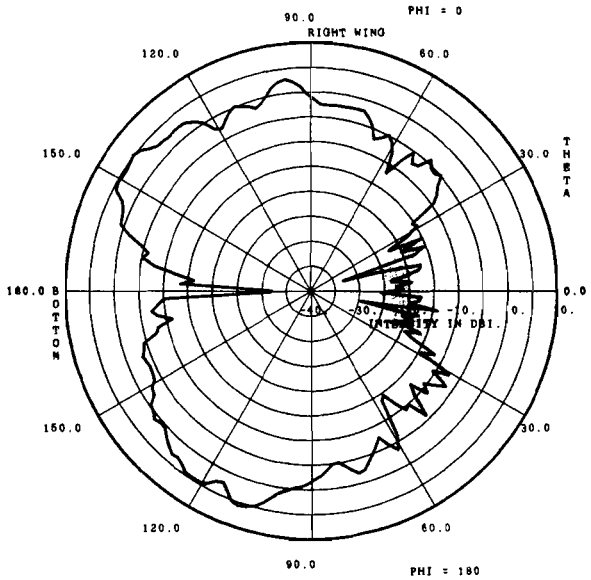

(b) wing to wing

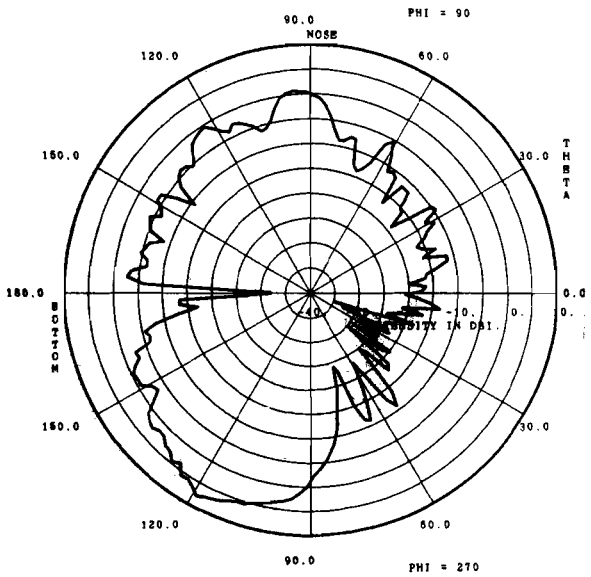

(c) nose to tail

ATC-47(B.2-12)

Fig. B.2-12. Piper Cherokee bottom-mounted front, flaps up, wheels down

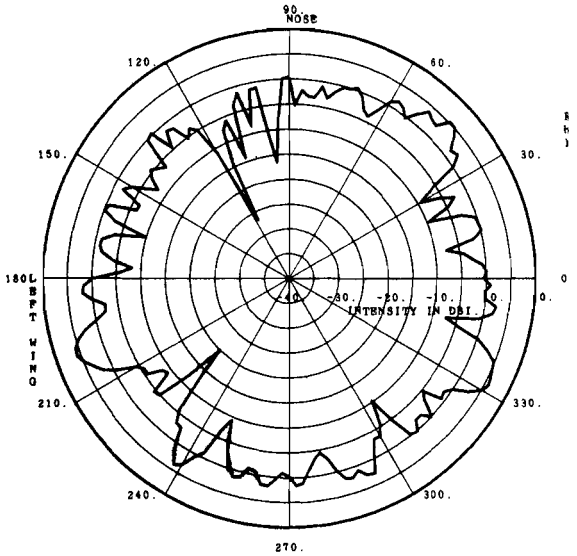

(a) horizontal plane

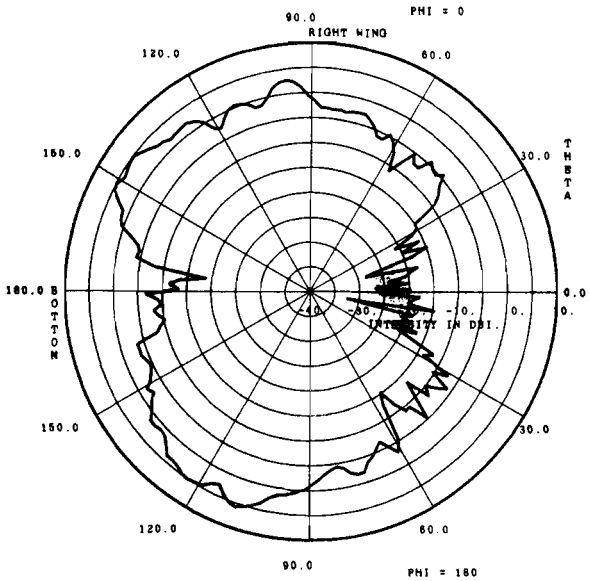

(b) wing to wing

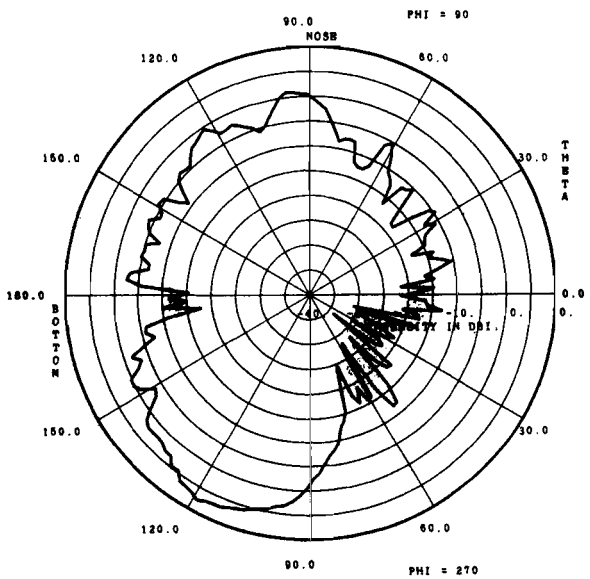

(c) nose to tail

ATC-47(B.2-13)

Fig. B.2-13. Piper Cherokee bottom-mounted front, flaps down, wheels down

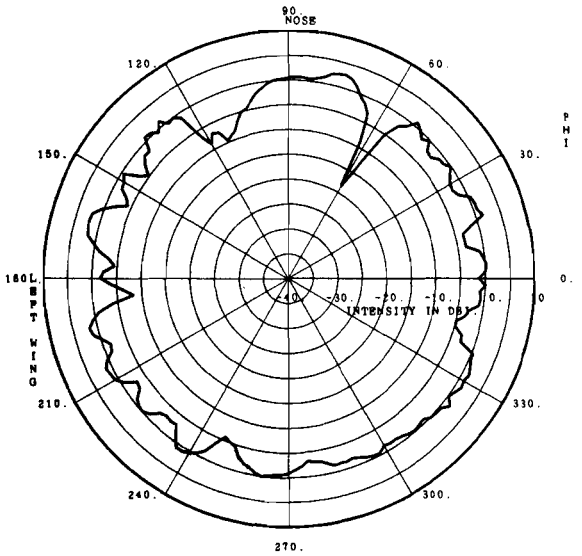

(a) horizontal plane

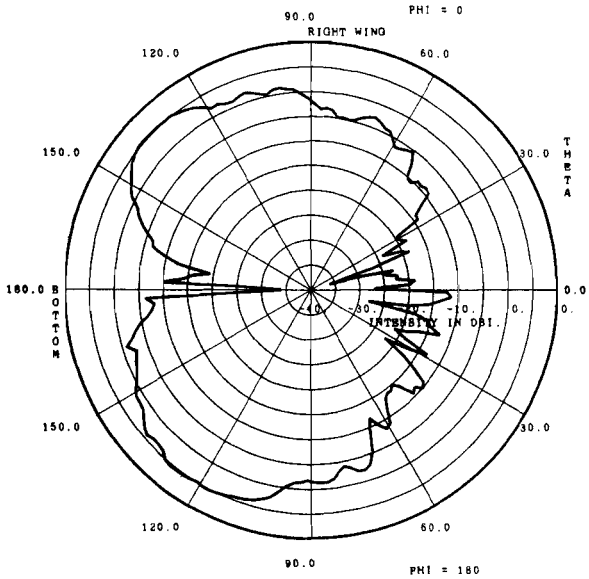

(b) wing to wing

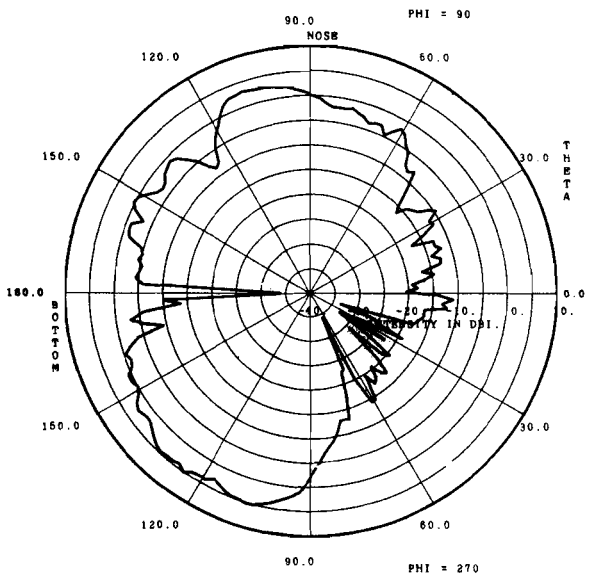

(c) nose to tail

ATC-47(B.2-14)

Fig. B. 2-14. Piper Cherokee bottom-mounted front, flaps down, wheels up

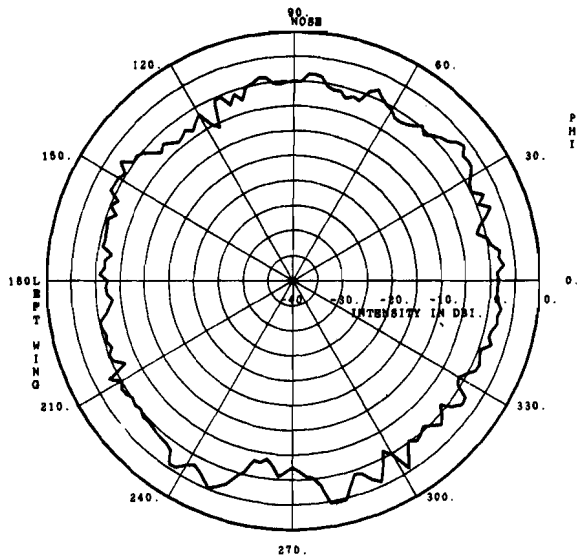

(a) horizontal plane

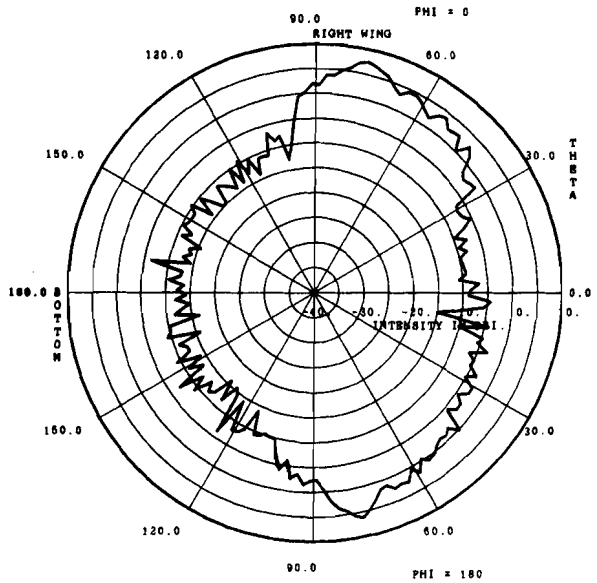

(b) wing to wing

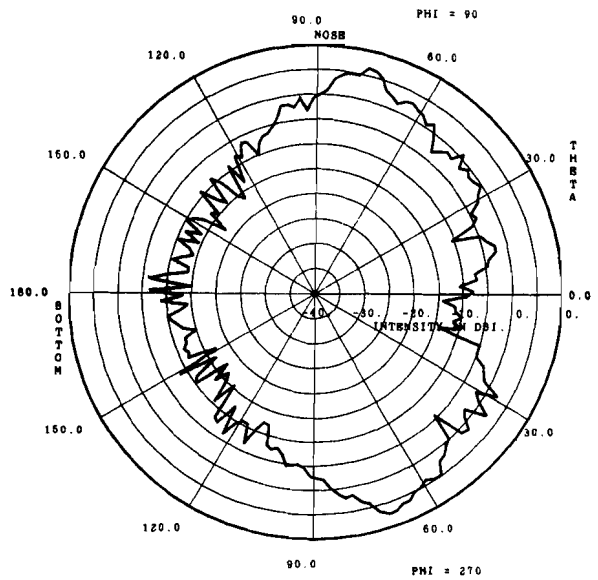

(c) nose to tail

ATC-47(B.4-1)

Fig. B.4-1. Cessna 150 top-mounted rear, flaps up, wheels down

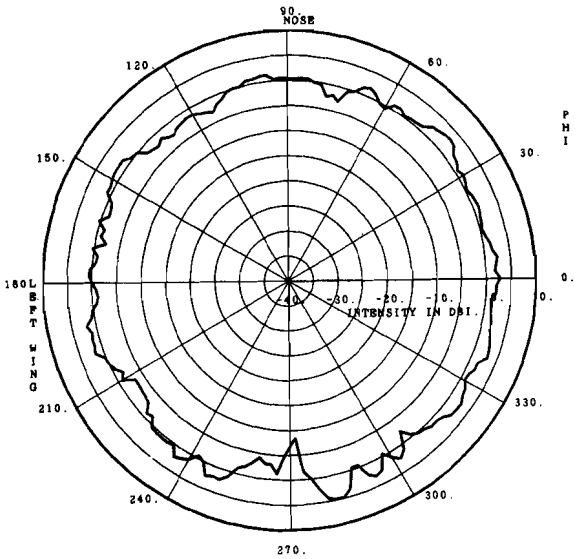

(a) horizontal plane

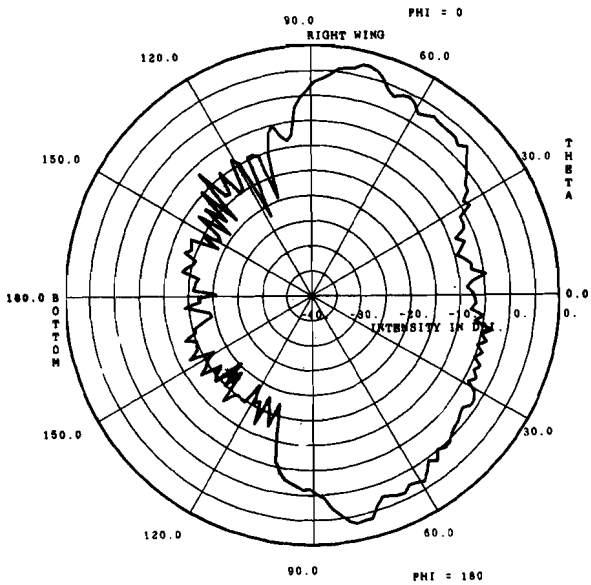

(b) wing to wing

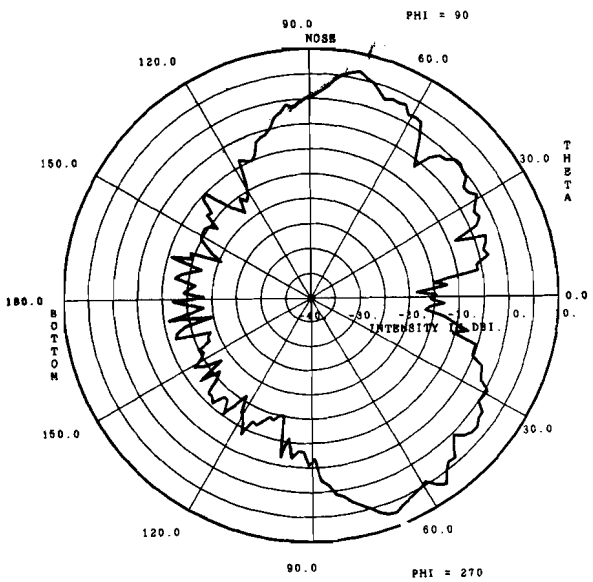

(c) nose to tail

ATC-47(B.4-2)

Fig. B. 4-2. Cessna 150 top-mounted rear, flaps down, wheels down

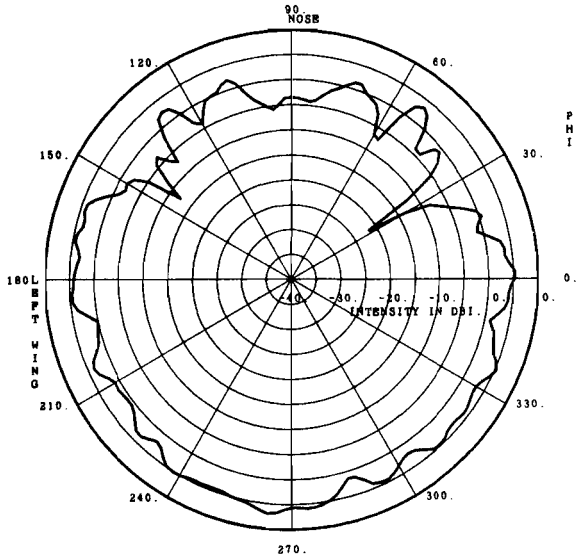

(a) horizontal plane

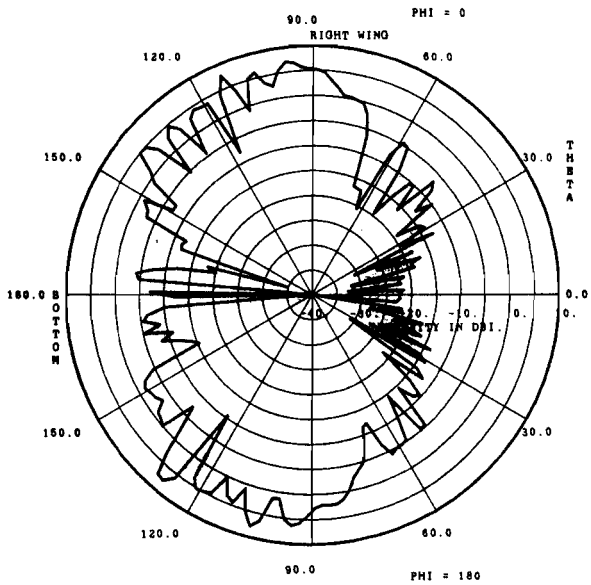

(b) wing to wing

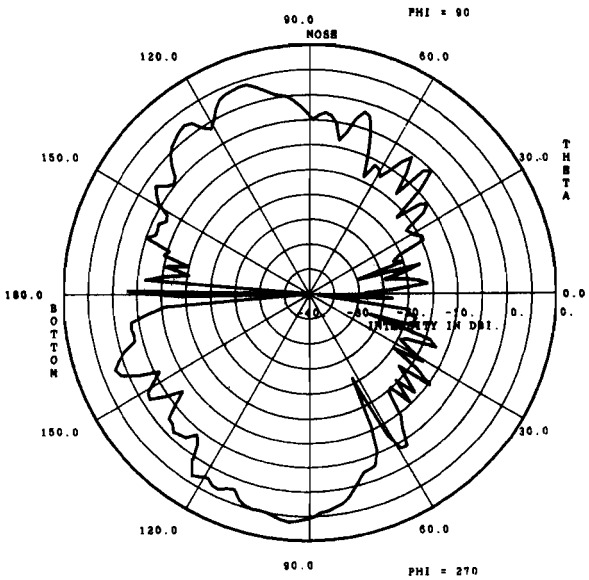

(c) nose to tail

ATC-47(B.4-3)

Fig. B. 4-3. Cessna 150 bottom-mounted rear, flaps up, wheels down

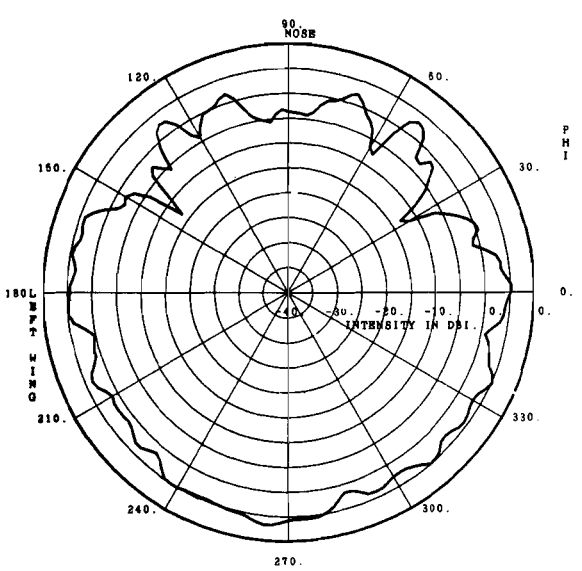

(a) horizontal plane

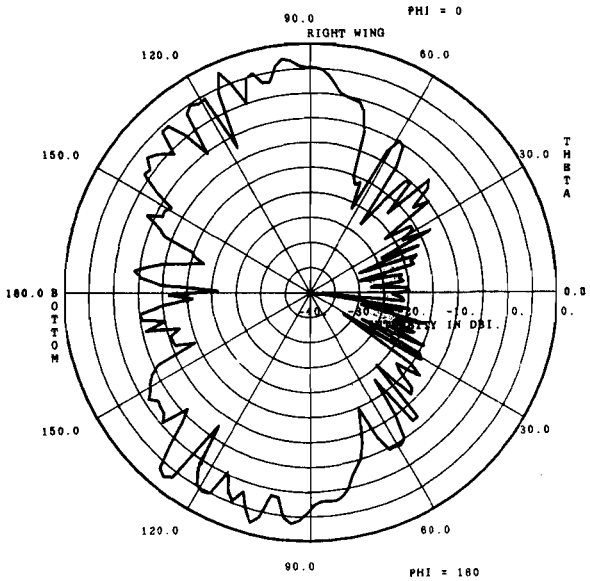

(b) wing to wing

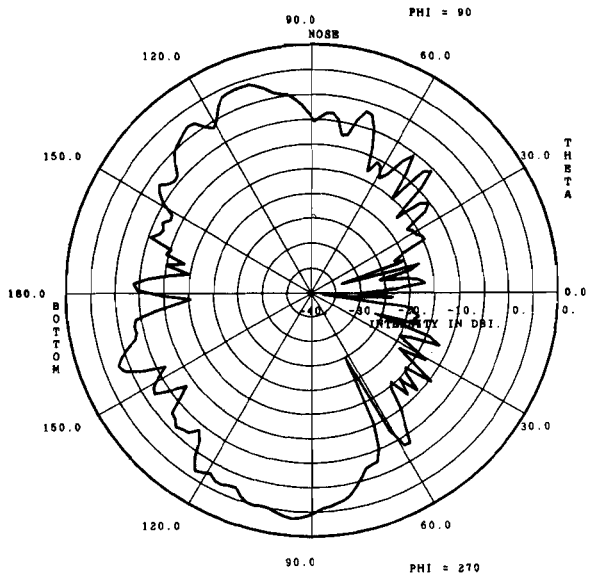

(c) nose to tail

ATC-47(B.4-4)

Fig. B.4-4. Cessna 150 bottom-mounted rear, flaps down, wheels down

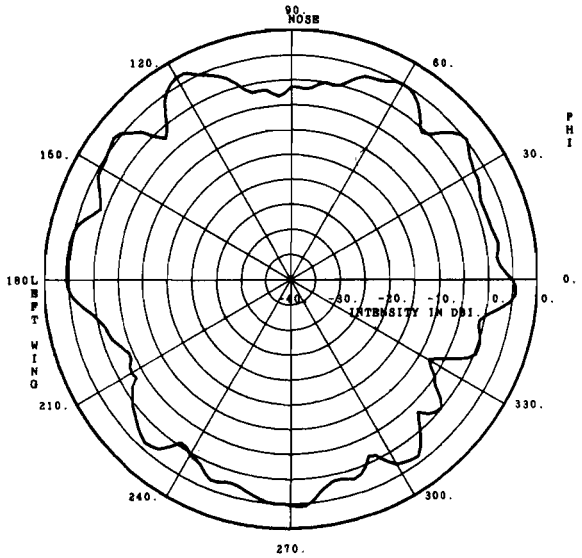

(a) horizontal plane

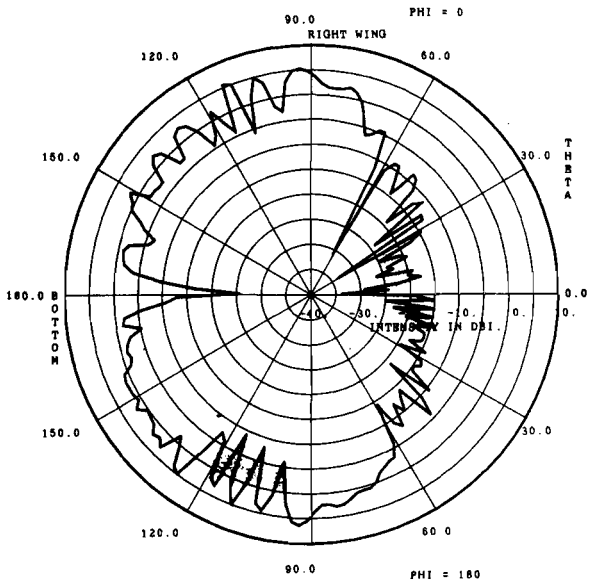

(b) wing to wing

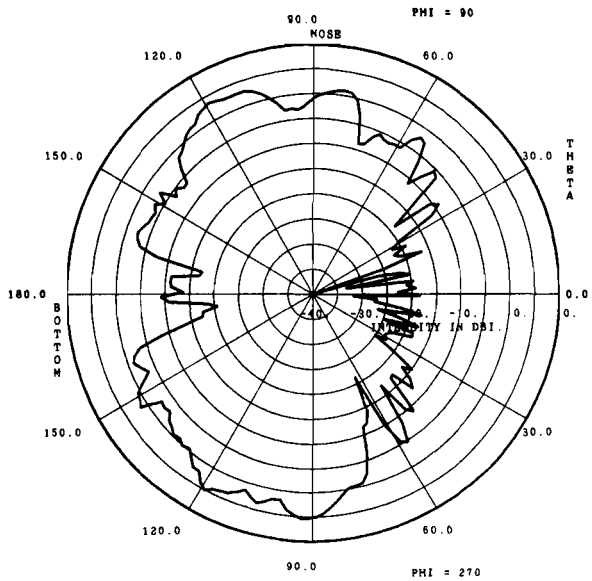

(c) nose to tail

ATC-47(B.4-5)

Fig. B. 4-5. Cessna 150 bottom-mounted center, flaps up, wheels down

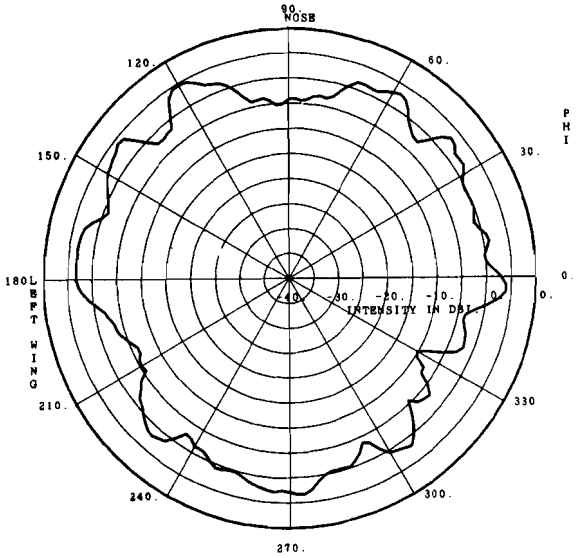

(a) horizontal plane

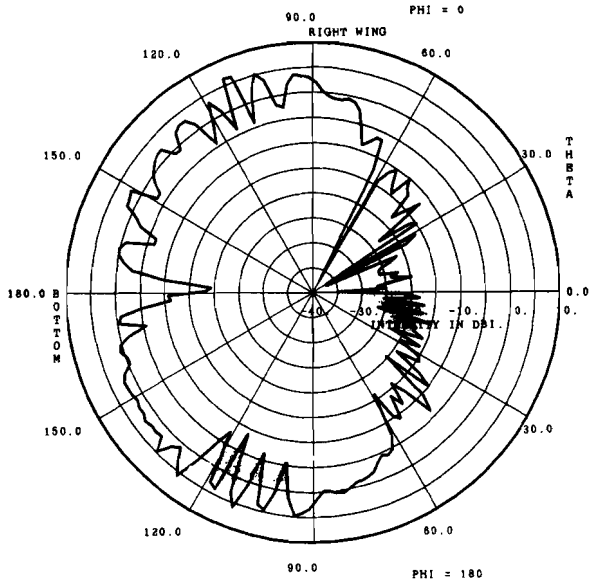

(b) wing to wing

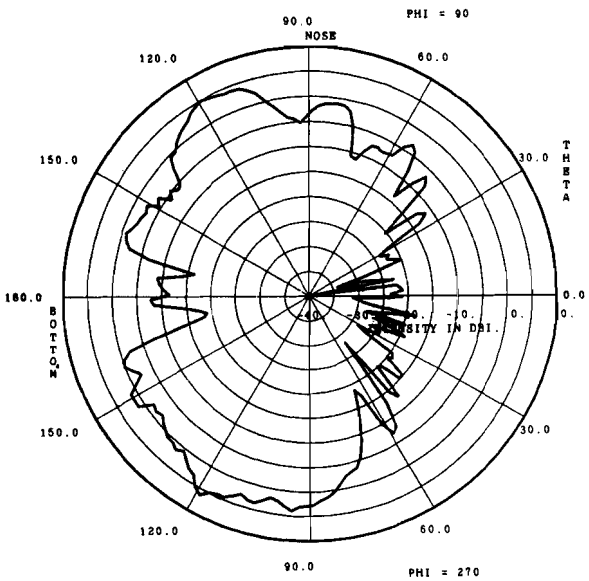

(c) nose to tail

ATC-47(B.4-6)

Fig. B. 4-6. Cessna 150 bottom-mounted center, flaps down, wheels down

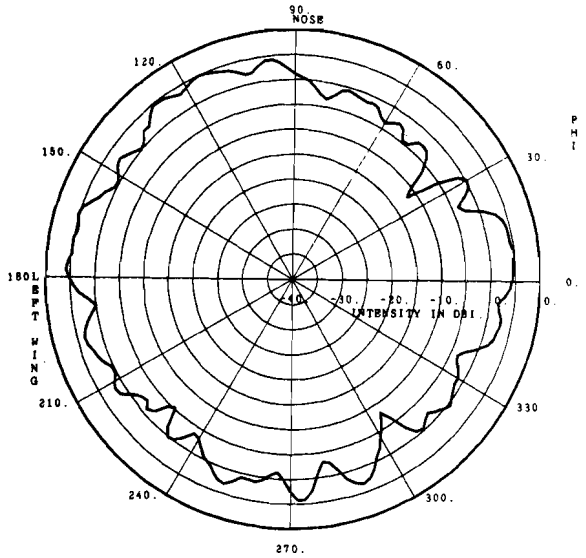

(a) horizontal plane

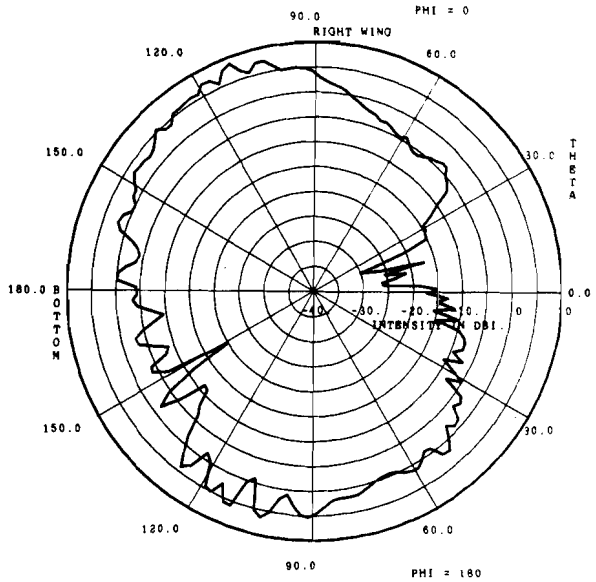

(b) wing to wing

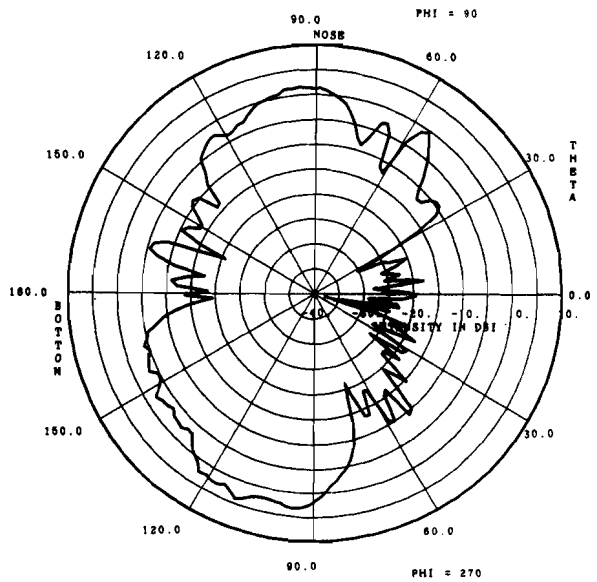

(c) nose to tail

ATC-47(B.4-7)

Fig. B. 4-7. Cessna 150 bottom-mounted front, flaps up, wheels down

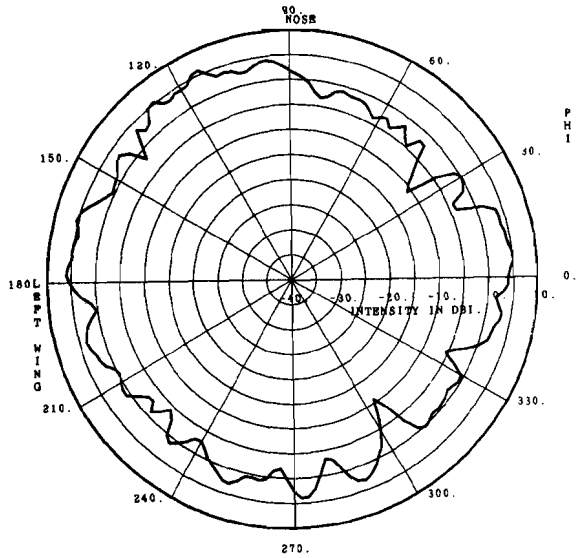

(a) horizontal plane

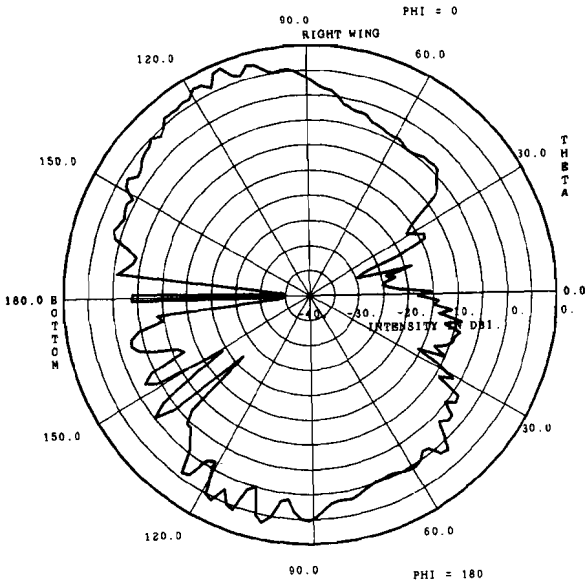

(b) wing to wing

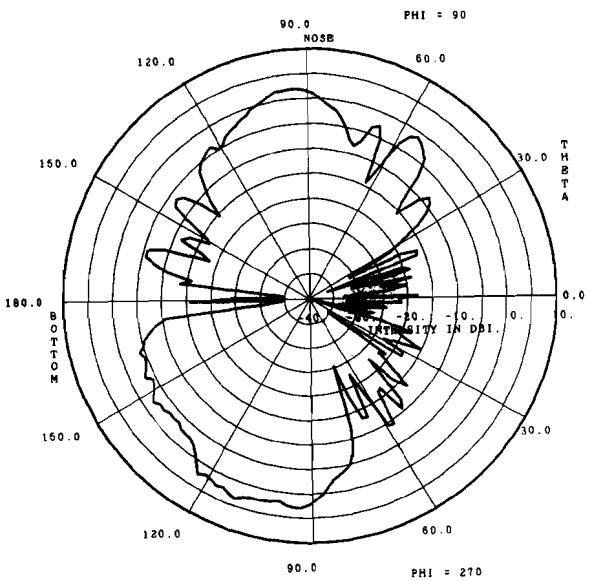

(c) nose to tail

ATC-47(B.4-8)

Fig. B. 4-8. Cessna 150 bottom-mounted front, flaps down, wheels down

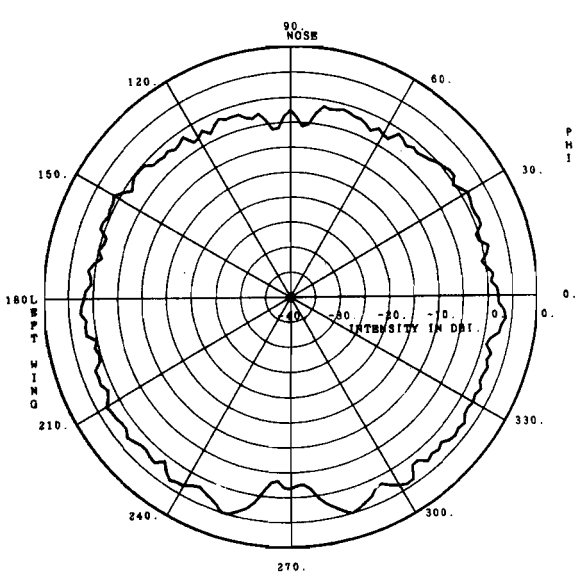

(a) horizontal plane

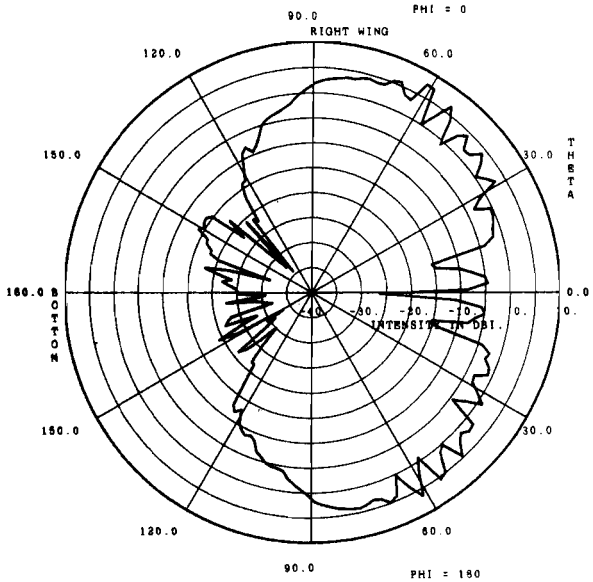

(b) wing to wing

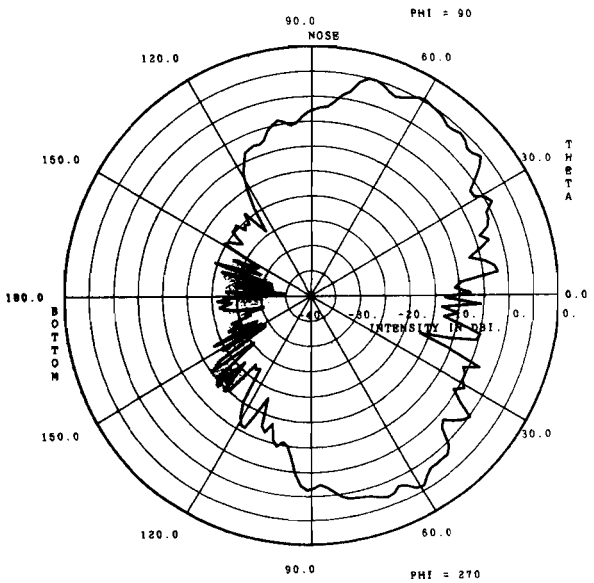

(c) nose to tail

ATC-47(B.7-1)

Fig. B. 7-1. Beech Baron top-mounted rear, flaps up, wheels down

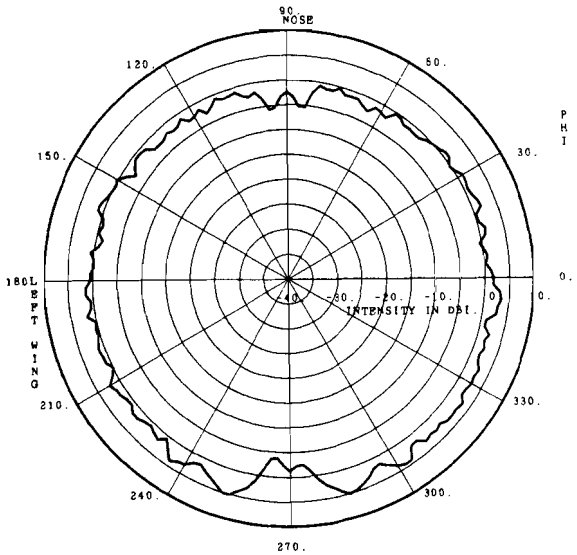

(a) horizontal plane

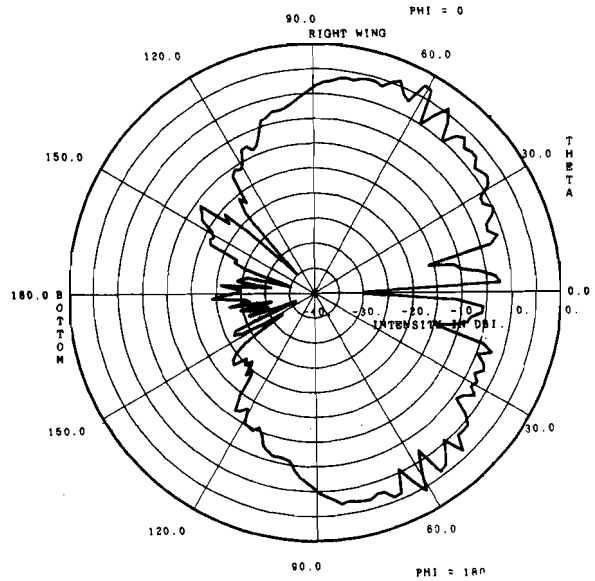

(b) wing to wing

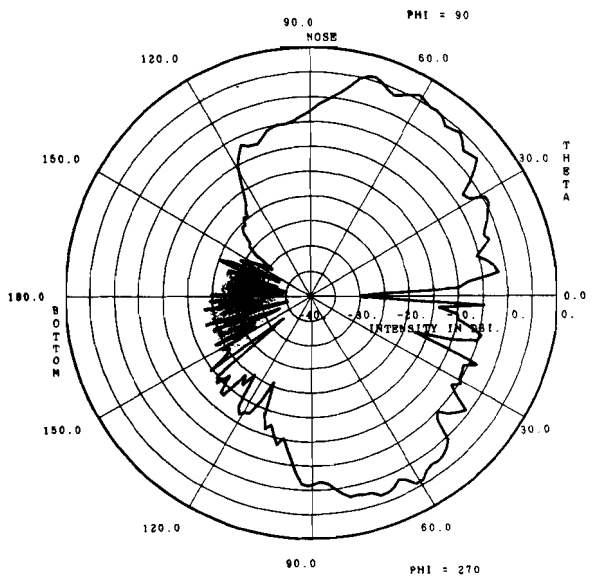

(c) nose to tail

ATC-47(B,7-2)

Fig. B. 7-2. Beech Baron top-mounted rear, flaps down, wheels down

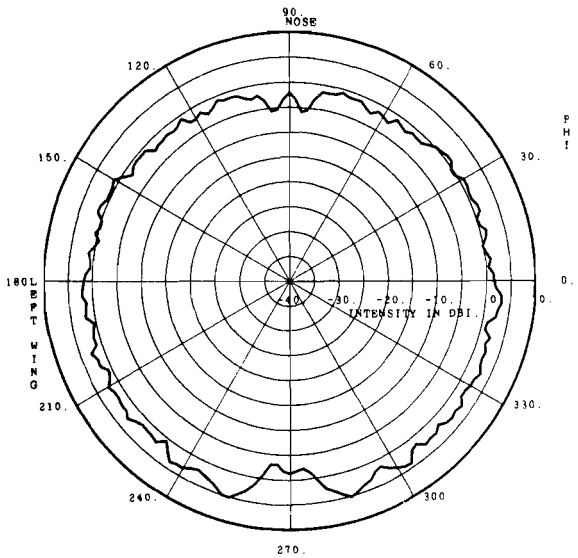

(a) horizontal plane

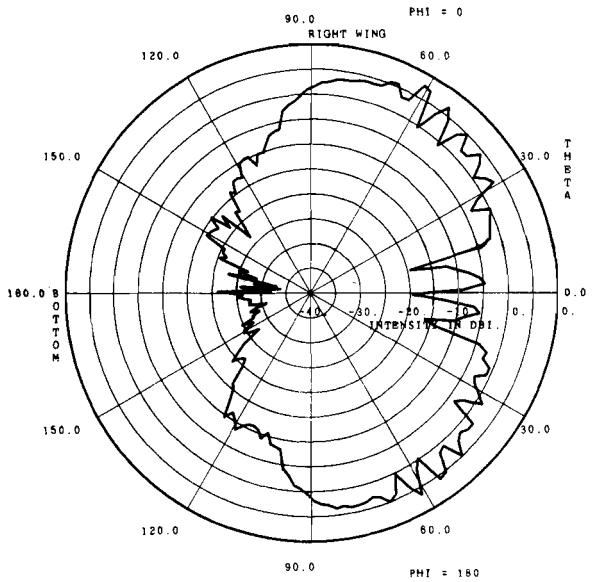

(b) wing to wing

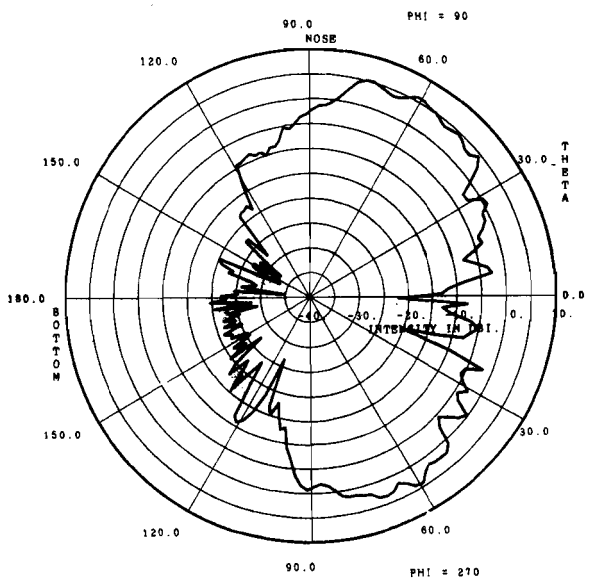

(c) nose to tail

ATC-47(B.7-3)

Fig. B. 7-3. Beech Baron top-mounted rear, flaps up, wheels down

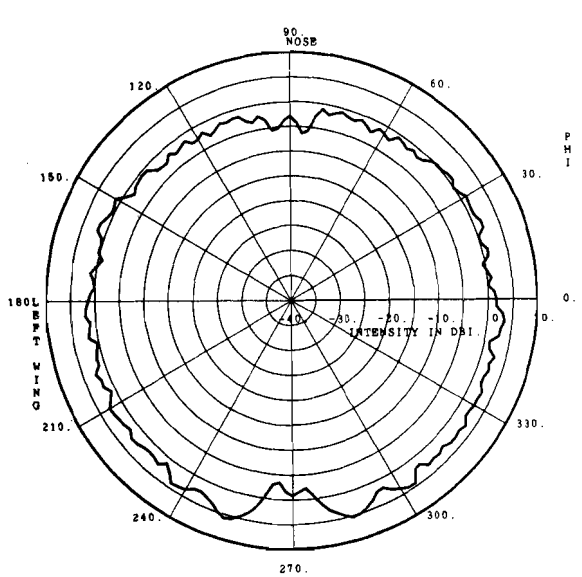

(a) horizontal plane

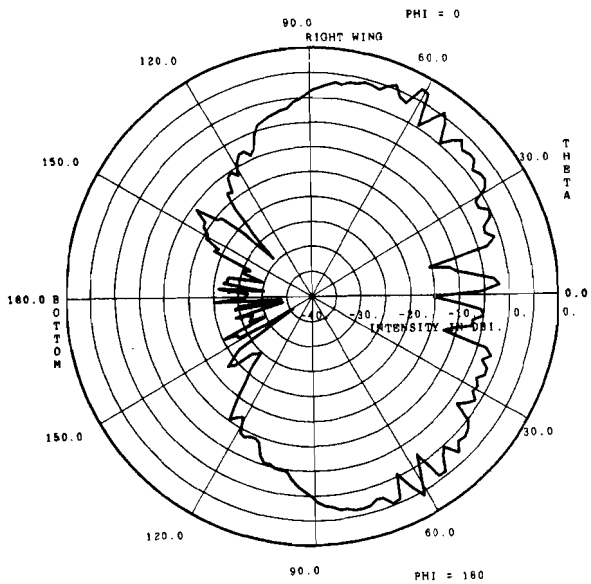

(b) wing to wing

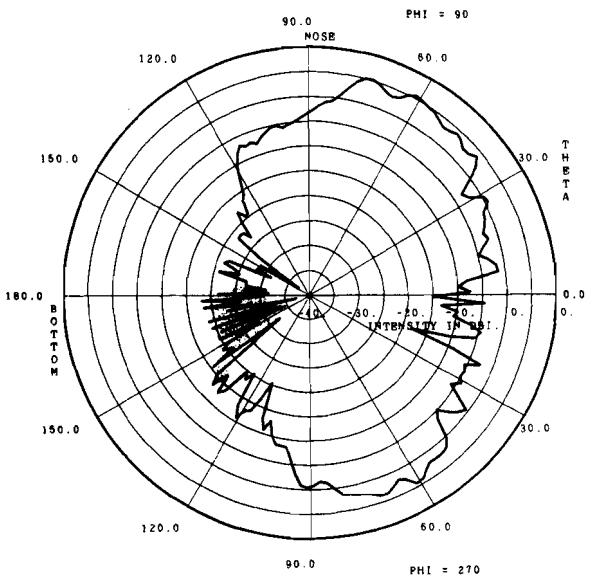

(c) nose to tail

ATC-47(B.7-4)

Fig. B. 7-4. Beech Baron top-mounted rear, flaps down, wheels up

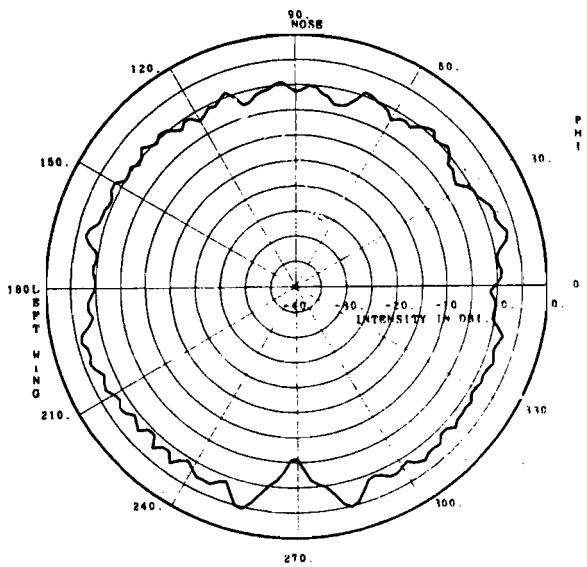

(a) horizontal plane

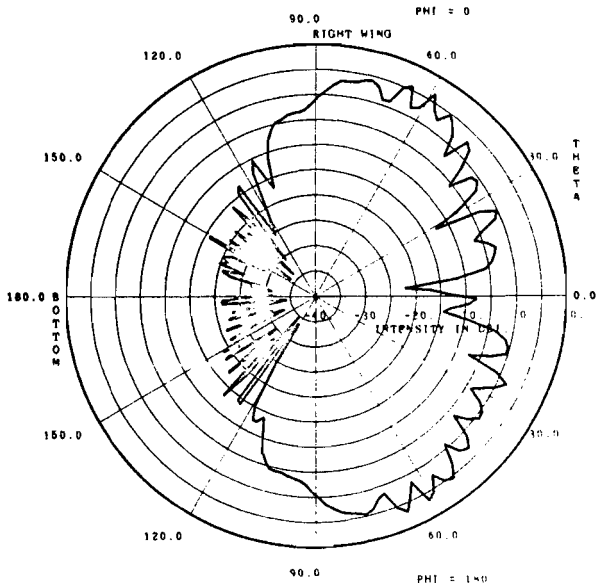

(b) wing to wing

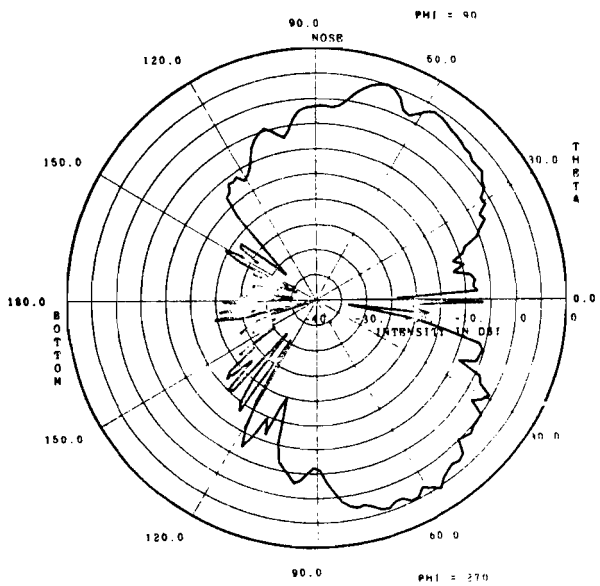

(c) nose to tail

ATC-47(B.7-5)

Fig. B.7-5. Beech Baron top-mounted front, flaps up, wheels down

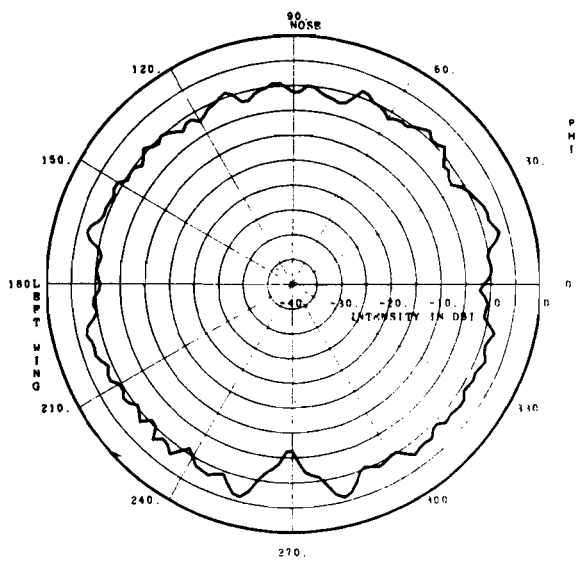

(a) horizontal plane

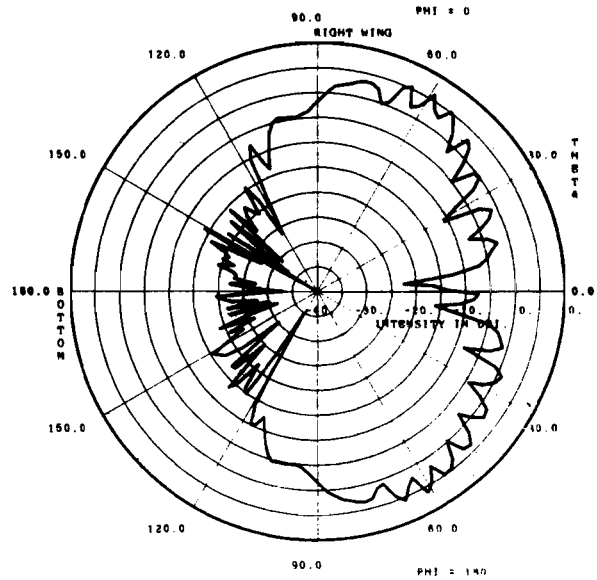

(b) wing to wing

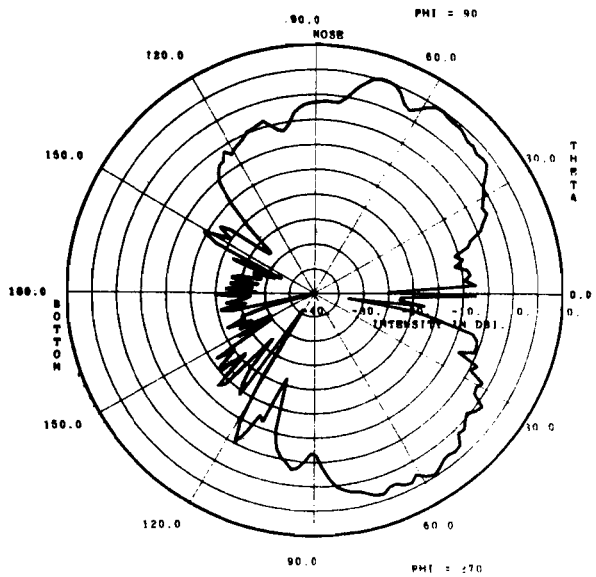

(c) nose to tail

ATC-47(B.7-6)

Fig. B.7-6. Beech Baron top-mounted front, flaps down, wheels down

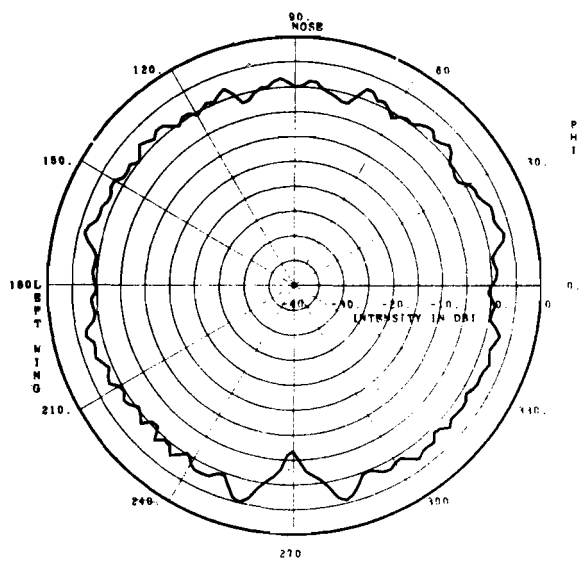

(a) horizontal plane

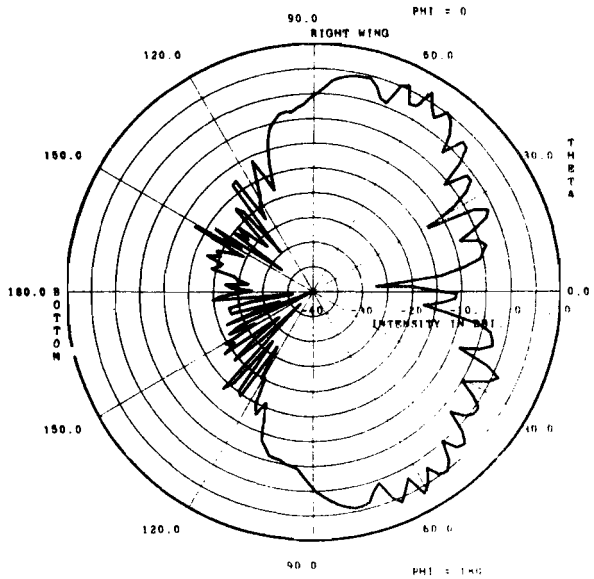

(b) wing to wing

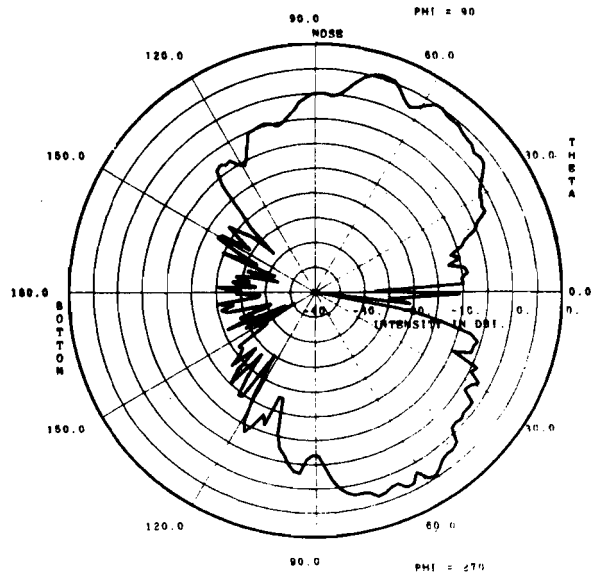

(c) nose to tail

ATC-47(B.7-7)

Fig. B. 7-7. Beech Baron top-mounted front, flaps up, wheels up

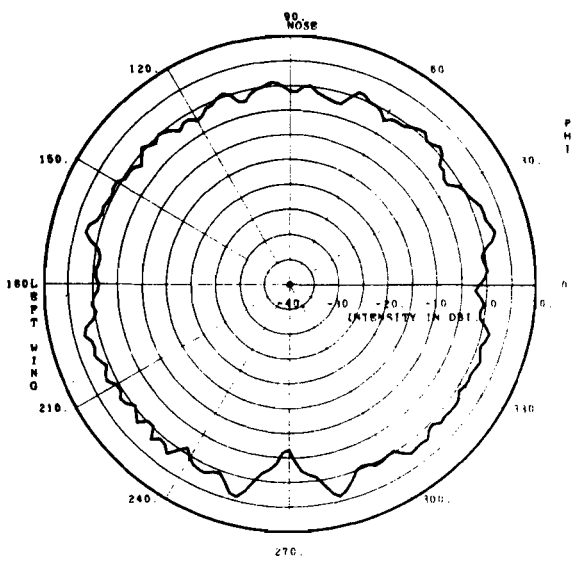

(a) horizontal plane

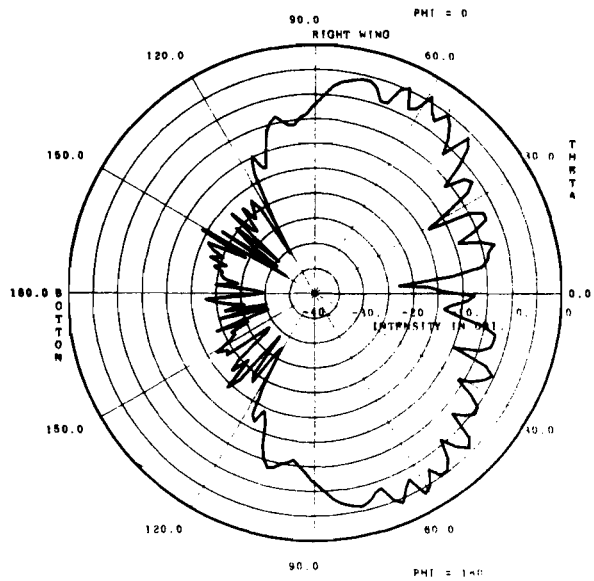

(b) wing to wing

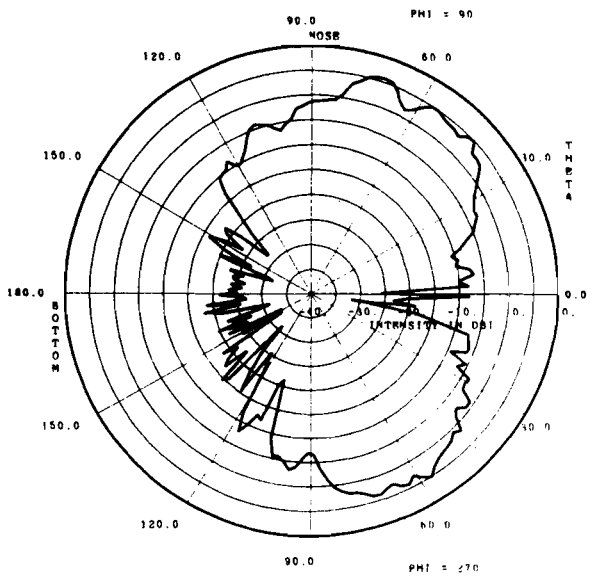

(c) nose to tail

ATC-47(B.7-8)

Fig. B.7-8. Beech Baron top-mounted front, flaps down, wheels up

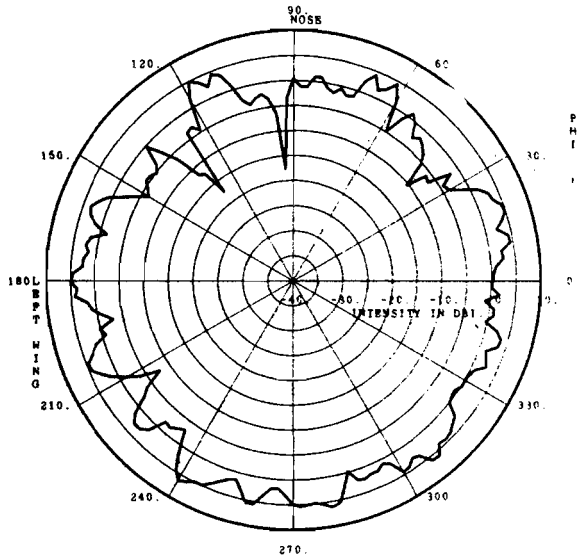

(a) horizontal plane

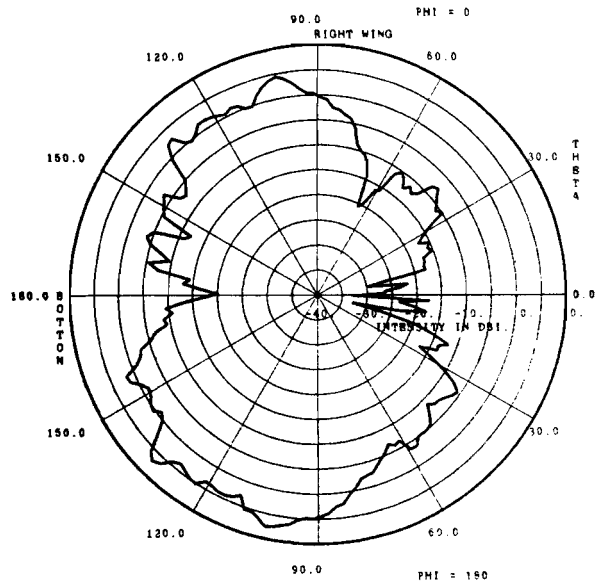

(b) wing to wing

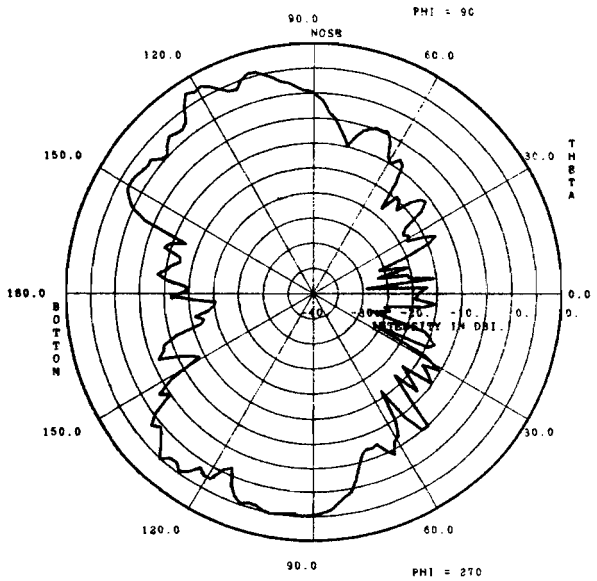

(c) nose to tail

ATC-47(B.7-9)

Fig. B. 7-9. Beech Baron bottom-mounted rear, flaps up, wheels down

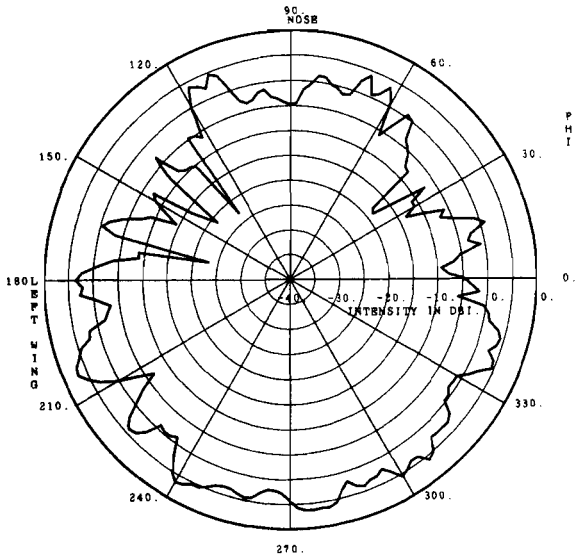

(a) horizontal plane

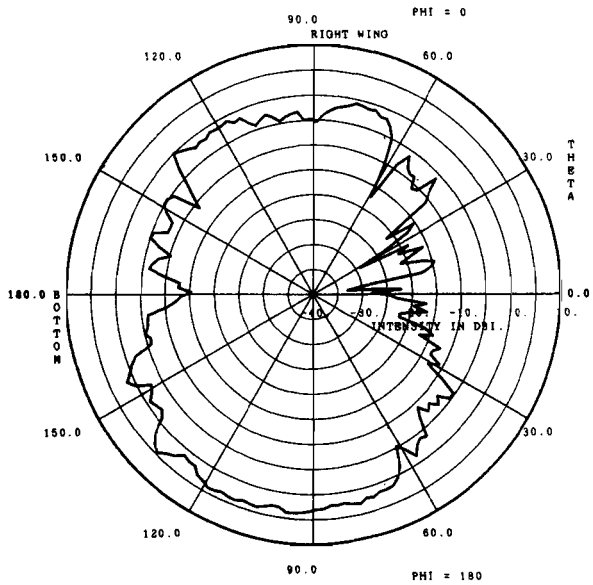

(b) wing to wing

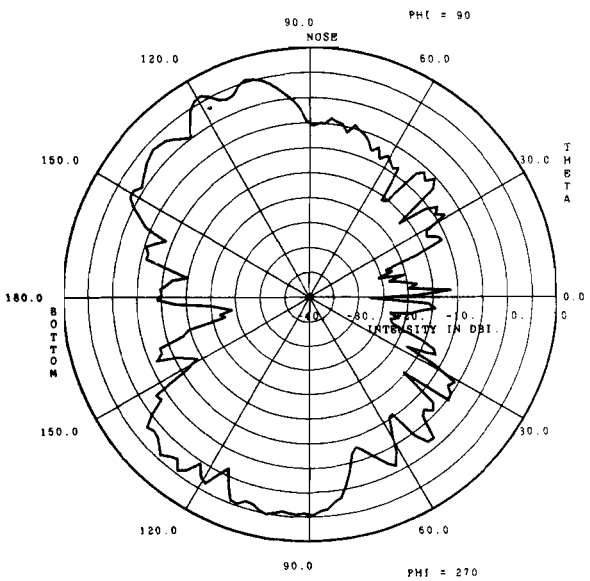

(c) nose to tail

ATC-47(B.7-10)

Fig. B.7-10. Beech Baron bottom-mounted rear, flaps down, wheels down

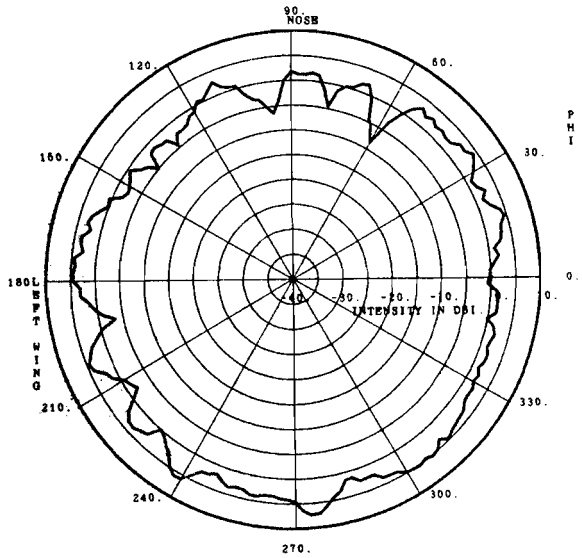

(a) horizontal plane

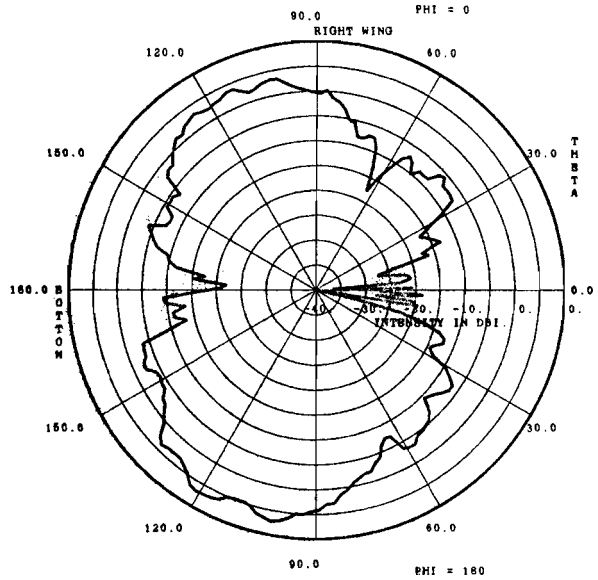

(b) wing to wing

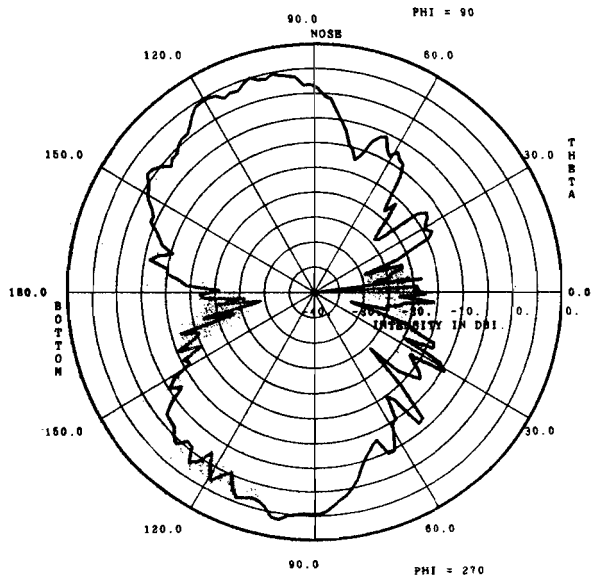

(c) nose to tail

ATC-47(B.7-11)

Fig. B. 7-11. Beech Baron bottom-mounted rear, flaps up, wheels up

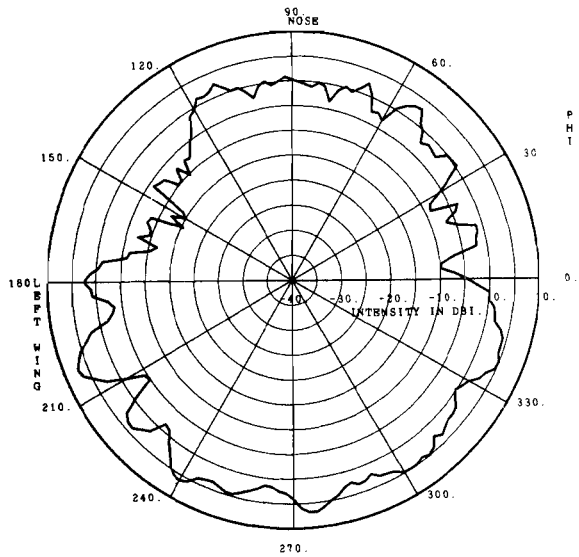

(a) horizontal plane

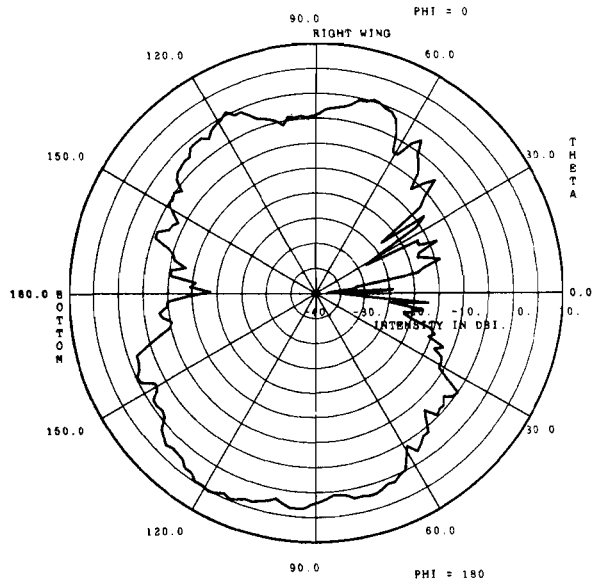

(b) wing to wing

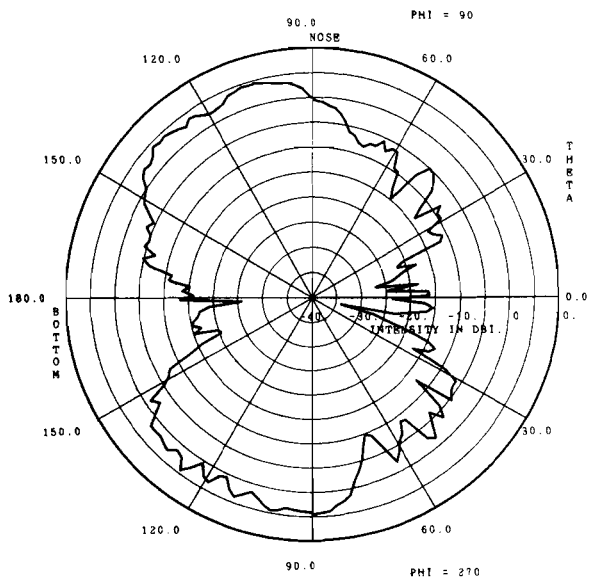

(c) nose to tail

ATC-47(B.7-12)

Fig. B.7-12. Beech Baron bottom-mounted rear, flaps down, wheels up

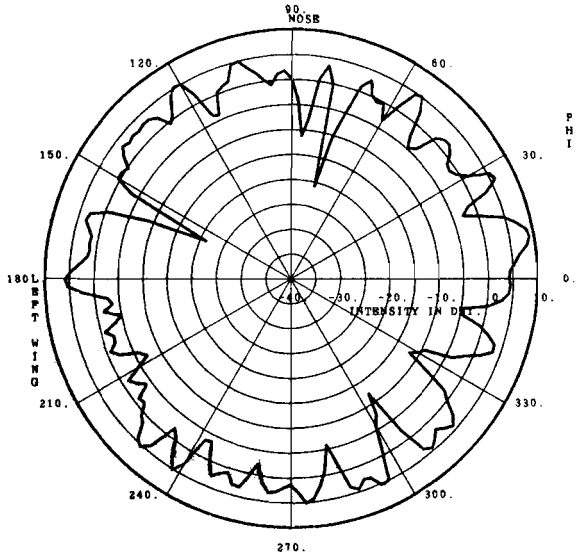

(a) horizontal plane

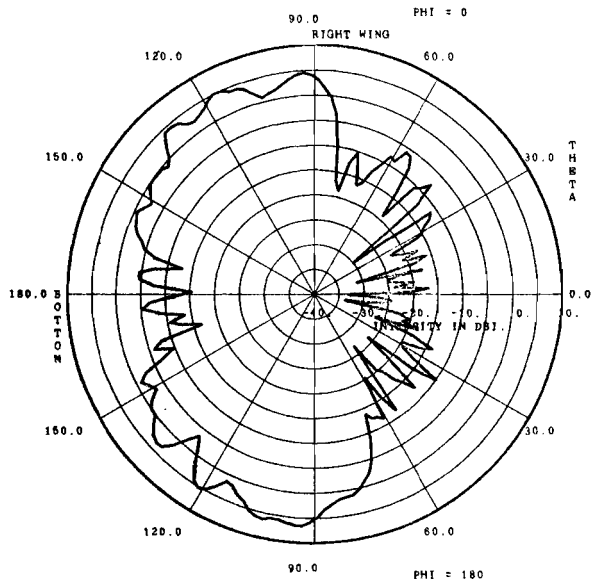

(b) wing to wing

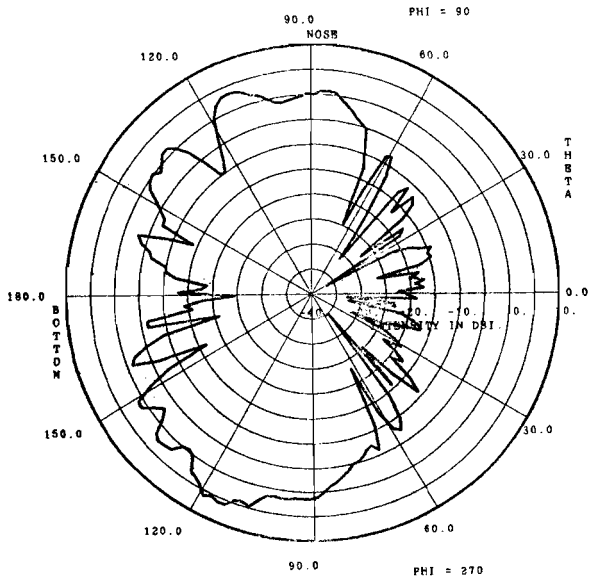

(c) nose to tail

ATC-47(B.7-13)

Fig. B. 7-13. Beech Baron bottom-mounted front, flaps down, wheels down

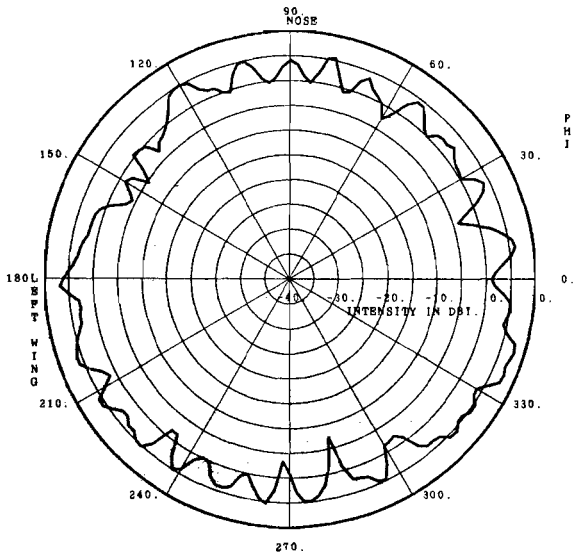

(a) horizontal plane

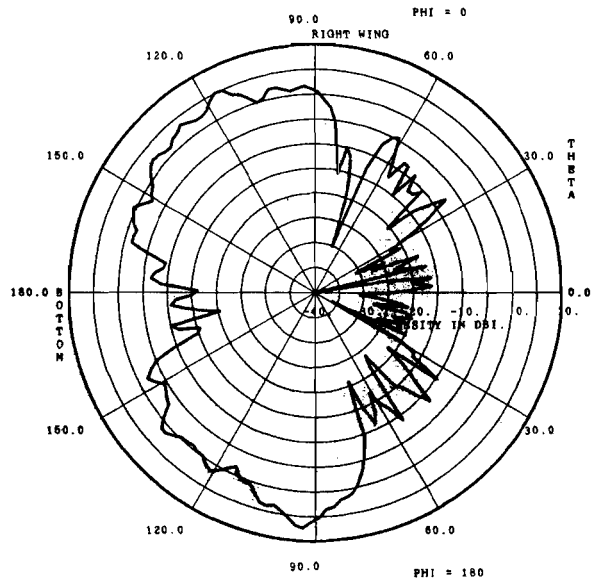

(b) wing to wing

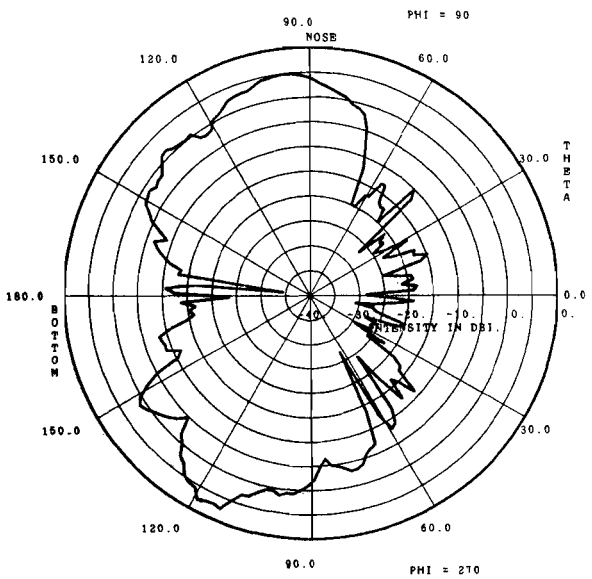

(c) nose to tail

ATC-47(B.7-14)

Fig. B. 7-14. Beech Baron bottom-mounted front, flaps up, wheels up

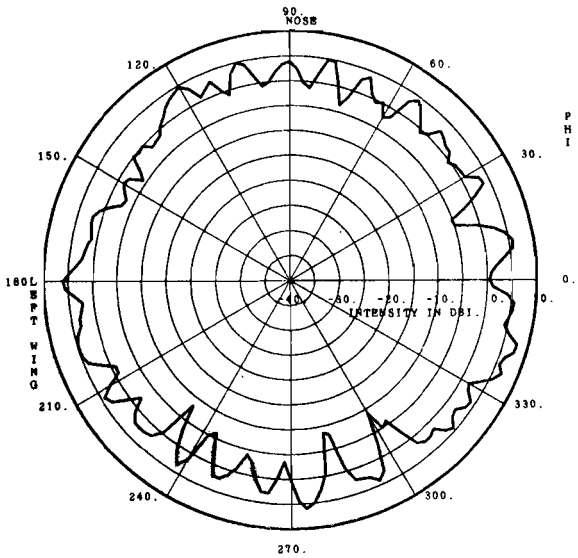

(a) horizontal plane

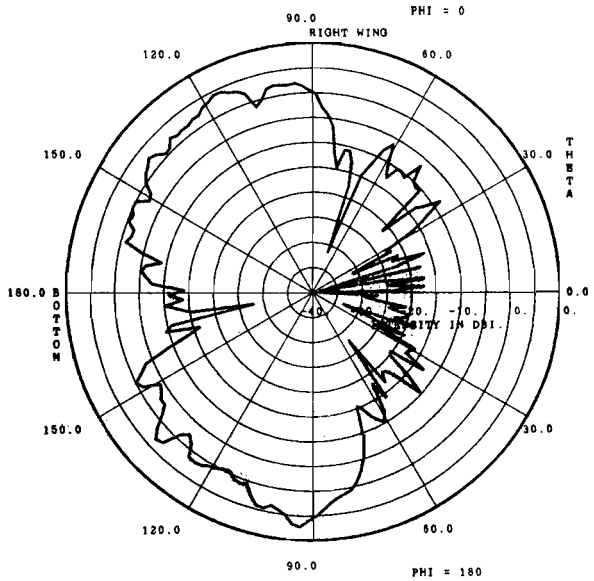

(b) wing to wing

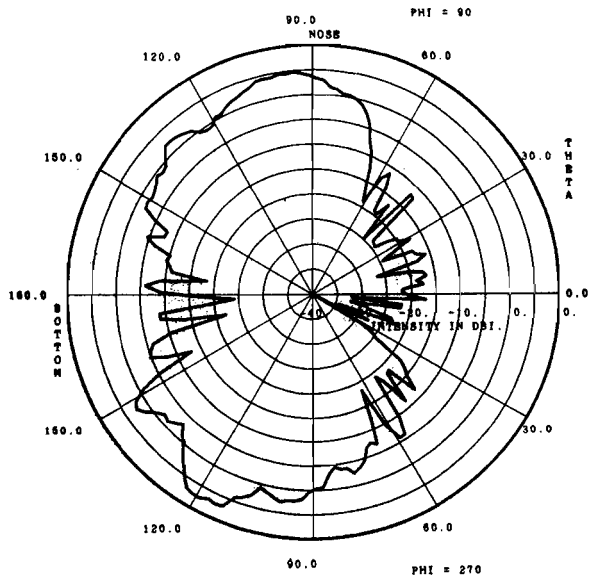

(c) nose to tail

ATC-47(B.7-15)

Fig. B. 7-15. Beech Baron bottom-mounted front, flaps down, wheels up

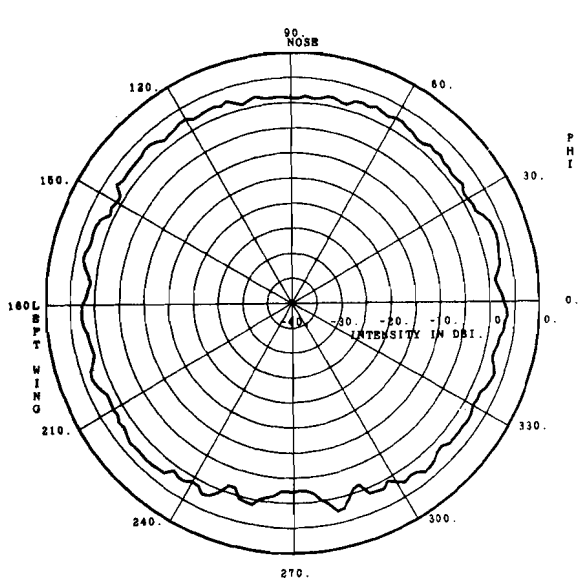

(a) horizontal plane

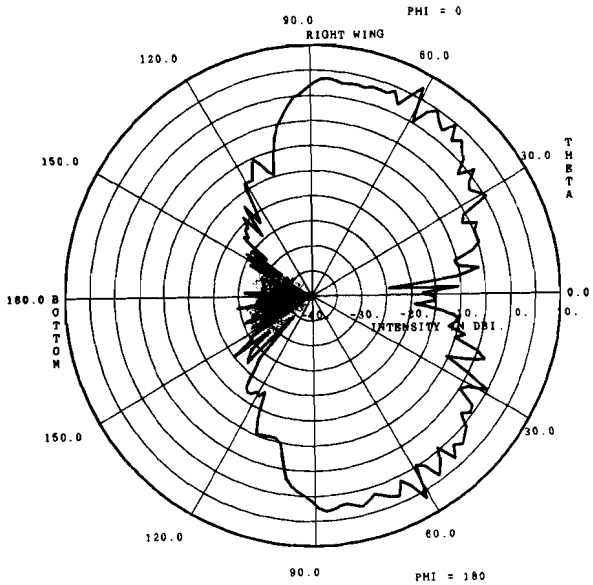

(b) wing to wing

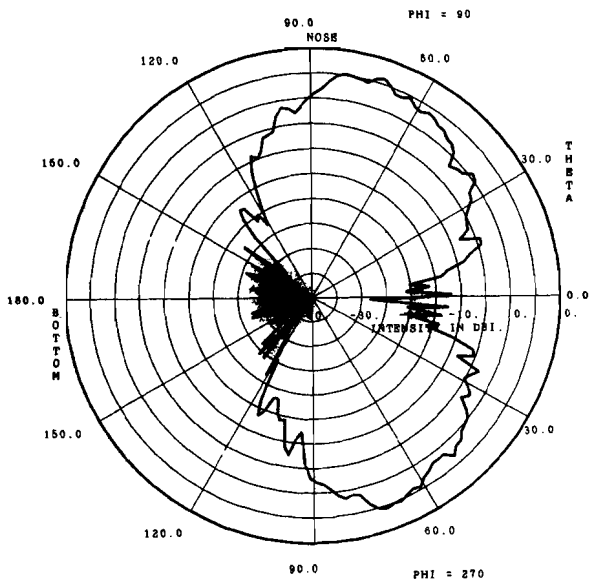

(c) nose to tail

ATC-47(B.8-1)

Fig. B. 8-1. Beech B-99 top-mounted rear, flaps up, wheels down

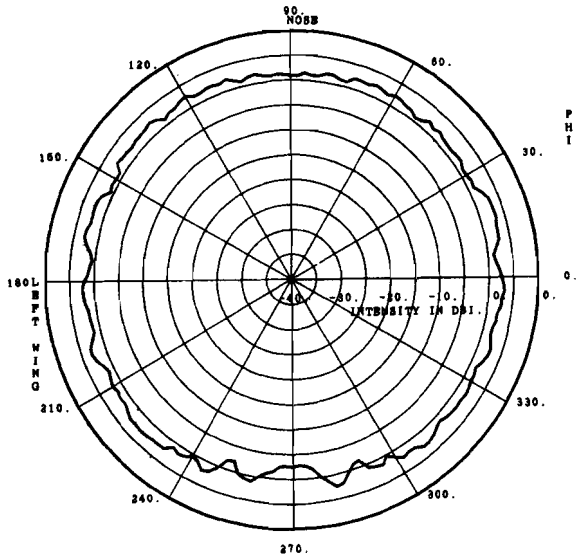

(a) horizontal plane

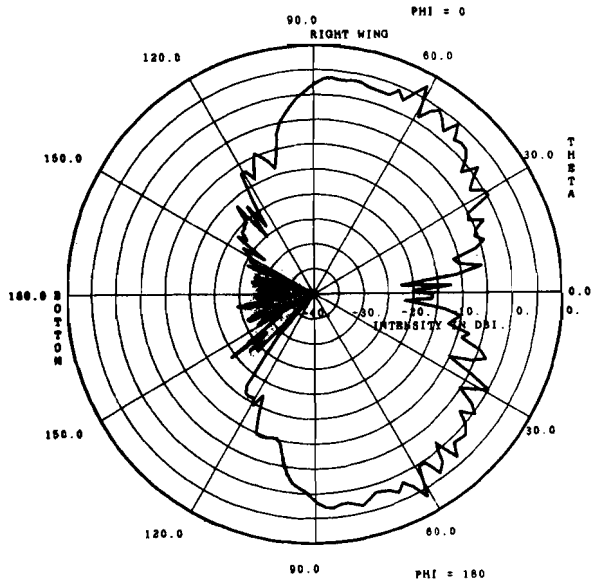

(b) wing to wing

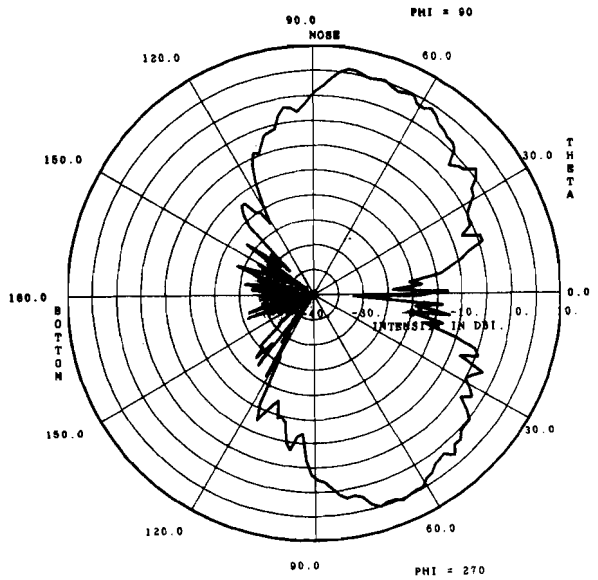

(c) nose to tail

ATC-47(B.8-2)

Fig. B.8-2. Beech B-99 top-mounted rear, flaps down, wheels down

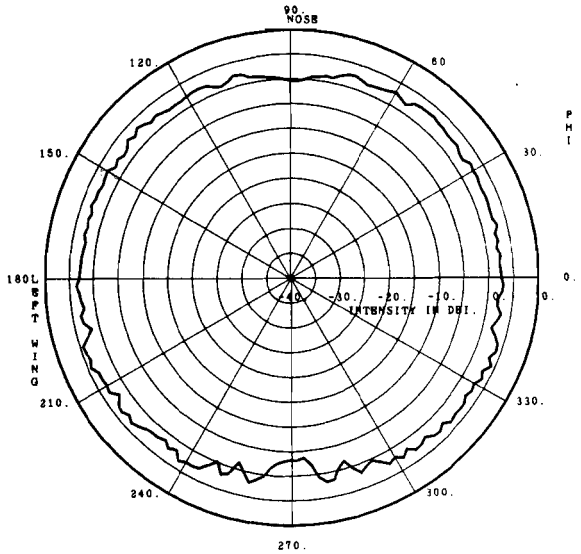

(a) horizontal plane

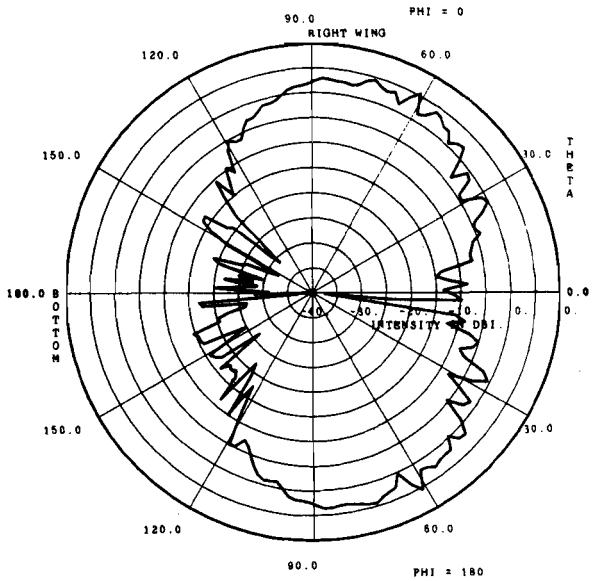

(b) wing to wing

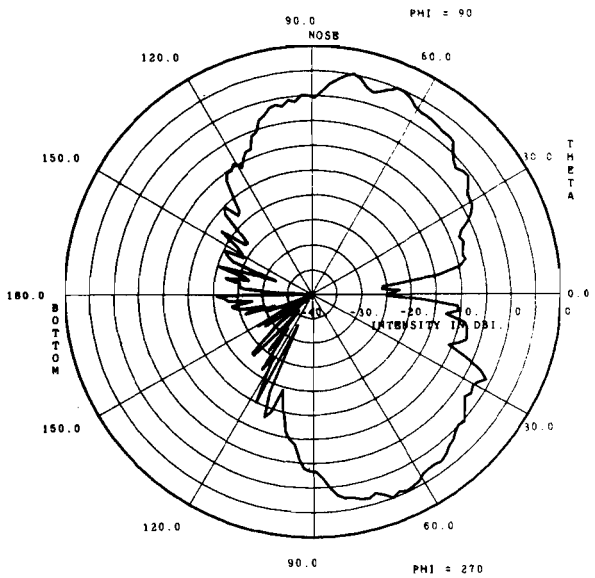

(c) nose to tail

ATC-47(B.8-3)

Fig. B.8-3. Beech B-99 top-mounted front, flaps down, wheels down

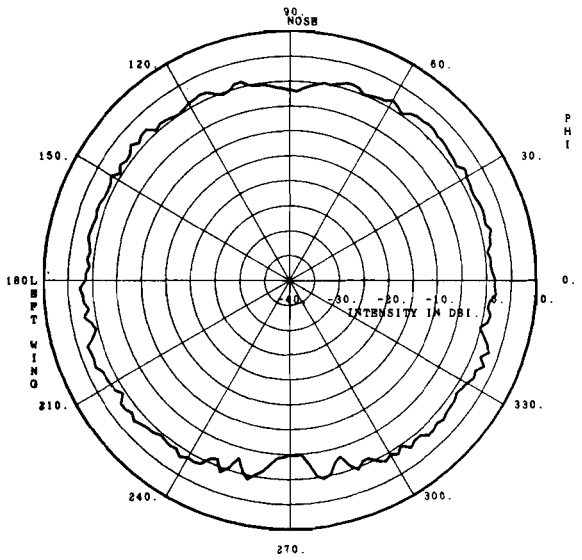

(a) horizontal plane

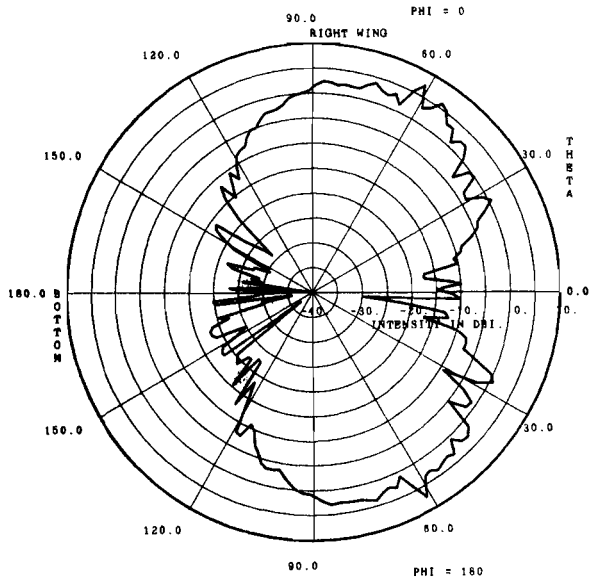

(b) wing to wing

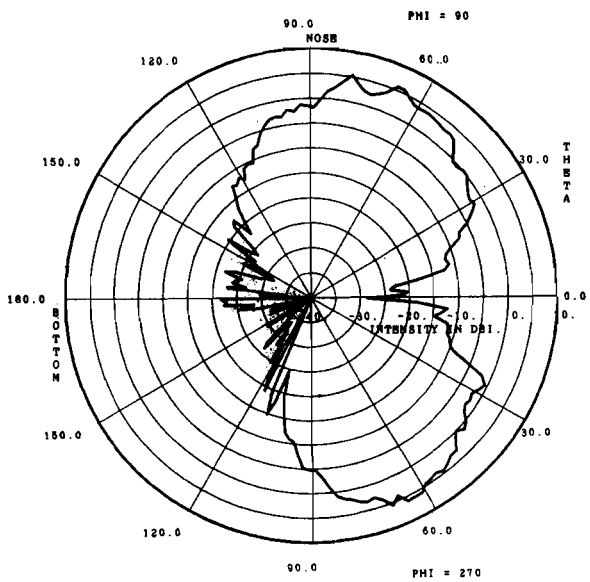

(c) nose to tail

ATC-47(B.8-4)

Fig. B. 8-4. Beech B-99 top-mounted front, flaps up, wheels up

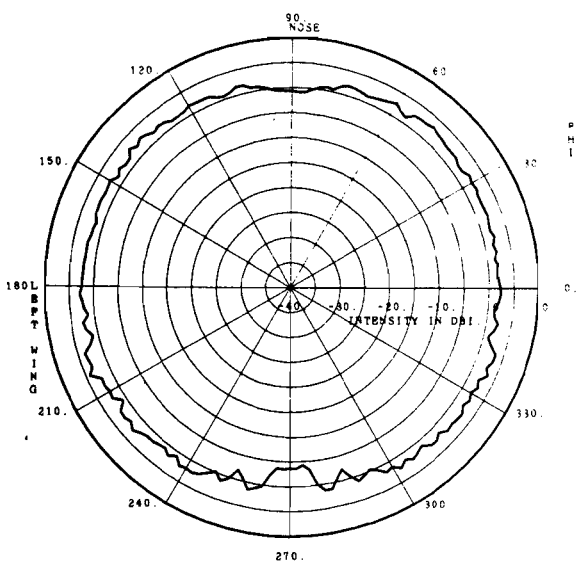

(a) horizontal plane

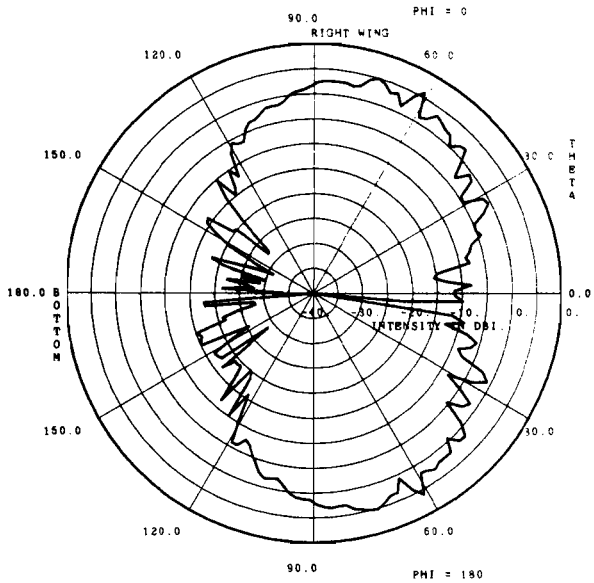

(b) wing to wing

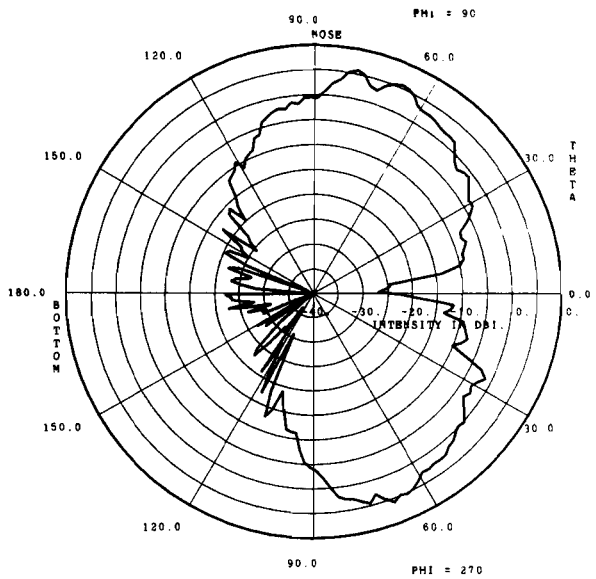

(c) nose to tail

ATC-47(B.8-5)

Fig. B.8-5. Beech B-99 top-mounted front, flaps down, wheels up

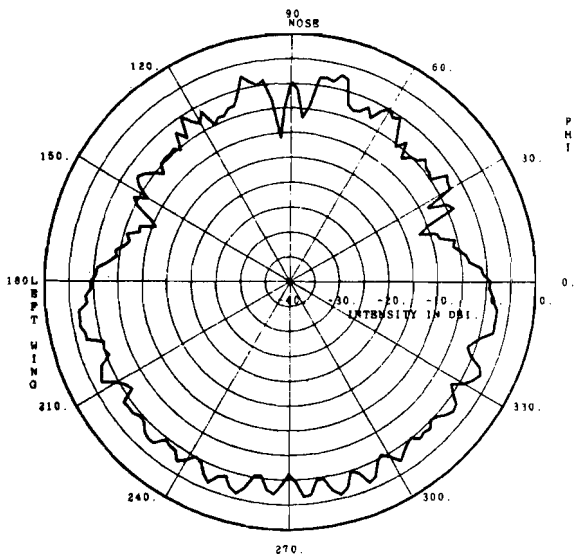

(a) horizontal plane

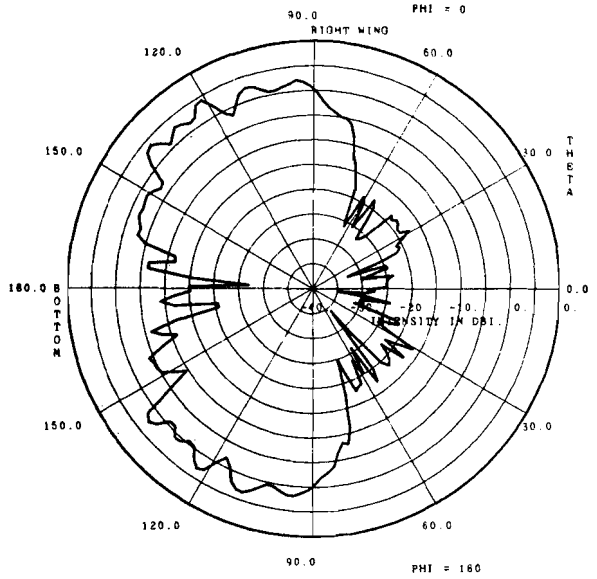

(b) wing to wing

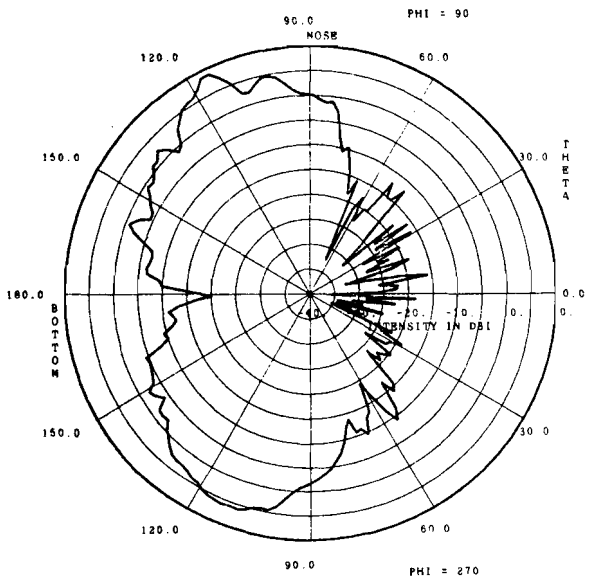

(c) nose to tail

ATC-47(B.8-6)

Fig. B.8-6. Beech B-99 bottom-mounted rear, flaps up, wheels down

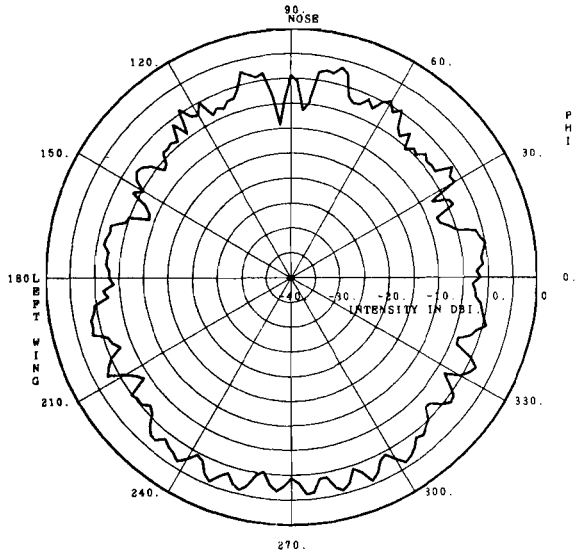

(a) horizontal plane

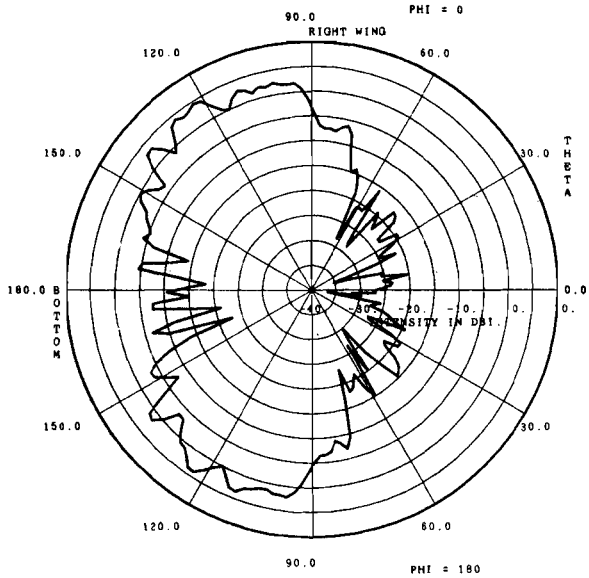

(b) wing to wing

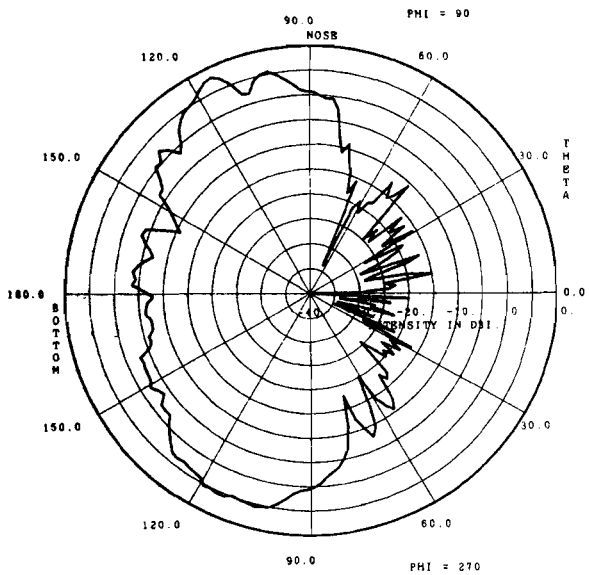

(c) nose to tail

ATC-47(B.8-7)

Fig. B. 8-7. Beech B-99 bottom-mounted rear, flaps down, wheels down

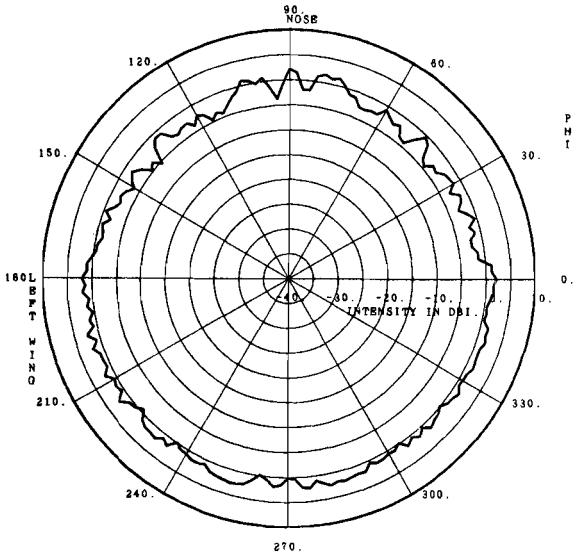

(a) horizontal plane

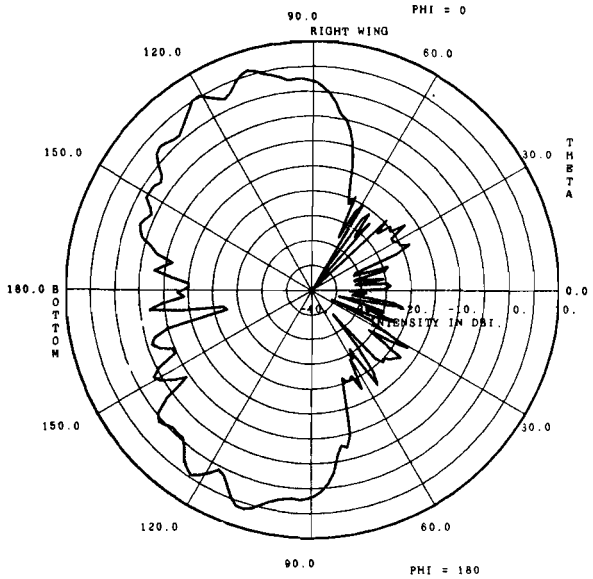

(b) wing to wing

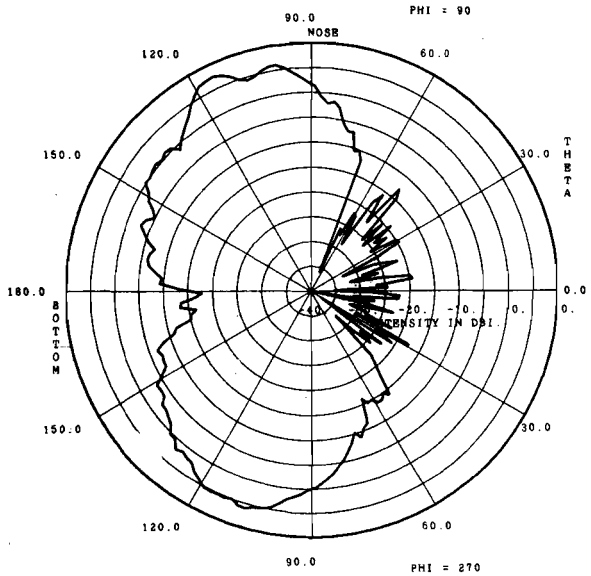

(c) nose to tail

ATC-47(B.8-8)

Fig. B. 8-8. Beech B-99 bottom-mounted rear, flaps up, wheels up

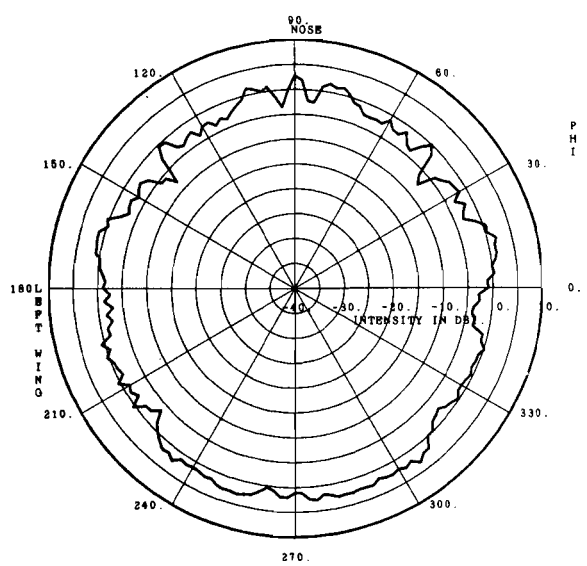

(a) horizontal plane

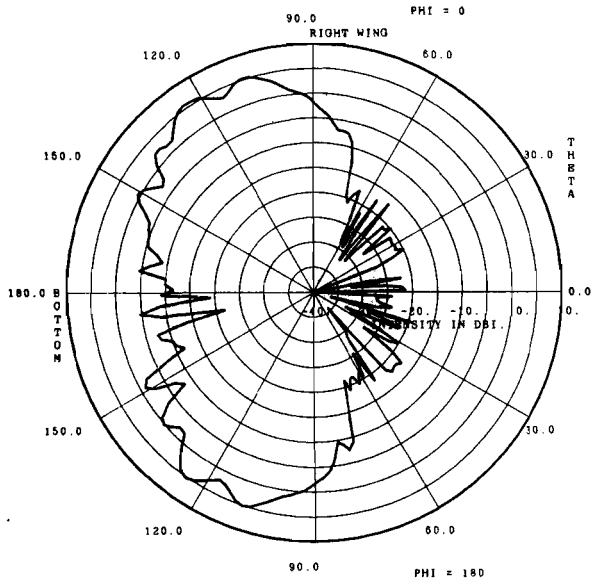

(b) wing to wing

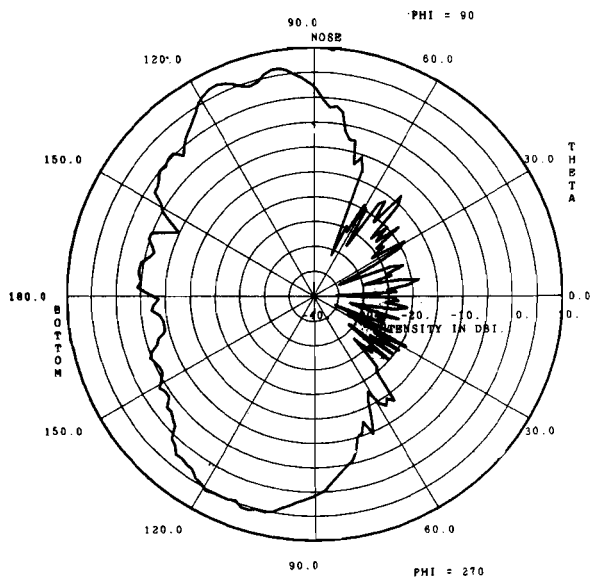

(c) nose to tail

ATC-47(B.8-9)

Fig. B. 8-9. Beech B-99 bottom-mounted rear, flaps down, wheels up

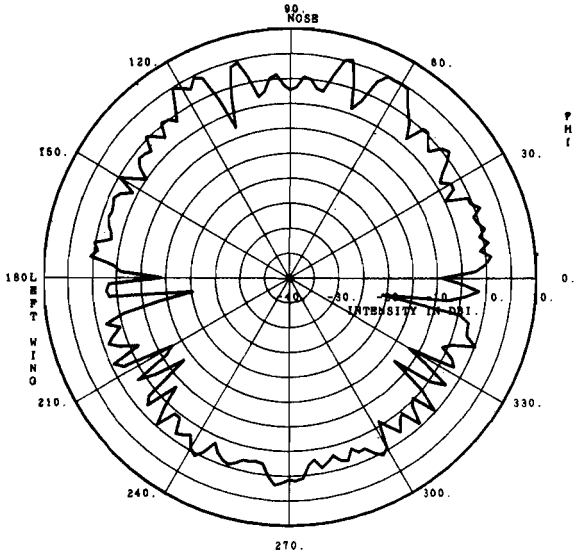

(a) horizontal plane

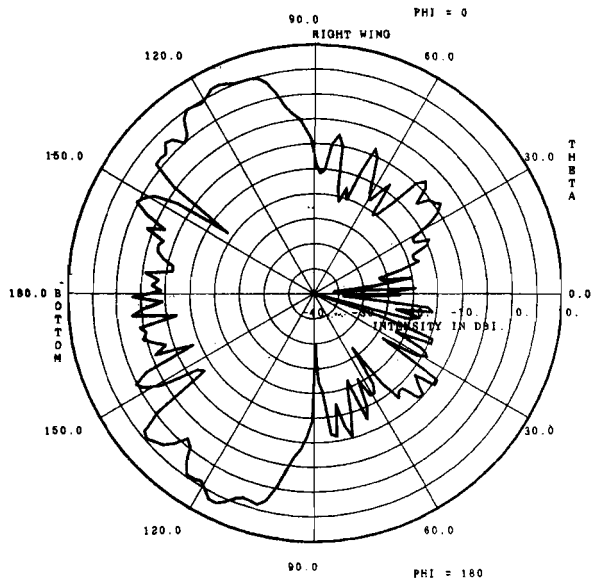

(b) wing to wing

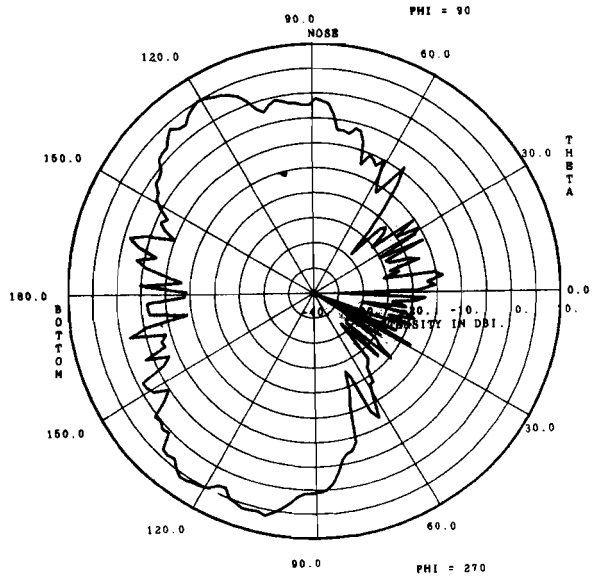

(c) nose to tail

ATC-47(B.8-10)

Fig. B.8-10. Beech B-99 bottom-mounted center, flaps down, wheels down

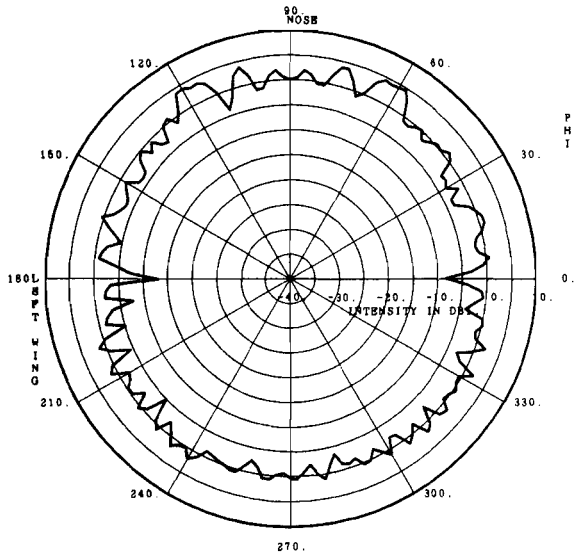

(a) horizontal plane

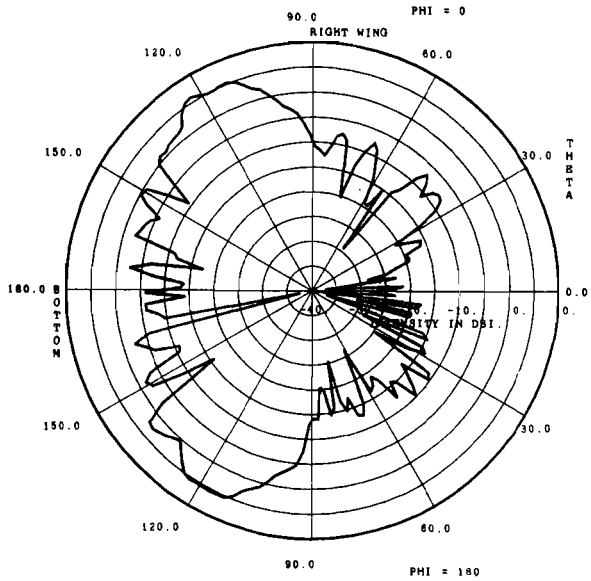

(b) wing to wing

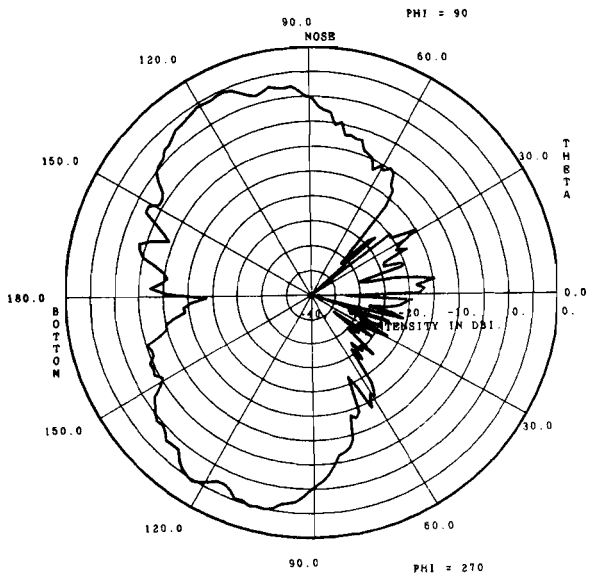

(c) nose to tail

ATC-47(B.8-11)

Fig. B.8-11. Beech B-99 bottom-mounted center, flaps up, wheels up

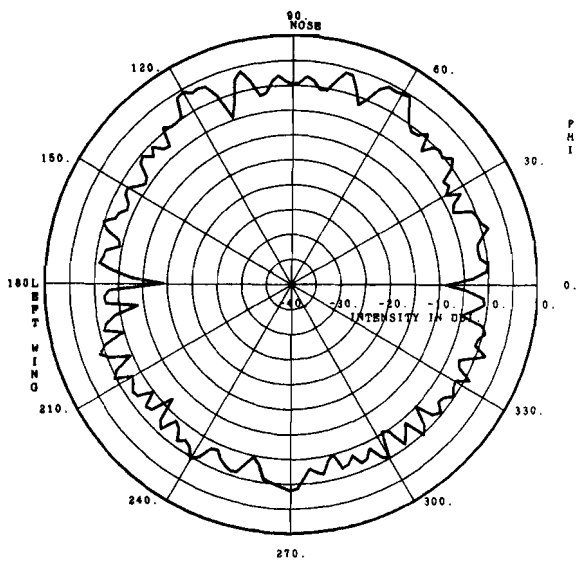

(a) horizontal plane

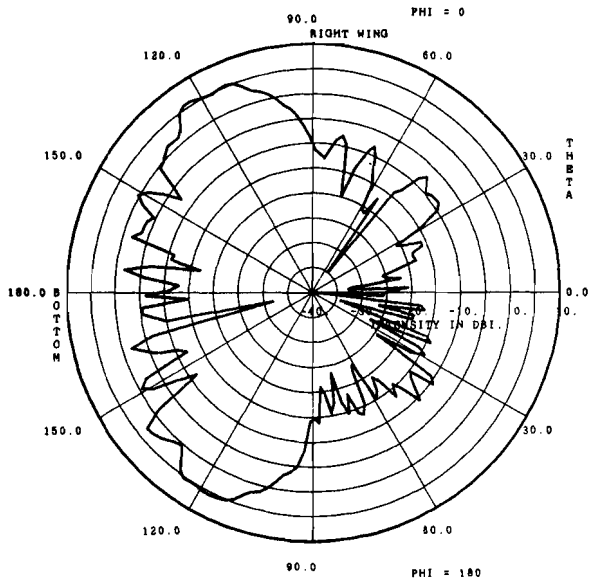

(b) wing to wing

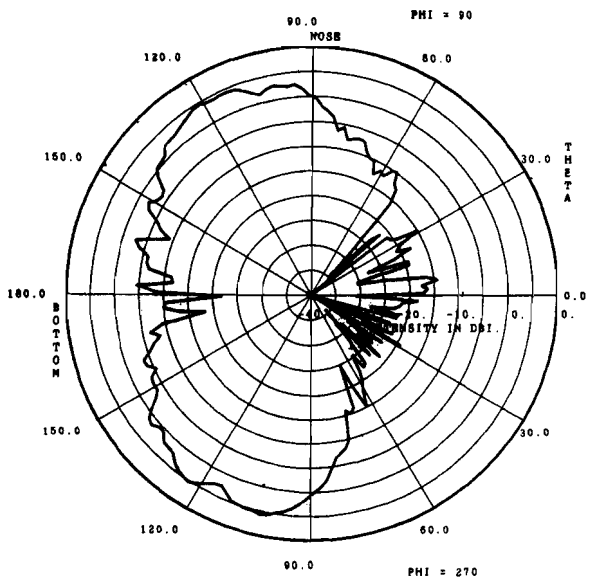

(c) nose to tail

ATC-47(B.8-12)

Fig. B.8-12. Beech B-99 bottom-mounted center, flaps down, wheels up

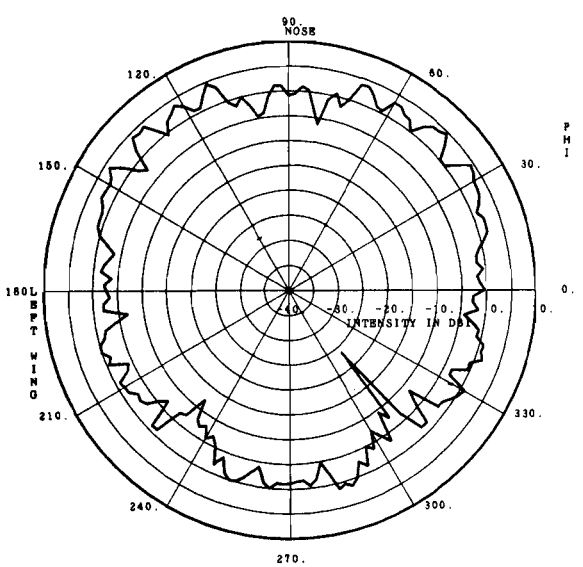

(a) horizontal plane

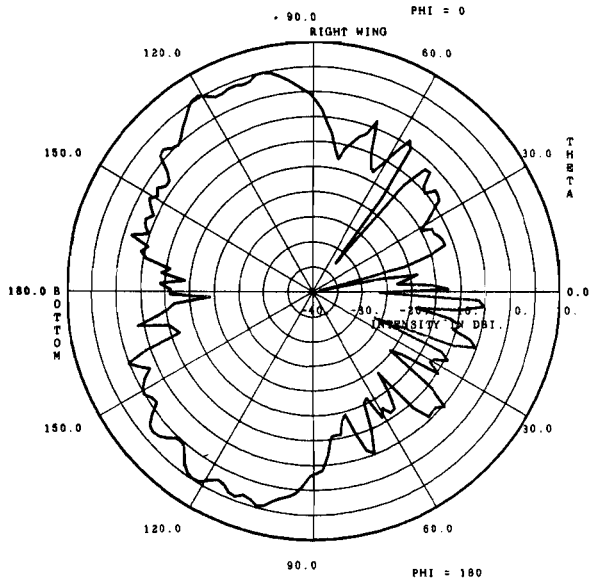

(b) wing to wing

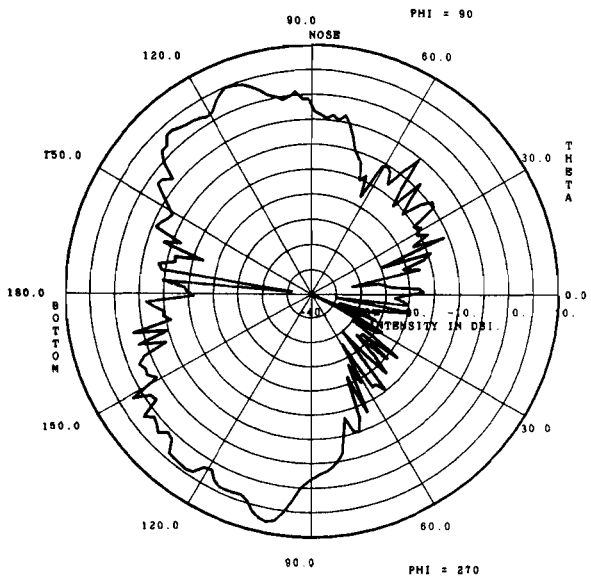

(c) nose to tail

ATC-47(B.8-13)

Fig. B.8-13. Beech B-99 bottom-mounted front, flaps down, wheels down

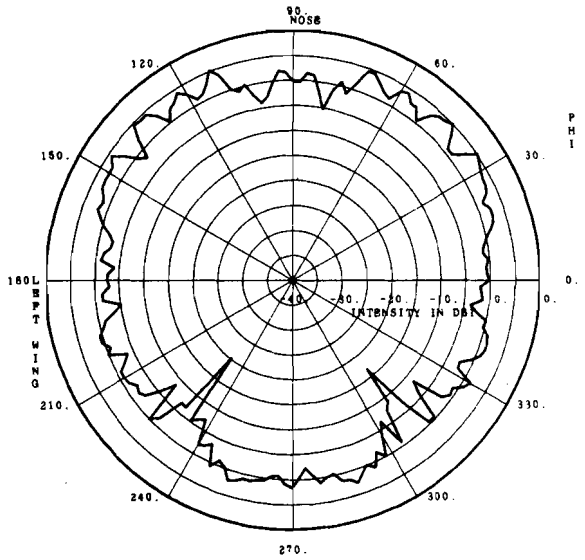

(a) horizontal plane

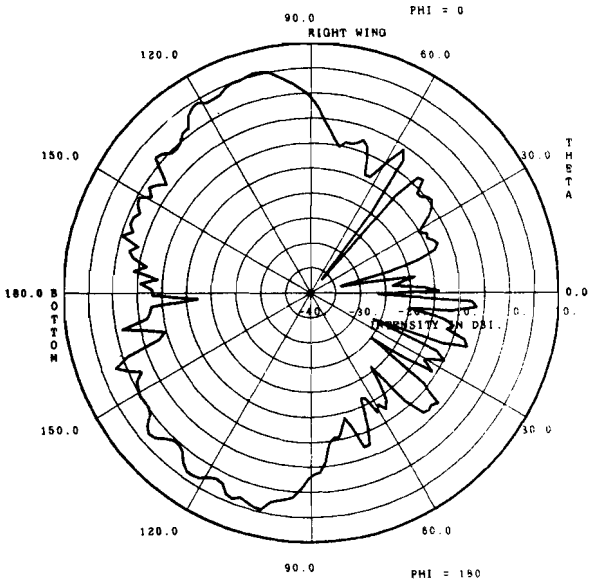

(b) wing to wing

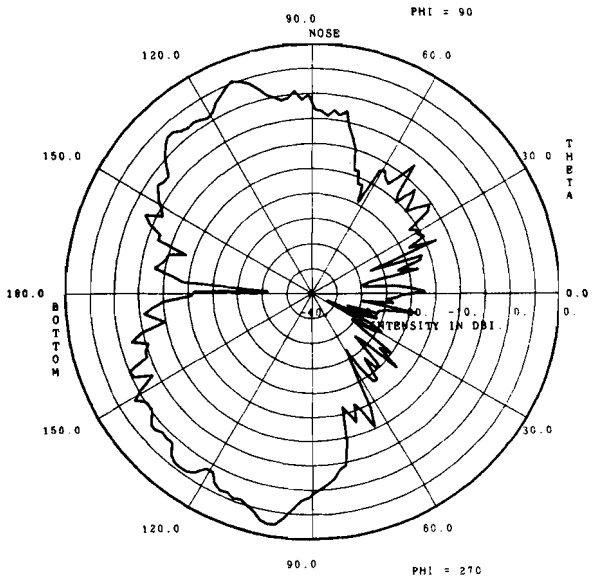

(c) nose to tail

ATC-47(B.8-14)

Fig. B.8-14. Beech B-99 bottom-mounted front, flaps up, wheels up

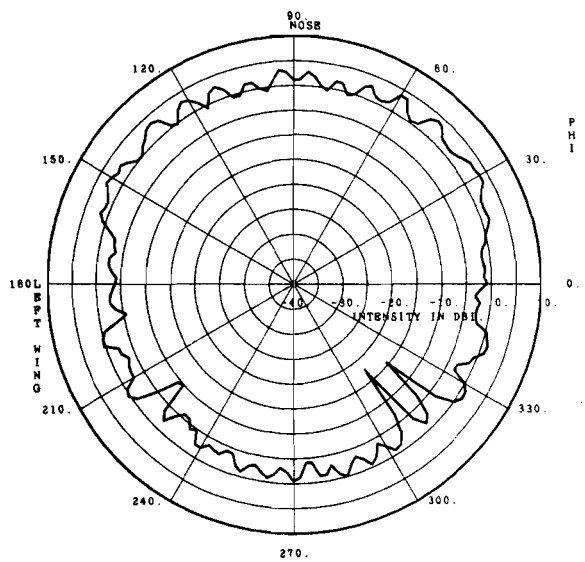

(a) horizontal plane

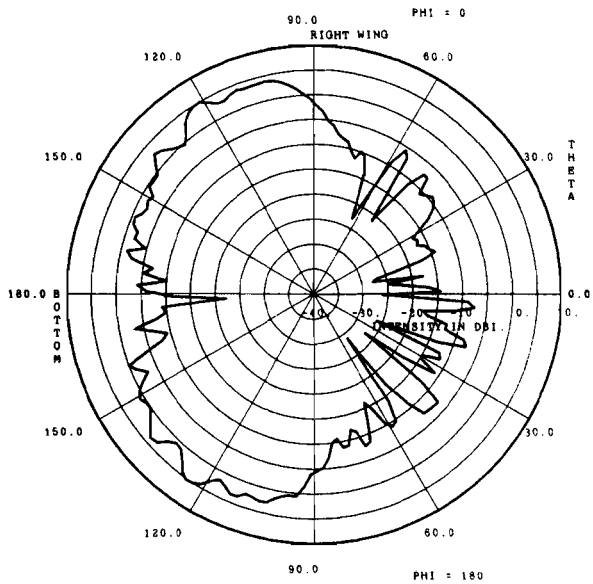

(b) wing to wing

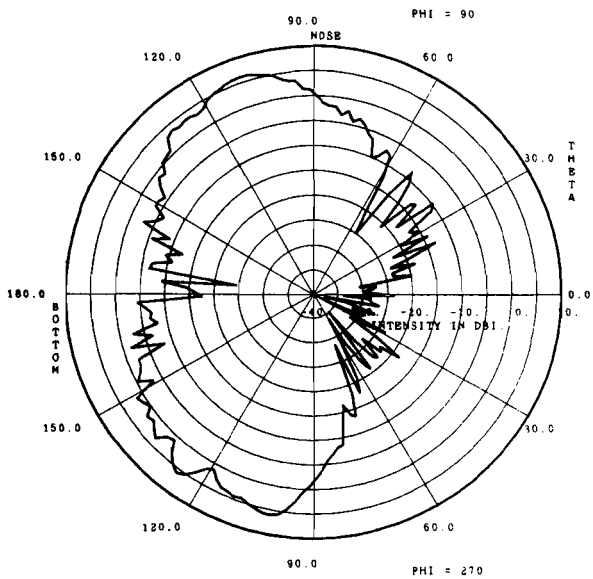

(c) nose to tail

ATC-47(B.8-15)

Fig. B. 8-15. Beech B-99 bottom-mounted front, flaps down, wheels up

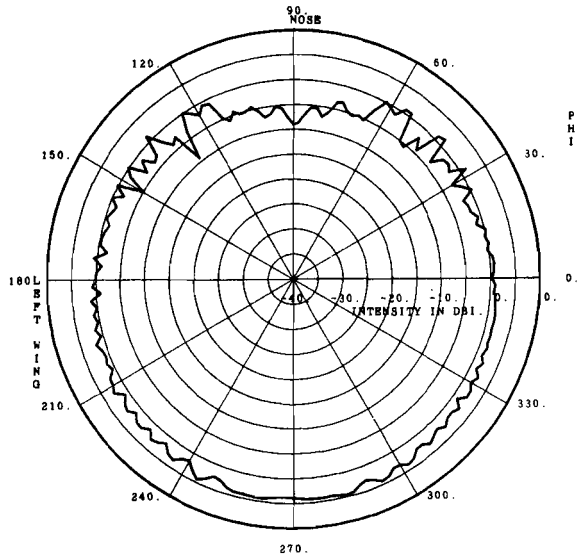

(a) horizontal plane

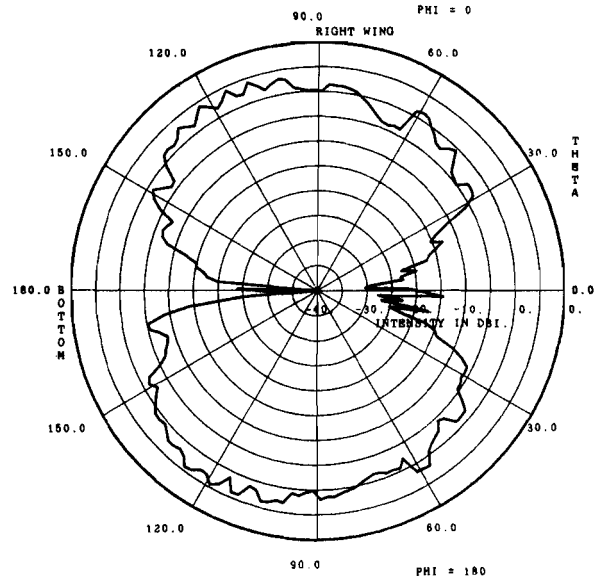

(b) wing to wing

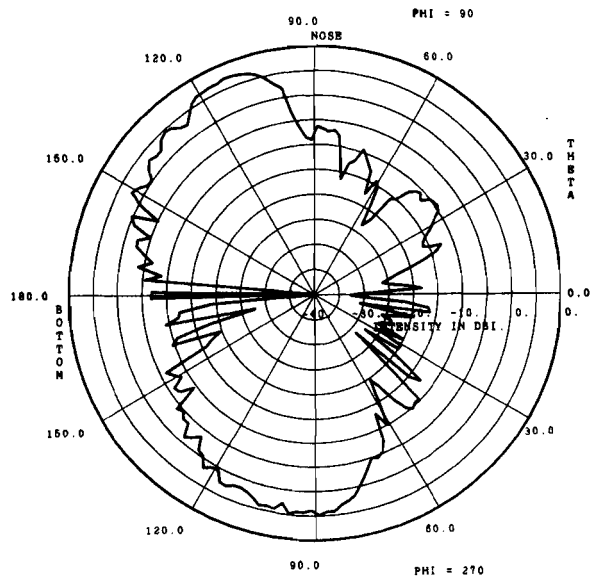

(c) nose to tail

ATC-47(B.10-1)

Fig. B.10-1. Helio U-10/D bottom-mounted rear, flaps up, wheels down

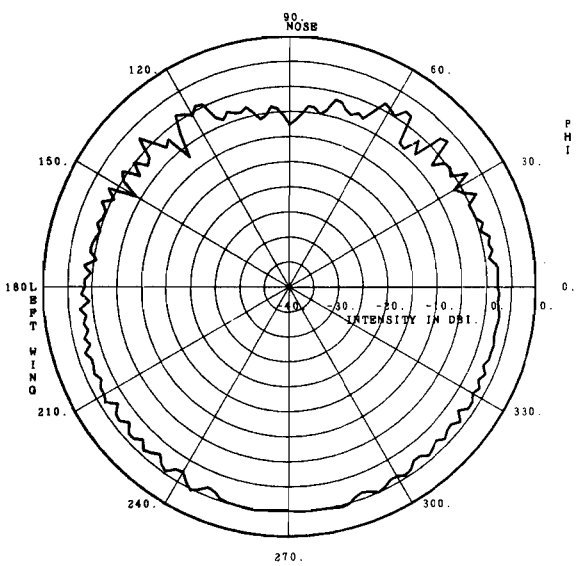

(a) horizontal plane

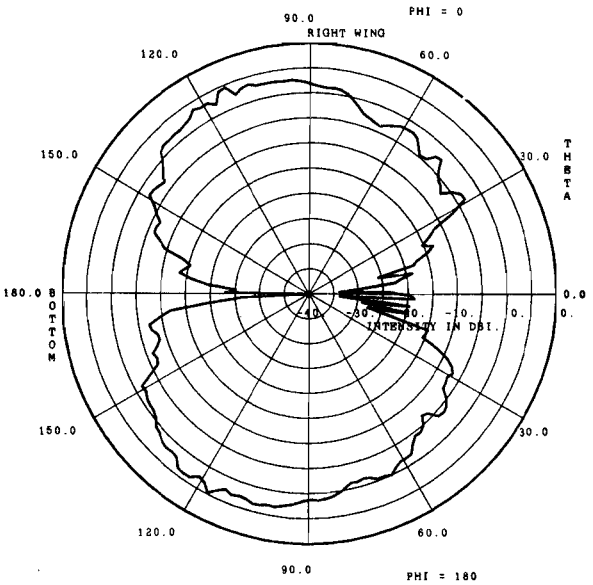

(b) wing to wing

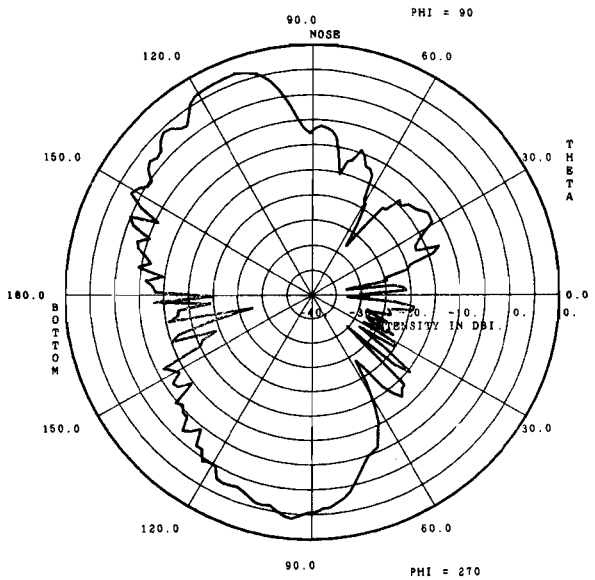

(c) nose to tail

ATC-47(B.10-2)

Fig. B.10-2. Helio U-10/D bottom-mounted rear, flaps down, wheels down

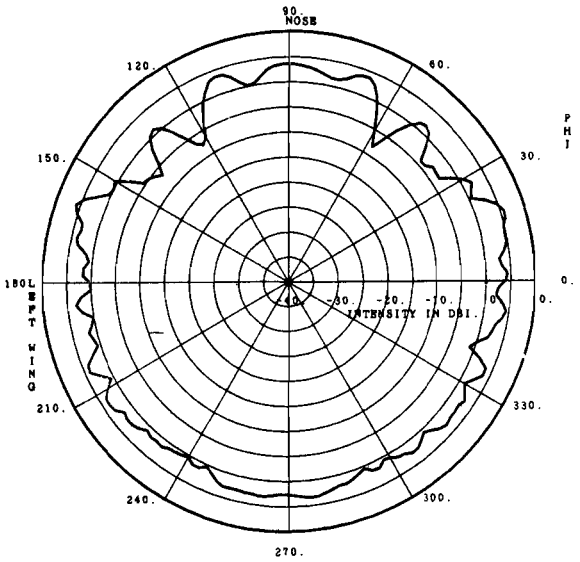

(a) horizontal plane

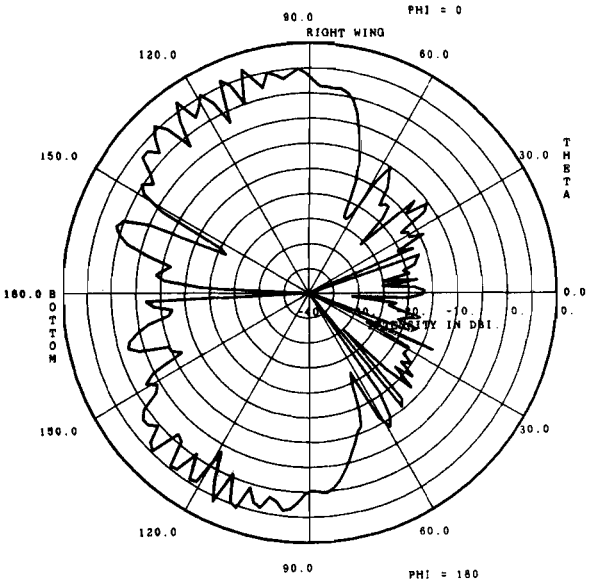

(b) wing to wing

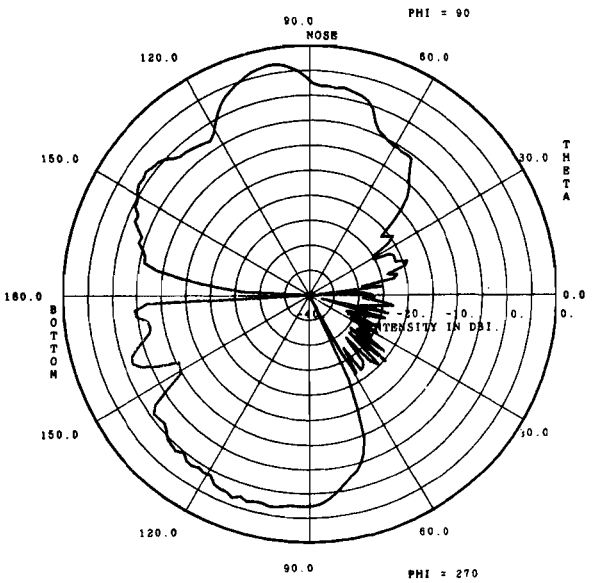

(c) nose to tail

ATC-47(B.10-3)

Fig. B. 10-3. Helio U-10/D bottom-mounted front, flaps up, wheels down

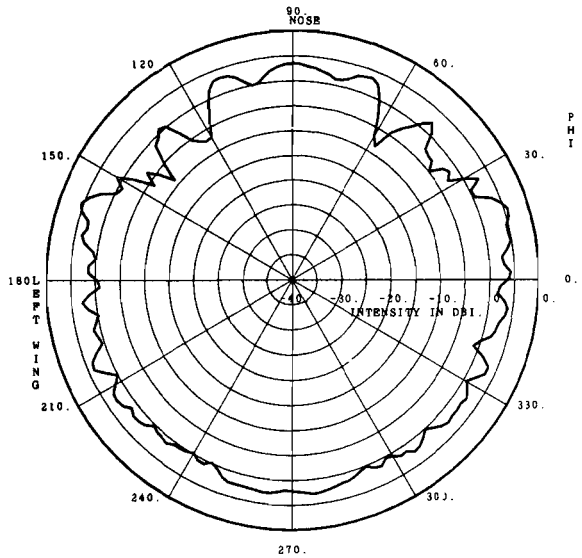

(a) horizontal plane

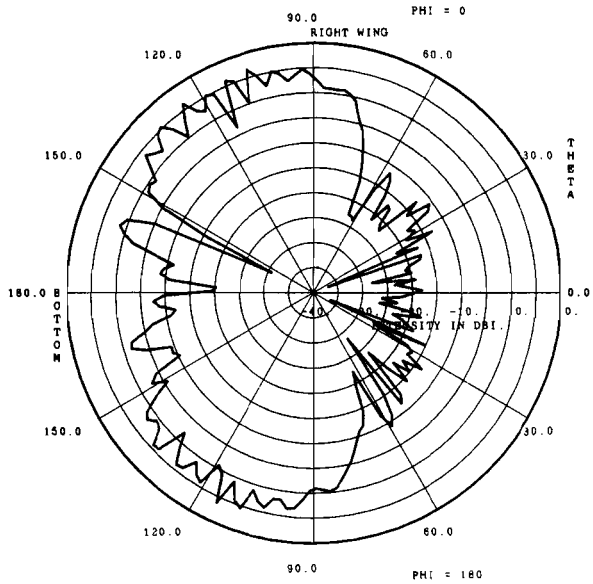

(b) wing to wing

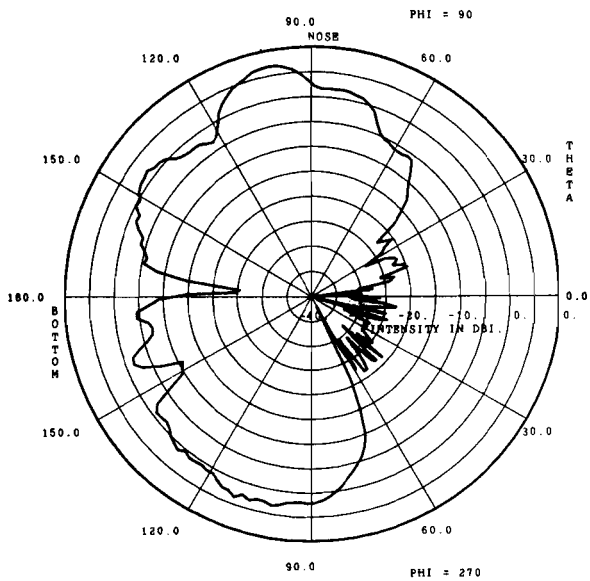

(c) nose to tail

ATC-47(B.10-4)

Fig. B.10-4. Helio U-10/D bottom-mounted front, flaps down, wheels down

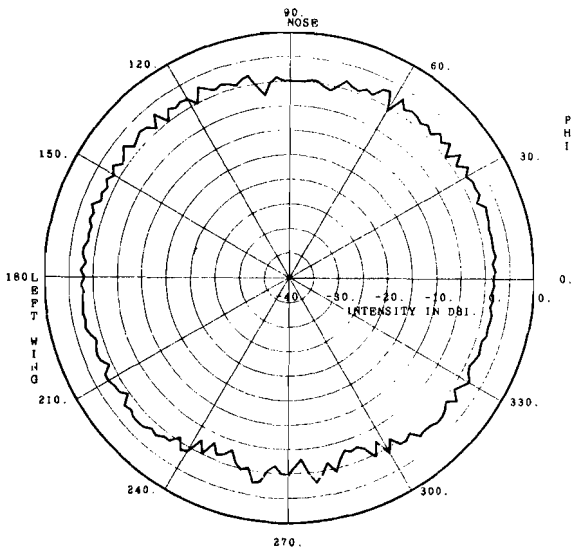

(a) horizontal plane

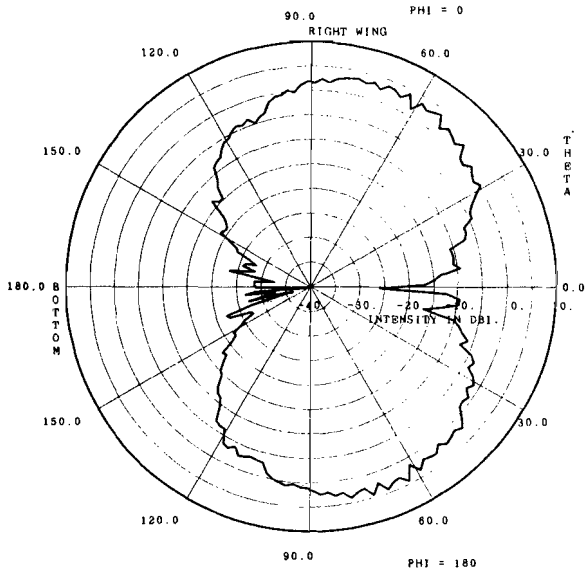

(b) wing to wing

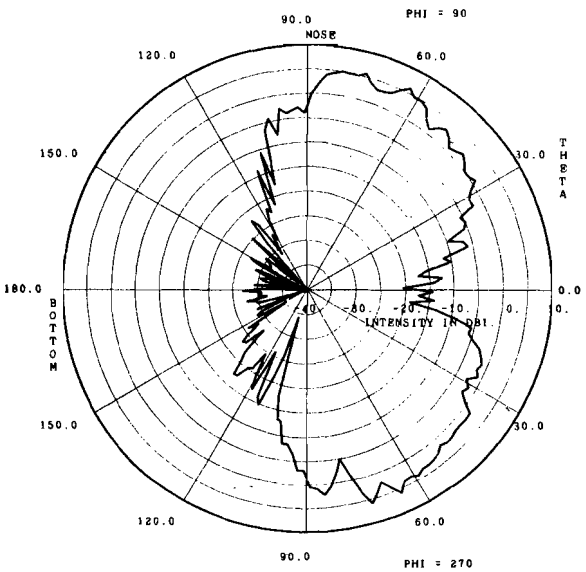

(c) nose to tail

ATC-47(B.11-1)

Fig. B.11-1. Grumman Gulfstream top-mounted rear, flaps up, wheels down

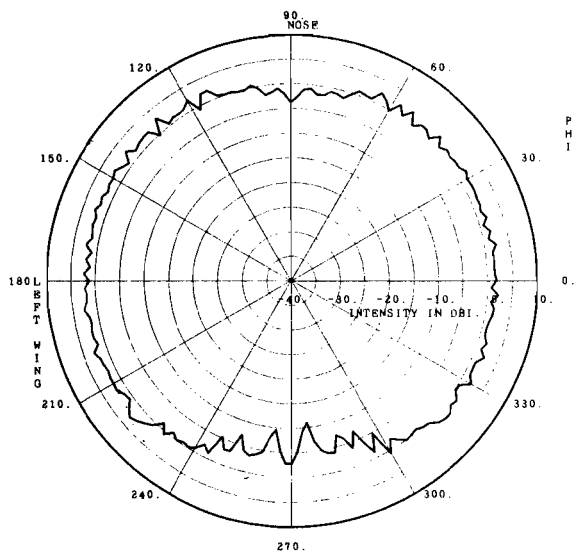

(a) horizontal plane

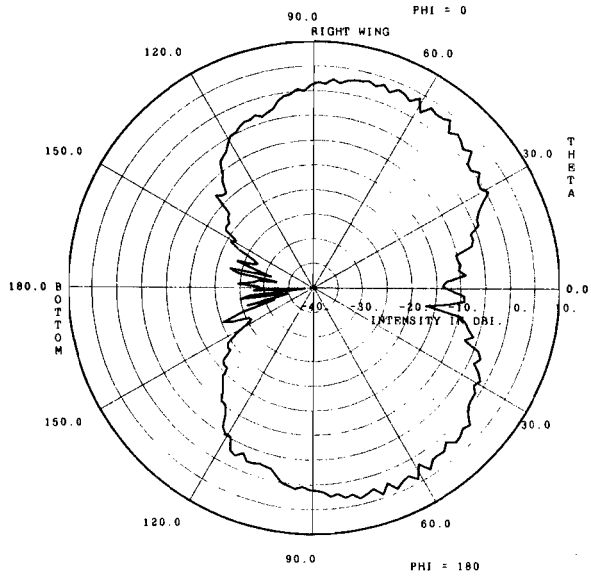

(b) wing to wing

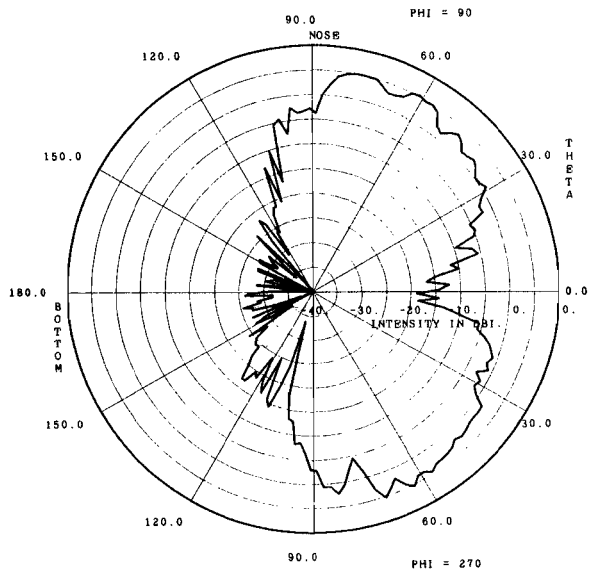

(c) nose to tail

ATC-47(B.11-2)

Fig. B.11-2. Grumman Gulfstream top-mounted rear, flaps down, wheels down

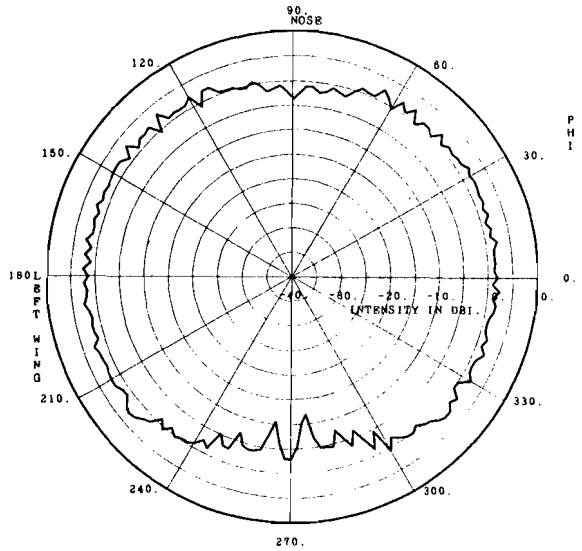

(a) horizontal plane

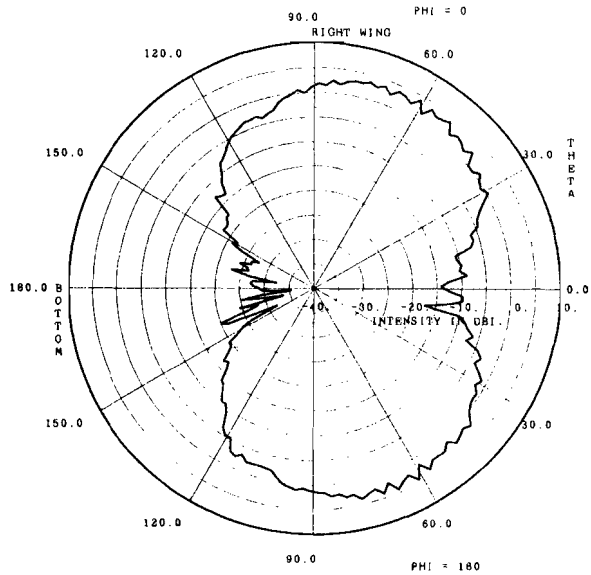

(b) wing to wing

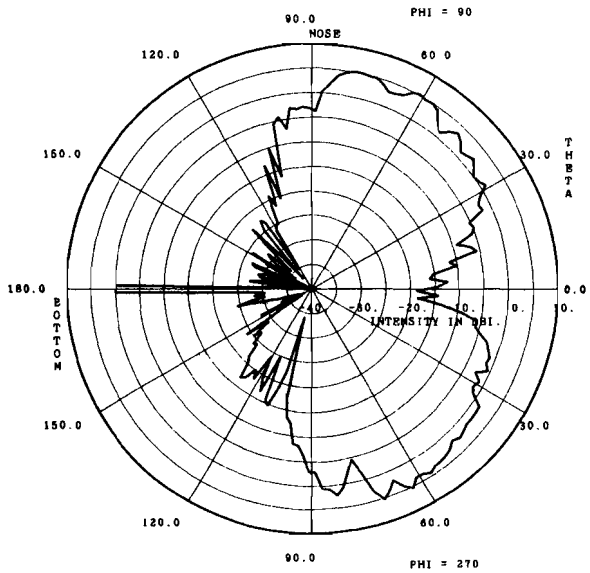

(c) nose to tail

ATC-47(B.11-3)

Fig. B.11-3. Grumman Gulfstream top-mounted rear, flaps down, wheels up

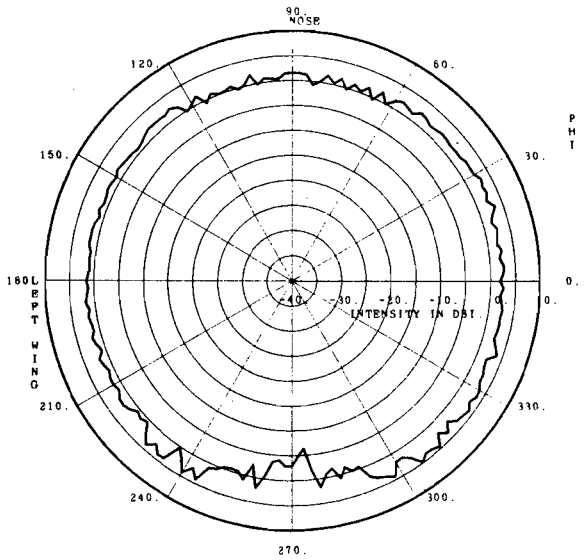

(a) horizontal plane

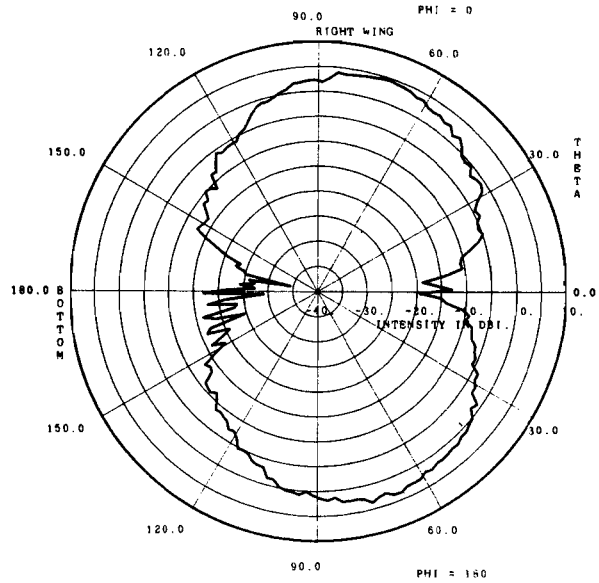

(b) wing to wing

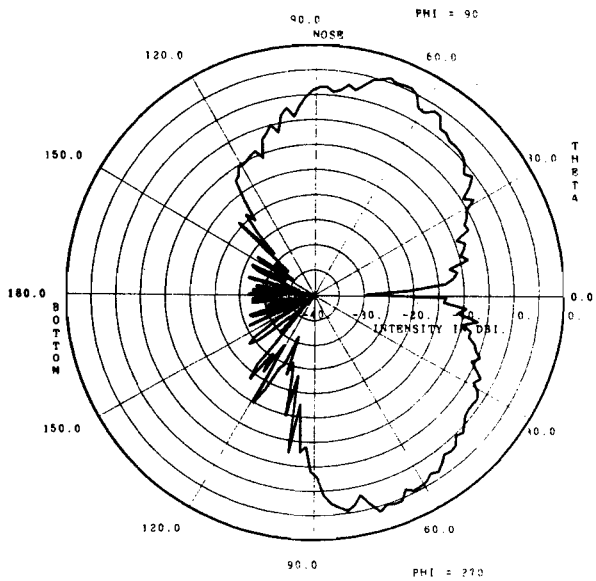

(c) nose to tail

ATC-47(B.11-4)

Fig. B.11-4. Grumman Gulfstream top-mounted front, flaps up, wheels down

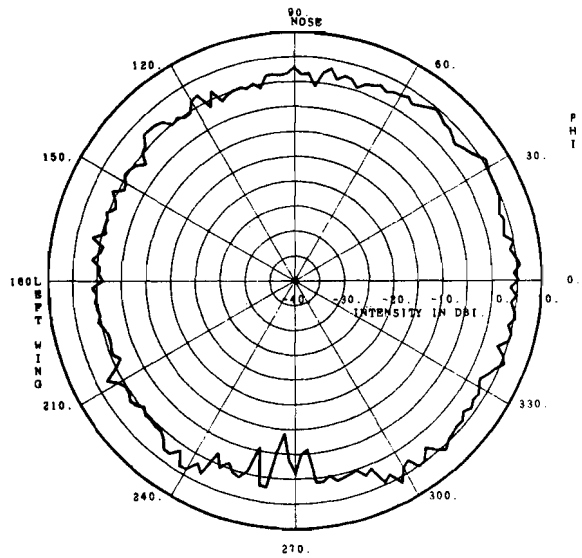

(a) horizontal plane

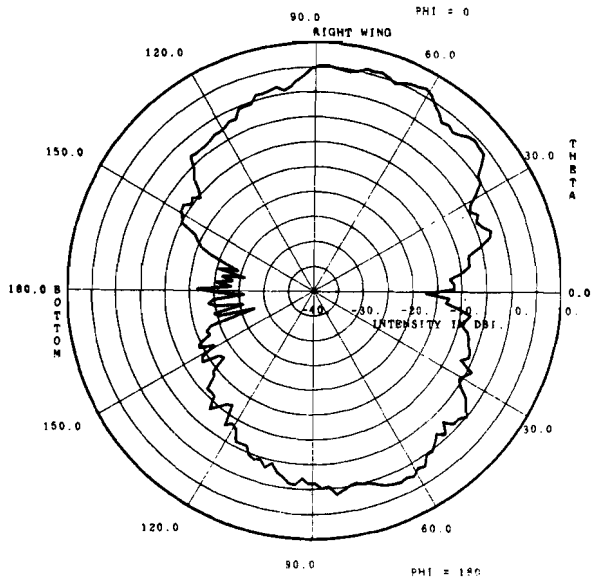

(b) wing to wing

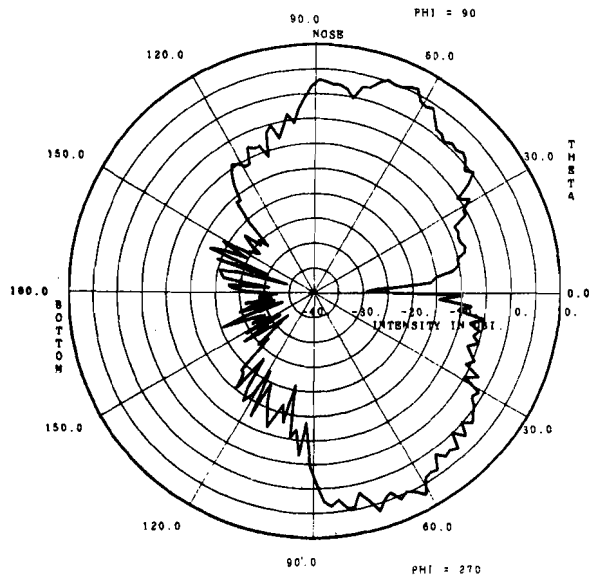

(c) nose to tail

ATC-47(B.11-5)

Fig. B. 11-5. Grumman Gulfstream top-mounted front, flaps up, wheels up

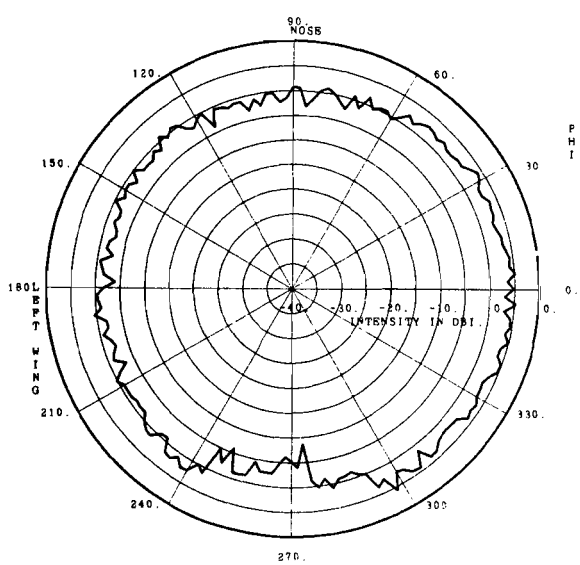

(a) horizontal plane

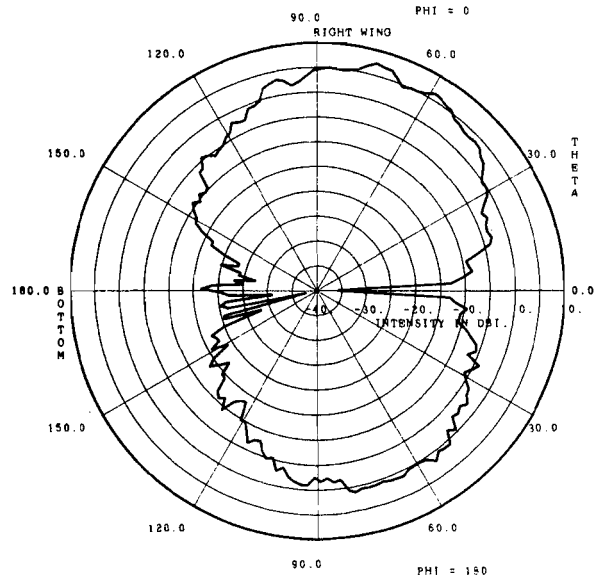

(b) wing to wing

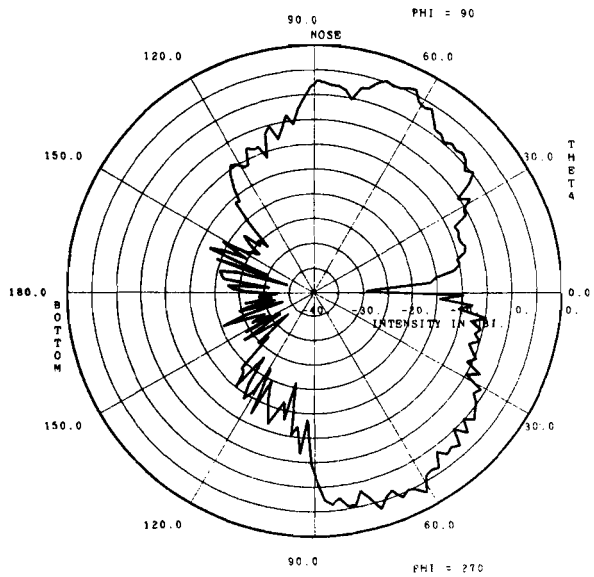

(c) nose to tail

ATC-47(B.11-6)

Fig. B.11-6. Grumman Gulfstream top-mounted front, flaps down, wheels up

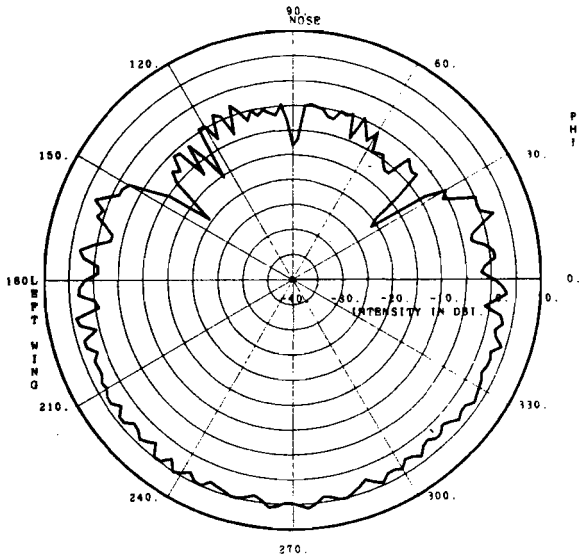

(a) horizontal plane

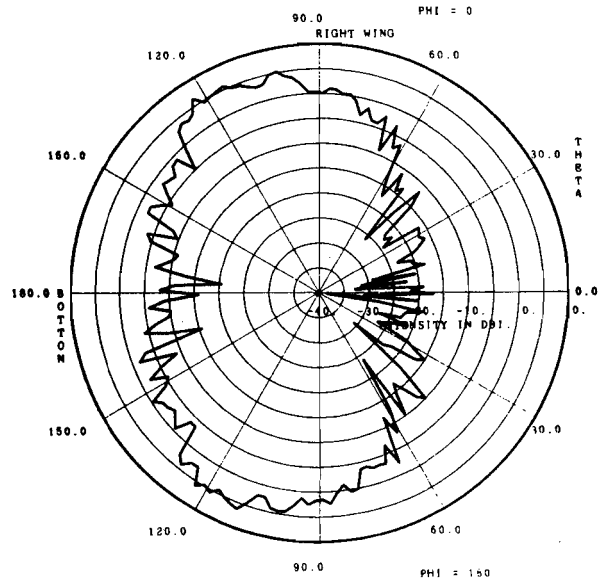

(b) wing to wing

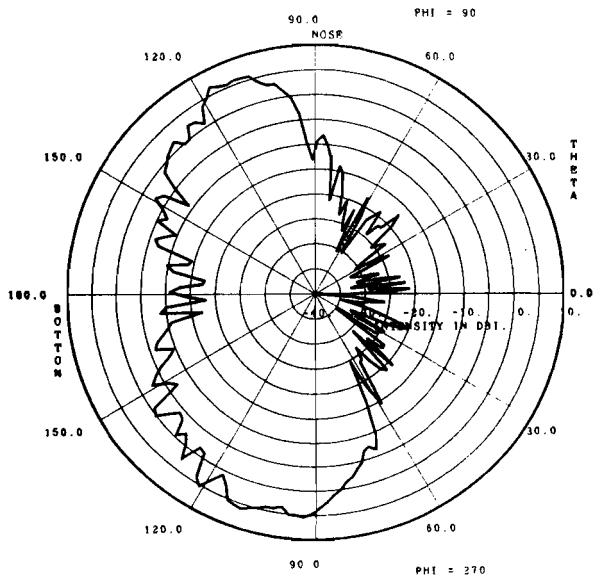

(c) nose to tail

ATC-47(B.11-7)

Fig. B.11-7. Grumman Gulfstream bottom-mounted rear, flaps up, wheels down

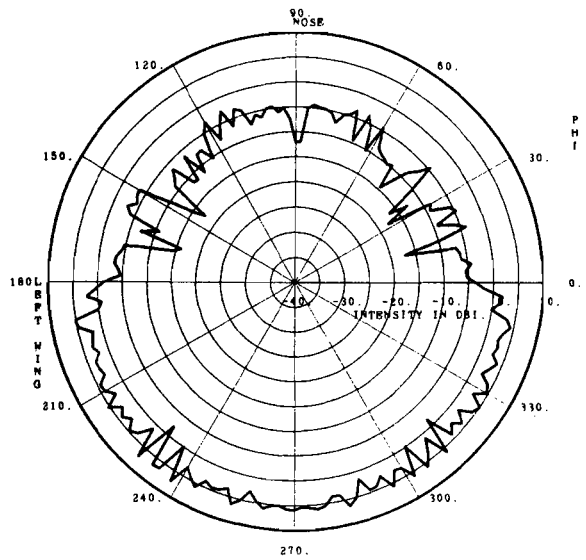

(a) horizontal plane

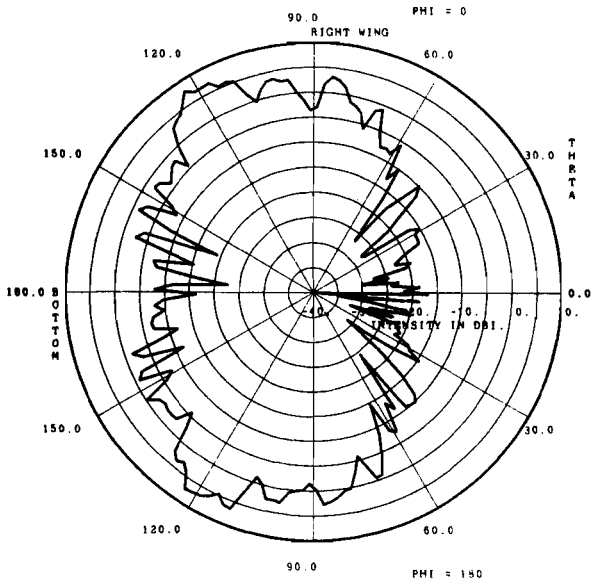

(b) wing to wing

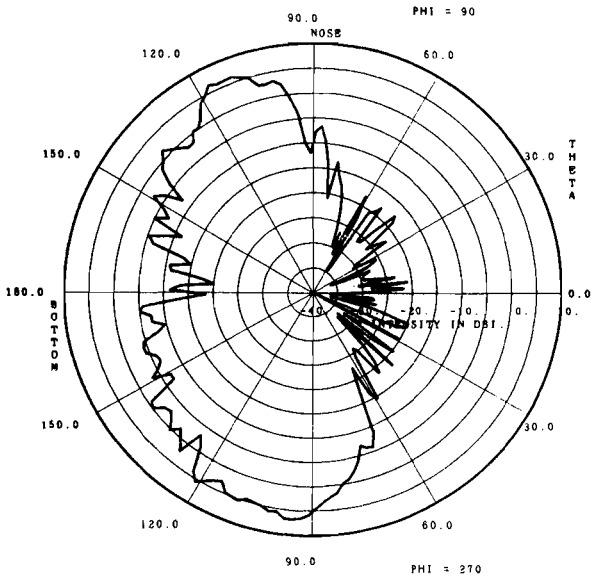

(c) nose to tail

ATC-47(B.11-8)

Fig. B.11-8. Grumman Gulfstream bottom-mounted rear, flaps down, wheels down

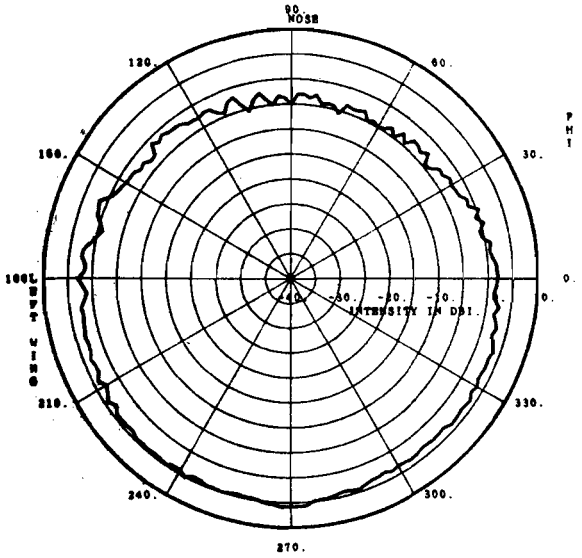

(a) horizontal plane

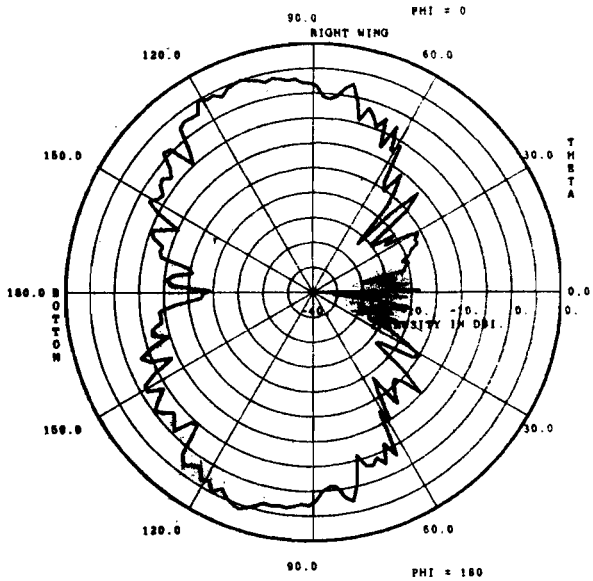

(b) wing to wing

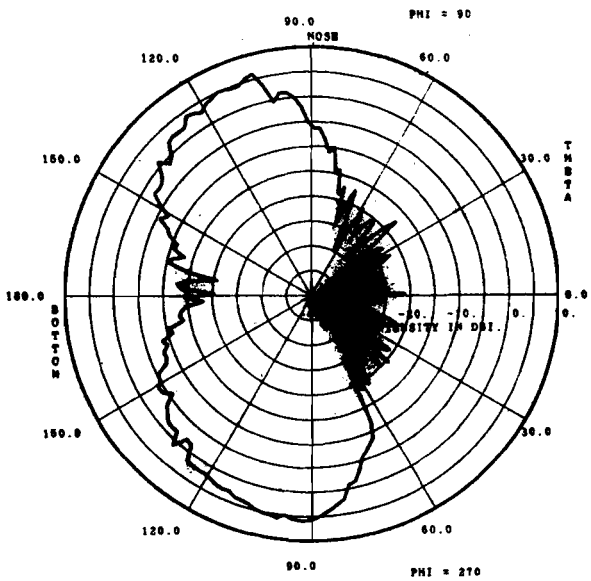

(c) nose to tail

ATC-47(B.11-9)

Fig. B.11-9. Grumman Gulfstream bottom-mounted rear, flaps up, wheels up

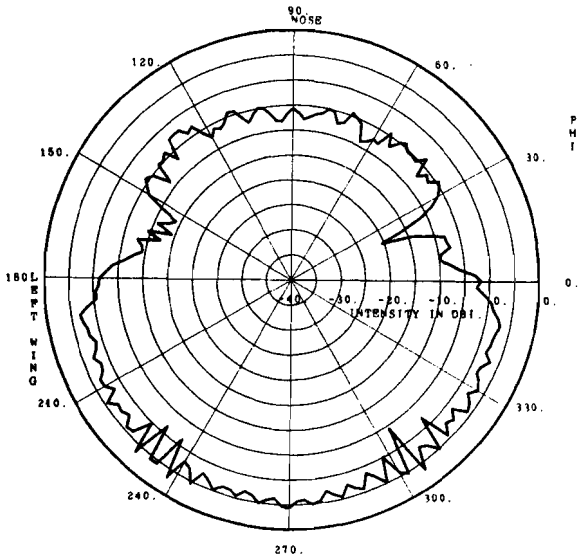

(a) horizontal plane

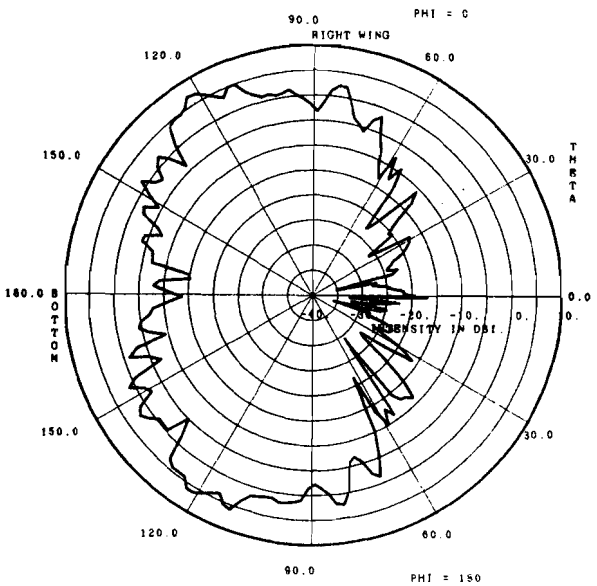

(b) wing to wing

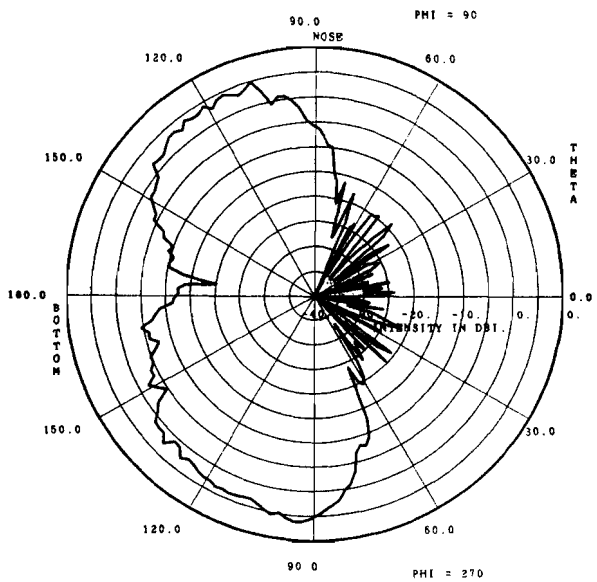

(c) nose to tail

ATC-47(B.11-10)

Fig. B.11-10. Grumman Gulfstream bottom-mounted rear, flaps down, wheels up

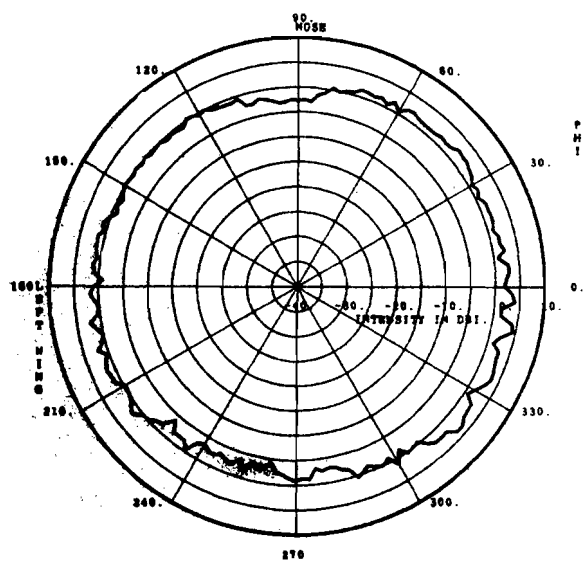

(a) horizontal plane

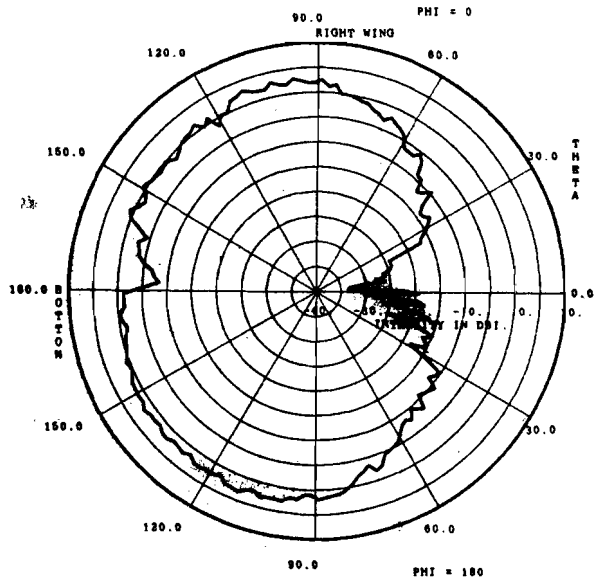

(b) wing to wing

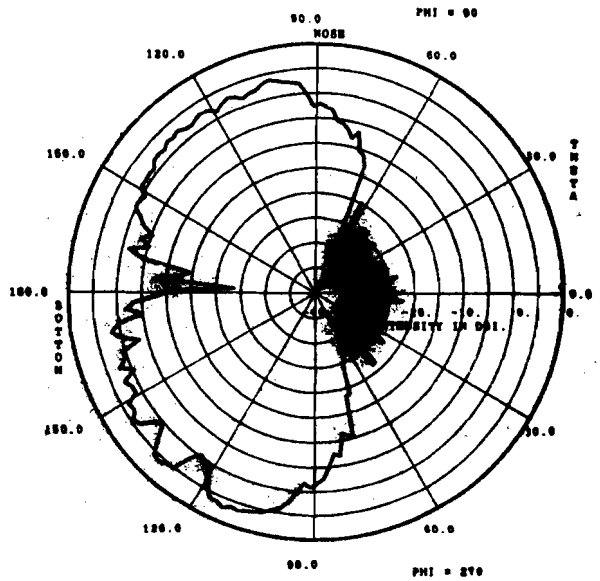

(c) nose to tail

ATC-47(B.11-11)

Fig. B.11-11. Grumman Gulfstream bottom-mounted front, flaps up, wheels up

APPENDIX C

CROSS-POLARIZATION LOSS AND COORDINATE CONVERSION

Figure 4 shows the model aircraft and tower geometry. The polarization vector lies in the plane defined by the yaw axis of the model aircraft and the line joining the transmitter to the model aircraft. This happens to be the horizontal plane in this case and this condition is maintained throughout the whole measurement process. When an aircraft in flight receives radiation from a vertically polarized antenna on the ground, there is correspondence to the experimental setup as long as the aircraft is in straight and level flight. However, any change in flying conditions involving rolling, climbing, or diving will result in the polarization vector flying outside of the above mentioned plane.

In vector notation the polarization vector $\vec{p}$ can be expressed as follows:

Let $\vec{i}_z$ be a unit vector in the axis of the transmitting dipole elements of a ground antenna and $\vec{\rho}$ be a unit vector in the line joining the origin of coordinates in the aircraft to the point of observation, i.e., the transmitting antenna on the ground

then $$\vec{p} = \left(\frac{\vec{i}_z \times \vec{\rho}}{|\vec{i}_z \times \vec{\rho}|} \right) \times \vec{\rho}$$

where x signifies vector cross product.

Let $\vec{i}_{yaw}$ be a unit vector defining the yaw axis of the aircraft (and the aircraft antenna) and let N be a unit vector normal to the plane defined by $\vec{\rho}$ and $\vec{i}_{yaw}$

then $$\vec{N} = \frac{\left(\vec{i}_{yaw} \times \vec{\rho}\right)}{\left|\vec{i}_{yaw} \times \vec{\rho}\right|} \quad .$$

The fraction of the incident signal voltage which is sensed by the aircraft antenna is $\left|\vec{N} \times \vec{r}\right|$, a quantity always less than or equal to unity. The other component of $\vec{p}$ is cross-polarized and contributes nothing to the received signal. Therefore, in practical situations involving aircraft maneuvers, $20 \log_{10} \left|\vec{N} \times \vec{p}\right|$ should be added to the measured antenna directivity. This is one of the quantities computed in a subroutine which also obtains the required coordinate transformations described below.

Let X_I, Y_I, Z_I be the target aircraft coordinates with respect to the ground antenna. The positive directions of the corresponding axes are East, North and vertically up, respectively, and $\vec{i}_x$, $\vec{i}_y$, $\vec{i}_z$ are unit vectors on these axes. Target information expressed in any other form can always be transformed to fit the description.

Let ℓ, m and n be direction cosines defining the unit vector on the aircraft velocity vector, thus defining the aircraft heading in the horizontal plane and the pitch angle. Heading will be defined as the clockwise angle measured from North to the velocity vector and pitch is measured from the horizontal plane to the velocity vector. It is positive if up and negative if down.

Let R be the roll angle of the aircraft. This is zero in straight and level flight and is regarded as positive if the aircraft is rotated clockwise as seen from the tail.

The coordinates of the aircraft relative to the ground antenna define both $\vec{\rho}$ and $\vec{p}$

$$\vec{\rho} = \frac{1}{\sqrt{X_I^2 + Y_I^2 + Z_I^2}} \left\{ - X_I \vec{i}_x - Y_I \vec{i}_y - Z_I \vec{i}_z \right\}$$

$$\frac{\left(\vec{i}_z \times \vec{\rho}\right)}{\left|\vec{i}_z \times \vec{\rho}\right|} = \frac{1}{\sqrt{X_I^2 + Y_I^2}} \left\{ Y_I \vec{i}_x - X_I \vec{i}_y \right\}$$

$$\vec{p} = \frac{1}{\sqrt{X_I^2 + Y_I^2 + Z_I^2}\ \sqrt{X_I^2 + Y_I^2}} \left\{ -X_I Z_I \vec{i}_x - Y_I Z_I \vec{i}_y + (X_I^2 + Y_I^2) \vec{i}_z \right\} .$$

The velocity vector roll angle defines the roll, pitch and yaw axes of the aircraft

$\vec{i}_{yaw}$ is a unit vector on the yaw axis of the aircraft.

$\vec{i}_{roll}$ is a unit vector on the roll axis of the aircraft.

$\therefore \vec{i}_{roll} = \ell \vec{i}_x + m \vec{i}_y + n \vec{i}_z$.

Since the roll axis coincides with the velocity vector, $\vec{i}_{pitch}$ is a unit vector on the pitch axis of the aircraft. When the roll angle is zero

$$\begin{cases} \vec{i}_{pitch} = \dfrac{1}{\sqrt{m^2 + \ell^2}} \left\{ m\,\vec{i}_x - \ell\,\vec{i}_y \right\} \\ \vec{i}_{yaw} = \dfrac{1}{\sqrt{m^2 + \ell^2}} \left\{ -n\ell\,\vec{i}_x - nm\,\vec{i}_y + \sqrt{\ell^2 + m^2}\,\vec{i}_z \right\} \end{cases}$$

and when the roll angle can have any value

$$\vec{i}_{pitch} = \frac{1}{\sqrt{m^2 + \ell^2}} \left[(m \cos R - n\,\ell \sin R)\,\vec{i}_x - (\ell \cos R + nm \sin R)\,\vec{i}_y + (\ell^2 + m^2) \sin R\,\vec{i}_z \right]$$

$$\vec{i}_{yaw} = \frac{1}{\sqrt{m^2 + \ell^2}} \left[-(n\,\ell \cos R + m \sin R)\,\vec{i}_x - (nm \cos R - \ell \sin R)\,\vec{i}_y + (\ell^2 + m^2) \cos R\,\vec{i}_z \right] .$$

The necessary steps to obtain the correction for cross polarization are now obvious. Because of the cumbersome expressions involved, the results of the vector cross products will not be written in expanded form; but it is a simple computer operation and needs no further description.

The aircraft coordinate angles θ and ϕ are now very simply obtained as follows:

$$\cos\theta = \vec{i}_{yaw} \cdot \vec{\rho}$$

$$\therefore \theta = \cos^{-1}\left\{\vec{i}_{yaw} \cdot \vec{\rho}\right\}$$

$$\tan\phi = \left\{\frac{\vec{\rho} \cdot \vec{i}_{pitch}}{\vec{\rho} \cdot \vec{i}_{roll}}\right\}$$

$$\therefore \phi = \tan^{-1}\left\{\frac{\vec{\rho} \cdot \vec{i}_{pitch}}{\vec{\rho} \cdot \vec{i}_{roll}}\right\} \quad .$$

BIBLIOGRAPHY

1. "Technical Development Plan for a Discrete Address Beacon System," Report No. FAA-RD-71-79, October 1974 Final Report, IV -29, IV -30, IV -31, Department of Transportation, Federal Aviation Administration, Washington, D.C. 20590

2. Ibid., V -13.

3. Schlieckert, G. J., "An Analysis of Aircraft L-Band Beacon Antenna Patterns," M. I. T. Lincoln Laboratory, FAA-RD-74-144 (15 January 1975).

☆ U. S. GOVERNMENT PRINTING OFFICE: 1975--600-021--58